Fluid and Particle Dynamics*

James N. Tilton, Ph.D., P.E., *Senior Consultant, Process Engineering, E. I. du Pont de Nemours & Co.; Member, American Institute of Chemical Engineers; Registered Professional Engineer (Delaware)*

FLUID DYNAMICS

* The author acknowledges the contribution of B. C. Sakiadis, editor of this section in the sixth edition of the *Handbook.*

PARTICLE DYNAMICS

Nomenclature and Units*

In this listing, symbols used in this section are defined in a general way and appropriate SI units are given. Specific definitions, as denoted by subscripts, are stated at the place of application in the section. Some specialized symbols used in the section are defined only at the place of application. Some symbols have more than one definition; the appropriate one is identified at the place of application.

Symbol	Definition	SI units	U.S. customary units
a	Pressure wave velocity	m/s	ft/s
A	Area	m^2	ft^2
b	Wall thickness	m	in
b	Channel width	m	ft
c	Acoustic velocity	m/s	ft/s
c_f	Friction coefficient	Dimensionless	Dimensionless
C	Conductance	m^3/s	ft^3/s
Ca	Capillary number	Dimensionless	Dimensionless
C_0	Discharge coefficient	Dimensionless	Dimensionless
C_D	Drag coefficient	Dimensionless	Dimensionless
d	Diameter	m	ft
D	Diameter	m	ft
De	Dean number	Dimensionless	Dimensionless
D_{ij}	Deformation rate tensor components	1/s	1/s
E	Elastic modulus	Pa	lbf/in^2
$\dot{E}_v$	Energy dissipation rate	J/s	ft · lbf/s
Eo	Eotvos number	Dimensionless	Dimensionless
f	Fanning friction factor	Dimensionless	Dimensionless
f	Vortex shedding frequency	1/s	1/s
F	Force	N	lbf
F	Cumulative residence time distribution	Dimensionless	Dimensionless
Fr	Froude number	Dimensionless	Dimensionless
g	Acceleration of gravity	m/s^2	ft/s^2
G	Mass flux	$kg/(m^2 \cdot s)$	$lbm/(ft^2 \cdot s)$
h	Enthalpy per unit mass	J/kg	Btu/lbm
h	Liquid depth	m	ft
k	Ratio of specific heats	Dimensionless	Dimensionless
k	Kinetic energy of turbulence	J/kg	ft · lbf/lbm
K	Power law coefficient	$kg/(m \cdot s^{2-n})$	$lbm/(ft \cdot s^{2-n})$
l_v	Viscous losses per unit mass	J/kg	ft · lbf/lbm
L	Length	m	ft
$\dot{m}$	Mass flow rate	kg/s	lbm/s
M	Mass	kg	lbm
M	Mach number	Dimensionless	Dimensionless
M	Morton number	Dimensionless	Dimensionless
M_w	Molecular weight	kg/kgmole	lbm/lbmole
n	Power law exponent	Dimensionless	Dimensionless
N_b	Blend time number	Dimensionless	Dimensionless
N_D	Best number	Dimensionless	Dimensionless
N_P	Power number	Dimensionless	Dimensionless
N_Q	Pumping number	Dimensionless	Dimensionless
p	Pressure	Pa	lbf/in^2
q	Entrained flow rate	m^3/s	ft^3/s
Q	Volumetric flow rate	m^3/s	ft^3/s
Q	Throughput (vacuum flow)	$Pa \cdot m^3/s$	$lbf \cdot ft^3/s$
δQ	Heat input per unit mass	J/kg	Btu/lbm
r	Radial coordinate	m	ft
R	Radius	m	ft
R	Ideal gas universal constant	J/(kgmole · K)	Btu/(lbmole · R)
R_i	Volume fraction of phase i	Dimensionless	Dimensionless
Re	Reynolds number	Dimensionless	Dimensionless
s	Density ratio	Dimensionless	Dimensionless
s	Entropy per unit mass	J/(kg · K)	Btu/(lbm · R)
S	Slope	Dimensionless	Dimensionless
S	Pumping speed	m^3/s	ft^3/s
S	Surface area per unit volume	l/m	l/ft
St	Strouhal number	Dimensionless	Dimensionless
t	Time	s	s
t	Force per unit area	Pa	lbf/in^2
T	Absolute temperature	K	R
u	Internal energy per unit mass	J/kg	Btu/lbm
u	Velocity	m/s	ft/s
U	Velocity	m/s	ft/s
v	Velocity	m/s	ft/s
V	Velocity	m/s	ft/s
V	Volume	m^3	ft^3
We	Weber number	Dimensionless	Dimensionless
$\dot{W}_s$	Rate of shaft work	J/s	Btu/s
δW_s	Shaft work per unit mass	J/kg	Btu/lbm
x	Cartesian coordinate	m	ft
y	Cartesian coordinate	m	ft
z	Cartesian coordinate	m	ft
z	Elevation	m	ft
	Greek symbols		
α	Velocity profile factor	Dimensionless	Dimensionless
α	Included angle	Radians	Radians
β	Velocity profile factor	Dimensionless	Dimensionless
β	Bulk modulus of elasticity	Pa	lbf/in^2
$\dot{\gamma}$	Shear rate	l/s	l/s
Γ	Mass flow rate per unit width	$kg/(m \cdot s)$	$lbm/(ft \cdot s)$
δ	Boundary layer or film thickness	m	ft
δ_{ij}	Kronecker delta	Dimensionless	Dimensionless
ϵ	Pipe roughness	m	ft
ϵ	Void fraction	Dimensionless	Dimensionless
ϵ	Turbulent dissipation rate	$J/(kg \cdot s)$	$ft \cdot lbf/(lbm \cdot s)$
θ	Residence time	s	s
θ	Angle	Radians	Radians
λ	Mean free path	m	ft
μ	Viscosity	$Pa \cdot s$	$lbm/(ft \cdot s)$
ν	Kinematic viscosity	m^2/s	ft^2/s
ρ	Density	kg/m^3	lbm/ft^3
σ	Surface tension	N/m	lbf/ft
σ	Cavitation number	Dimensionless	Dimensionless
σ_{ij}	Components of total stress tensor	Pa	lbf/in^2
τ	Shear stress	Pa	lbf/in^2
τ	Time period	s	s
τ_{ij}	Components of deviatoric stress tensor	Pa	lbf/in^2
Φ	Energy dissipation rate per unit volume	$J/(m^3 \cdot s)$	$ft \cdot lbf/(ft^3 \cdot s)$
ϕ	Angle of inclination	Radians	Radians
ω	Vorticity	1/s	1/s

* Note that with U.S. Customary units, the conversion factor g_c may be required to make equations in this section dimensionally consistent; $g_c = 32.17$ (lbm·ft)/lbf·s^2).

FLUID DYNAMICS

General References: Batchelor, *An Introduction to Fluid Dynamics,* Cambridge University, Cambridge, 1967; Bird, Stewart, and Lightfoot, *Transport Phenomena,* Wiley, New York, 1960; Brodkey, *The Phenomena of Fluid Motions,* Addison-Wesley, Reading, Mass., 1967; Denn, *Process Fluid Mechanics,* Prentice-Hall, Englewood Cliffs, N.J., 1980; Landau and Lifshitz, *Fluid Mechanics,* 2d ed., Pergamon, 1987; Govier and Aziz, *The Flow of Complex Mixtures in Pipes,* Van Nostrand Reinhold, New York, 1972, Krieger, Huntington, N.Y., 1977; Panton, *Incompressible Flow,* Wiley, New York, 1984; Schlichting, *Boundary Layer Theory,* 8th ed., McGraw-Hill, New York, 1987; Shames, *Mechanics of Fluids,* 3d ed., McGraw-Hill, New York, 1992; Streeter, *Handbook of Fluid Dynamics,* McGraw-Hill, New York, 1971; Streeter and Wylie, *Fluid Mechanics,* 8th ed., McGraw-Hill, New York, 1985; Vennard and Street, *Elementary Fluid Mechanics,* 5th ed., Wiley, New York, 1975; Whitaker, *Introduction to Fluid Mechanics,* Prentice-Hall, Englewood Cliffs, N.J., 1968, Krieger, Huntington, N.Y., 1981.

NATURE OF FLUIDS

Deformation and Stress A **fluid** is a substance which undergoes continuous deformation when subjected to a shear stress. Figure 6-1 illustrates this concept. A fluid is bounded by two large parallel plates, of area A, separated by a small distance H. The bottom plate is held fixed. Application of a force F to the upper plate causes it to move at a velocity U. The fluid continues to deform as long as the force is applied, unlike a solid, which would undergo only a finite deformation.

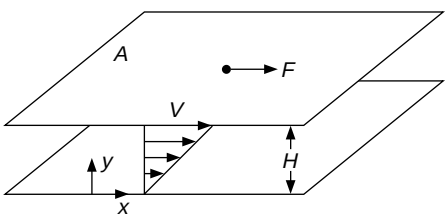

FIG. 6-1 Deformation of a fluid subjected to a shear stress.

The force is directly proportional to the area of the plate; the shear stress is $\tau = F/A$. Within the fluid, a linear velocity profile $u = Uy/H$ is established; due to the **no-slip condition,** the fluid bounding the lower plate has zero velocity and the fluid bounding the upper plate moves at the plate velocity U. The velocity gradient $\dot{\gamma} = du/dy$ is called the **shear rate** for this flow. Shear rates are usually reported in units of reciprocal seconds. The flow in Fig. 6-1 is a **simple shear flow.**

Viscosity The ratio of shear stress to shear rate is the viscosity, μ.

$$\mu = \frac{\tau}{\dot{\gamma}} \tag{6-1}$$

The SI units of viscosity are kg/(m · s) or Pa · s (pascal second). The cgs unit for viscosity is the poise; 1 Pa · s equals 10 poise or 1000 centipoise (cP) or 0.672 lbm/(ft · s). The terms *absolute viscosity* and *shear viscosity* are synonymous with the viscosity as used in Eq. (6-1). **Kinematic viscosity** $\nu \equiv \mu/\rho$ is the ratio of viscosity to density. The SI units of kinematic viscosity are m^2/s. The cgs stoke is 1 cm^2/s.

Rheology In general, fluid flow patterns are more complex than the one shown in Fig. 6-1, as is the relationship between fluid deformation and stress. Rheology is the discipline of fluid mechanics which studies this relationship. One goal of rheology is to obtain **constitutive equations** by which stresses may be computed from deformation rates. For simplicity, fluids may be classified into rheological types in reference to the simple shear flow of Fig. 6-1. Complete definitions require extension to multidimensional flow. For more information, several good references are available, including Bird, Armstrong, and Hassager, (*Dynamics of Polymeric Liquids,* vol. 1: *Fluid Mechanics,* Wiley, New York, 1977); Metzner, ("Flow of Non-Newtonian Fluids" in Streeter, *Handbook of Fluid Dynamics,* McGraw-Hill, New York, 1971); and Skelland (*Non-Newtonian Flow and Heat Transfer,* Wiley, New York, 1967).

Fluids without any solidlike elastic behavior do not undergo any reverse deformation when shear stress is removed, and are called **purely viscous** fluids. The shear stress depends only on the rate of deformation, and not on the extent of deformation (strain). Those which exhibit both viscous and elastic properties are called **viscoelastic** fluids.

Purely viscous fluids are further classified into time-independent and time-dependent fluids. For time-independent fluids, the shear stress depends only on the instantaneous shear rate. The shear stress for time-dependent fluids depends on the past history of the rate of deformation, as a result of structure or orientation buildup or breakdown during deformation.

A **rheogram** is a plot of shear stress versus shear rate for a fluid in simple shear flow, such as that in Fig. 6-1. Rheograms for several types of time-independent fluids are shown in Fig. 6-2. The **Newtonian** fluid rheogram is a straight line passing through the origin. The slope of the line is the viscosity. For a Newtonian fluid, the viscosity is independent of shear rate, and may depend only on temperature and perhaps pressure. By far, the Newtonian fluid is the largest class of fluid of engineering importance. Gases and low molecular weight liquids are generally Newtonian. Newton's law of viscosity is a rearrangement of Eq. (6-1) in which the viscosity is a constant:

$$\tau = \mu\dot{\gamma} = \mu \frac{du}{dy} \tag{6-2}$$

All fluids for which the viscosity varies with shear rate are **non-Newtonian fluids.** For non-Newtonian fluids the viscosity, defined as the ratio of shear stress to shear rate, is often called the **apparent viscosity** to emphasize the distinction from Newtonian behavior. Purely viscous, time-independent fluids, for which the apparent viscosity may be expressed as a function of shear rate, are called **generalized Newtonian fluids.**

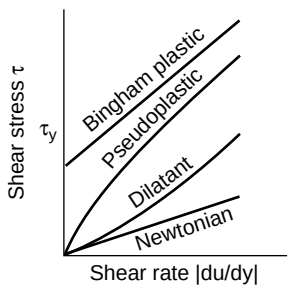

FIG. 6-2 Shear diagrams.

Non-Newtonian fluids include those for which a finite stress τ_y is required before continuous deformation occurs; these are called **yield-stress** materials. The **Bingham plastic** fluid is the simplest yield-stress material; its rheogram has a constant slope μ_∞, called the *infinite shear* viscosity.

$$\tau = \tau_y + \mu_\infty\dot{\gamma} \tag{6-3}$$

Highly concentrated suspensions of fine solid particles frequently exhibit Bingham plastic behavior.

Shear-thinning fluids are those for which the slope of the rheogram decreases with increasing shear rate. These fluids have also been called *pseudoplastic,* but this terminology is outdated and discouraged. Many polymer melts and solutions, as well as some solids suspensions, are shear-thinning. Shear-thinning fluids without yield stresses typically obey a power law model over a range of shear rates.

$$\tau = K\dot{\gamma}^n \tag{6-4}$$

The apparent viscosity is

$$\mu = K\dot{\gamma}^{n-1} \tag{6-5}$$

The factor K is the consistency index or power law coefficient, and n is the power law exponent. The exponent n is dimensionless, while K is in units of kg/(m · s^{2-n}). For shear-thinning fluids, $n < 1$. The power law model typically provides a good fit to data over a range of one to two orders of magnitude in shear rate; behavior at very low and very high shear rates is often Newtonian. Shear-thinning power law fluids with yield stresses are sometimes called *Herschel-Bulkley fluids.* Numerous other rheological model equations for shear-thinning fluids are in common use.

Dilatant, or shear-thickening, fluids show increasing viscosity with increasing shear rate. Over a limited range of shear rate, they may be described by the power law model with $n > 1$. Dilatancy is rare, observed only in certain concentration ranges in some particle suspensions (Govier and Aziz, pp. 33–34). Extensive discussions of dilatant suspensions, together with a listing of dilatant systems, are given by Green and Griskey (*Trans. Soc. Rheol,* **12**[1], 13–25 [1968]); Griskey and Green (*AIChE J.,* **17,** 725–728 [1971]); and Bauer and Collins ("Thixotropy and Dilatancy," in Eirich, *Rheology,* vol. 4, Academic, New York, 1967).

Time-dependent fluids are those for which structural rearrangements occur during deformation at a rate too slow to maintain equilibrium configurations. As a result, shear stress changes with duration of shear. **Thixotropic** fluids, such as mayonnaise, clay suspensions used as drilling muds, and some paints and inks, show decreasing shear stress with time at constant shear rate. A detailed description of thixotropic behavior and a list of thixotropic systems is found in Bauer and Collins (ibid.).

Rheopectic behavior is the opposite of thixotropy. Shear stress increases with time at constant shear rate. Rheopectic behavior has been observed in bentonite sols, vanadium pentoxide sols, and gypsum suspensions in water (Bauer and Collins, ibid.) as well as in some polyester solutions (Steg and Katz, *J. Appl. Polym. Sci.,* **9,** 3, 177 [1965]).

Viscoelastic fluids exhibit elastic recovery from deformation when stress is removed. Polymeric liquids comprise the largest group of fluids in this class. A property of viscoelastic fluids is the *relaxation time,* which is a measure of the time required for elastic effects to decay. Viscoelastic effects may be important with sudden changes in rates of deformation, as in flow startup and stop, rapidly oscillating flows, or as a fluid passes through sudden expansions or contractions where accelerations occur. In many fully developed flows where such effects are absent, viscoelastic fluids behave as if they were purely viscous. In viscoelastic flows, normal stresses perpendicular to the direction of shear are different from those in the parallel direction. These give rise to such behaviors as the *Weissenberg effect,* in which fluid climbs up a shaft rotating in the fluid, and *die swell,* where a stream of fluid issuing from a tube may expand to two or more times the tube diameter.

A parameter indicating whether viscoelastic effects are important is the **Deborah number,** which is the ratio of the characteristic relaxation time of the fluid to the characteristic time scale of the flow. For small Deborah numbers, the relaxation is fast compared to the characteristic time of the flow, and the fluid behavior is purely viscous. For very large Deborah numbers, the behavior closely resembles that of an elastic solid.

Analysis of viscoelastic flows is very difficult. Simple constitutive equations are unable to describe all the material behavior exhibited by viscoelastic fluids even in geometrically simple flows. More complex constitutive equations may be more accurate, but become exceedingly difficult to apply, especially for complex geometries, even with advanced numerical methods. For good discussions of viscoelastic fluid behavior, including various types of constitutive equations, see Bird, Armstrong, and Hassager (*Dynamics of Polymeric Liquids,* vol. 1: *Fluid Mechanics,* vol. 2: *Kinetic Theory,* Wiley, New York, 1977); Middleman (*The Flow of High Polymers,* Interscience (Wiley) New York, 1968); or Astarita and Marrucci (*Principles of Non-Newtonian Fluid Mechanics,* McGraw-Hill, New York, 1974).

Polymer processing is the field which depends most on the flow of non-Newtonian fluids. Several excellent texts are available, including Middleman (*Fundamentals of Polymer Processing,* McGraw-Hill, New York, 1977) and Tadmor and Gogos (*Principles of Polymer Processing,* Wiley, New York, 1979).

There is a wide variety of instruments for measurement of Newtonian viscosity, as well as rheological properties of non-Newtonian fluids. They are described in Van Wazer, Lyons, Kim, and Colwell, (*Viscosity and Flow Measurement,* Interscience, New York, 1963); Coleman, Markowitz, and Noll (*Viscometric Flows of Non-Newtonian Fluids,* Springer-Verlag, Berlin, 1966); Dealy and Wissbrun (*Melt Rheology and its Role in Plastics Processing,* Van Nostrand Reinhold, 1990). Measurement of rheological behavior requires well-characterized flows. Such *rheometric* flows are thoroughly discussed by Astarita and Marrucci (*Principles of Non-Newtonian Fluid Mechanics,* McGraw-Hill, New York, 1974).

KINEMATICS OF FLUID FLOW

Velocity The term *kinematics* refers to the quantitative description of fluid motion or deformation. The rate of deformation depends on the distribution of velocity within the fluid. Fluid velocity **v** is a vector quantity, with three cartesian components v_x, v_y, and v_z. The velocity vector is a function of spatial position and time. A **steady** flow is one in which the velocity is independent of time, while in **unsteady** flow **v** varies with time.

Compressible and Incompressible Flow An incompressible flow is one in which the density of the fluid is constant or nearly constant. Liquid flows are normally treated as incompressible, except in the context of hydraulic transients (see following). Compressible fluids, such as gases, may undergo incompressible flow if pressure and/or temperature changes are small enough to render density changes insignificant. Frequently, compressible flows are regarded as flows in which the density varies by more than 5 to 10 percent.

Streamlines, Pathlines, and Streaklines These are curves in a flow field which provide insight into the flow pattern. *Streamlines* are tangent at every point to the local instantaneous velocity vector. A *pathline* is the path followed by a material element of fluid; it coincides with a streamline if the flow is steady. In unsteady flow the pathlines generally do not coincide with streamlines. *Streaklines* are curves on which are found all the material particles which passed through a particular point in space at some earlier time. For example, a streakline is revealed by releasing smoke or dye at a point in a flow field. For steady flows, streamlines, pathlines, and streaklines are indistinguishable. In two-dimensional incompressible flows, streamlines are contours of the **stream function.**

One-dimensional Flow Many flows of great practical importance, such as those in pipes and channels, are treated as one-dimensional flows. There is a single direction called the *flow direction;* velocity components perpendicular to this direction are either zero or considered unimportant. Variations of quantities such as velocity, pressure, density, and temperature are considered only in the flow direction. The fundamental conservation equations of fluid mechanics are greatly simplified for one-dimensional flows. A broader category of one-dimensional flow is one where there is only one nonzero velocity component, which depends on only one coordinate direction, and this coordinate direction may or may not be the same as the flow direction.

Rate of Deformation Tensor For general three-dimensional flows, where all three velocity components may be important and may vary in all three coordinate directions, the concept of deformation previously introduced must be generalized. The rate of deformation tensor D_{ij} has nine components. In Cartesian coordinates,

$$D_{ij} = \left(\frac{\partial v_i}{\partial x_j} + \frac{\partial v_j}{\partial x_i} \right) \tag{6-6}$$

where the subscripts i and j refer to the three coordinate directions. Some authors define the deformation rate tensor as one-half of that given by Eq. (6-6).

Vorticity The relative motion between two points in a fluid can be decomposed into three components: rotation, dilatation, and deformation. The rate of deformation tensor has been defined. Dilatation refers to the volumetric expansion or compression of the fluid, and vanishes for incompressible flow. Rotation is described by a tensor $\omega_{ij} = \partial v_i/\partial x_j - \partial v_j/\partial x_i$. The vector of vorticity given by one-half the

curl of the velocity vector is another measure of rotation. In two-dimensional flow in the x-y plane, the vorticity ω is given by

$$\omega = \frac{1}{2}\left(\frac{\partial v_y}{\partial x} - \frac{\partial v_x}{\partial y}\right) \tag{6-7}$$

Here ω is the magnitude of the vorticity vector, which is directed along the z axis. An **irrotational** flow is one with zero vorticity. Irrotational flows have been widely studied because of their useful mathematical properties and applicability to flow regions where viscous effects may be neglected. Such flows without viscous effects are called **inviscid** flows.

Laminar and Turbulent Flow, Reynolds Number These terms refer to two distinct types of flow. In *laminar flow,* there are smooth streamlines and the fluid velocity components vary smoothly with position, and with time if the flow is unsteady. The flow described in reference to Fig. 6-1 is laminar. In *turbulent flow,* there are no smooth streamlines, and the velocity shows chaotic fluctuations in time and space. Velocities in turbulent flow may be reported as the sum of a time-averaged velocity and a velocity fluctuation from the average. For any given flow geometry, a dimensionless **Reynolds number** may be defined for a Newtonian fluid as $\mathrm{Re} = LU\rho/\mu$ where L is a characteristic length. Below a critical value of Re the flow is laminar, while above the critical value a transition to turbulent flow occurs. The geometry-dependent critical Reynolds number is determined experimentally.

CONSERVATION EQUATIONS

Macroscopic and Microscopic Balances Three postulates, regarded as laws of physics, are fundamental in fluid mechanics. These are *conservation of mass, conservation of momentum,* and *conservation of energy.* In addition, two other postulates, *conservation of moment of momentum* (angular momentum) and the *entropy inequality* (second law of thermodynamics) have occasional use. The conservation principles may be applied either to material systems or to control volumes in space. Most often, control volumes are used. The control volumes may be either of finite or differential size, resulting in either **algebraic** or **differential** conservation equations, respectively. These are often called **macroscopic** and **microscopic** balance equations.

Macroscopic Equations An arbitrary control volume of finite size V_a is bounded by a surface of area A_a with an outwardly directed unit normal vector **n.** The control volume is not necessarily fixed in space. Its boundary moves with velocity **w.** The fluid velocity is **v.** Figure 6-3 shows the arbitrary control volume.

Mass balance Applied to the control volume, the principle of conservation of mass may be written as (Whitaker, *Introduction to Fluid Mechanics,* Prentice-Hall, Englewood Cliffs, N.J., 1968, Krieger, Huntington, N.Y., 1981)

$$\frac{d}{dt}\int_{V_a} \rho\, dV + \int_{A_a} \rho(v - w)\cdot \mathbf{n}\, dA = 0 \tag{6-8}$$

This equation is also known as the **continuity** equation.

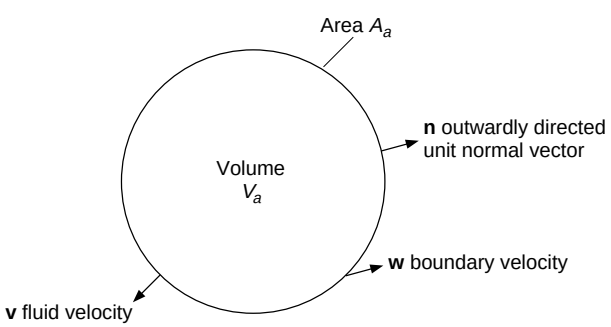

FIG. 6-3 Arbitrary control volume for application of conservation equations.

Simplified forms of Eq. (6-8) apply to special cases frequently found in practice. For a control volume fixed in space with one inlet of area A_1 through which an incompressible fluid enters the control volume at an average velocity V_1, and one outlet of area A_2 through which fluid leaves at an average velocity V_2, as shown in Fig. 6-4, the continuity equation becomes

$$V_1A_1 = V_2A_2 \tag{6-9}$$

The average velocity across a surface is given by

$$V = (1/A)\int_A v\, dA$$

where v is the local velocity component perpendicular to the inlet surface. The volumetric flow rate Q is the product of average velocity and the cross-sectional area, $Q = VA$. The average **mass velocity** is $G = \rho V$. For steady flows through fixed control volumes with multiple inlets and/or outlets, conservation of mass requires that the sum of inlet mass flow rates equals the sum of outlet mass flow rates. For incompressible flows through fixed control volumes, the sum of inlet flow rates (mass or volumetric) equals the sum of exit flow rates, whether the flow is steady or unsteady.

Momentum Balance Since momentum is a vector quantity, the momentum balance is a vector equation. Where gravity is the only body force acting on the fluid, the linear momentum principle, applied to the arbitrary control volume of Fig. 6-3, results in the following expression (Whitaker, ibid.).

$$\frac{d}{dt}\int_{V_a} \rho\mathbf{v}\, dV + \int_{A_a} \rho\mathbf{v}(\mathbf{v} - \mathbf{w})\cdot \mathbf{n}\, dA = \int_{V_a} \rho\mathbf{g}\, dV + \int_{A_a} \mathbf{t}_\mathbf{n}\, dA \tag{6-10}$$

Here $\mathbf{g}$ is the gravity vector and $\mathbf{t_n}$ is the force per unit area exerted by the surroundings on the fluid in the control volume. The integrand of the area integral on the left-hand side of Eq. (6-10) is nonzero only on the entrance and exit portions of the control volume boundary. For the special case of steady flow at a mass flow rate $\dot{m}$ through a control volume fixed in space with one inlet and one outlet, (Fig. 6-4) with the inlet and outlet velocity vectors perpendicular to planar inlet and outlet surfaces, giving average velocity vectors $\mathbf{V}_1$ and $\mathbf{V}_2$, the momentum equation becomes

$$\dot{m}(\beta_2\mathbf{V}_2 - \beta_1\mathbf{V}_1) = -p_1\mathbf{A}_1 - p_2\mathbf{A}_2 + \mathbf{F} + M\mathbf{g} \tag{6-11}$$

where M is the total mass of fluid in the control volume. The factor β arises from the averaging of the velocity across the area of the inlet or outlet surface. It is the ratio of the area average of the square of velocity magnitude to the square of the area average velocity magnitude. For a uniform velocity, $\beta = 1$. For turbulent flow, β is nearly unity, while for laminar pipe flow with a parabolic velocity profile, $\beta = 4/3$. The vectors $\mathbf{A}_1$ and $\mathbf{A}_2$ have magnitude equal to the areas of the inlet and outlet surfaces, respectively, and are outwardly directed normal to the surfaces. The vector $\mathbf{F}$ is the force exerted on the fluid by the nonflow boundaries of the control volume. It is also assumed that the stress vector $\mathbf{t_n}$ is normal to the inlet and outlet surfaces, and that its magnitude may be approximated by the pressure p. Equation (6-11) may be generalized to multiple inlets and/or outlets. In such cases, the mass flow rates for all the inlets and outlets are not equal. A distinct flow rate $\dot{m}_i$ applies to each inlet or outlet i. To generalize the equation, $-\mathbf{pA}$ terms for each inlet and outlet, $-\dot{m}\beta\mathbf{V}$ terms for each inlet, and $\dot{m}\beta\mathbf{V}$ terms for each outlet are included.

Balance equations for angular momentum, or moment of momentum, may also be written. They are used less frequently than the lin-

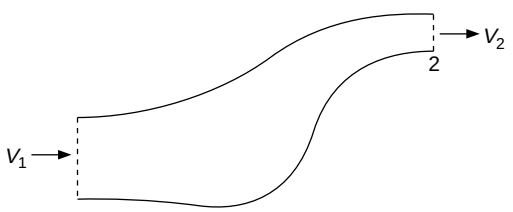

FIG. 6-4 Fixed control volume with one inlet and one outlet.

ear momentum equations. See Whitaker (*Introduction to Fluid Mechanics,* Prentice-Hall, Englewood Cliffs, N.J., 1968, Krieger, Huntington, N.Y., 1981; or Shames (*Mechanics of Fluids,* 3d ed., McGraw-Hill, New York, 1992).

Total Energy Balance The total energy balance derives from the first law of thermodynamics. Applied to the arbitrary control volume of Fig. 6-3, it leads to an equation for the rate of change of the sum of internal, kinetic, and gravitational potential energy. In this equation, u is the internal energy per unit mass, v is the magnitude of the velocity vector $\mathbf{v}$, z is elevation, g is the gravitational acceleration, and $\mathbf{q}$ is the heat flux vector:

$$\frac{d}{dt}\int_{V_a}\rho\left(u+\frac{v^2}{2}+gz\right)dV+\int_{A_a}\rho\left(u+\frac{v^2}{2}+gz\right)(\mathbf{v}-\mathbf{w})\cdot\mathbf{n}\,dA = \int_{A_a}(\mathbf{v}\cdot\mathbf{t_n})\,dA-\int_{A_a}(\mathbf{q}\cdot\mathbf{n})\,dA \quad (6\text{-}12)$$

The first integral on the right-hand side is the rate of work done on the fluid in the control volume by forces at the boundary. It includes both work done by moving solid boundaries and work done at flow entrances and exits. The work done by moving solid boundaries also includes that by such surfaces as pump impellers; this work is called **shaft work;** its rate is $\dot{W}_S$.

A useful simplification of the total energy equation applies to a particular set of assumptions. These are a control volume with fixed solid boundaries, except for those producing shaft work, steady state conditions, and mass flow at a rate $\dot{m}$ through a single planar entrance and a single planar exit (Fig. 6-4), to which the velocity vectors are perpendicular. As with Eq. (6-11), it is assumed that the stress vector $\mathbf{t_n}$ is normal to the entrance and exit surfaces and may be approximated by the pressure p. The **equivalent pressure,** $p+\rho gz$, is assumed to be uniform across the entrance and exit. The average velocity at the entrance and exit surfaces is denoted by V. Subscripts 1 and 2 denote the entrance and exit, respectively.

$$h_1+\alpha_1\frac{V_1^2}{2}+gz_1=h_2+\alpha_2\frac{V_2^2}{2}+gz_2-\delta Q-\delta W_S \quad (6\text{-}13)$$

Here, h is the enthalpy per unit mass, $h=u+p/\rho$. The shaft work per unit of mass flowing through the control volume is $\delta W_S=\dot{W}_s/\dot{m}$. Similarly, δQ is the heat input rate per unit of mass. The factor α is the ratio of the cross-sectional area average of the cube of the velocity to the cube of the average velocity. For a uniform velocity profile, $\alpha=1$. In turbulent flow, α is usually assumed to equal unity; in turbulent pipe flow, it is typically about 1.07. For laminar flow in a circular pipe with a parabolic velocity profile, $\alpha=2$.

Mechanical Energy Balance, Bernoulli Equation A balance equation for the sum of kinetic and potential energy may be obtained from the momentum balance by forming the scalar product with the velocity vector. The resulting equation, called the *mechanical energy balance,* contains a term accounting for the dissipation of mechanical energy into thermal energy by viscous forces. The mechanical energy equation is also derivable from the total energy equation in a way that reveals the relationship between the dissipation and entropy generation. The macroscopic mechanical energy balance for the arbitrary control volume of Fig. 6-3 may be written, with p = thermodynamic pressure, as

$$\frac{d}{dt}\int_{V_a}\rho\left(\frac{v^2}{2}+gz\right)dV+\int_{A_a}\rho\left(\frac{v^2}{2}+gz\right)(\mathbf{v}-\mathbf{w})\cdot\mathbf{n}\,dA = \int_{V_a}p\,\boldsymbol{\nabla}\cdot\mathbf{v}\,dV+\int_{A_a}(\mathbf{v}\cdot\mathbf{t}_n)\,dA-\int_{V_a}\Phi\,dV \quad (6\text{-}14)$$

The last term is the rate of viscous energy dissipation to internal energy, $\dot{E}_v=\int_{V_a}\Phi\,dV$, also called the rate of viscous losses. These losses are the origin of frictional pressure drop in fluid flow. Whitaker and Bird, Stewart, and Lightfoot provide expressions for the dissipation function Φ for Newtonian fluids in terms of the local velocity gradients. However, when using macroscopic balance equations the local velocity field within the control volume is usually unknown. For such cases additional information, which may come from empirical correlations, is needed.

For the same special conditions as for Eq. (6-13), the mechanical energy equation is reduced to

$$\alpha_1\frac{V_1^2}{2}+gz_1+\delta W_S=\alpha_2\frac{V_2^2}{2}+gz_2+\int_{p_1}^{p_2}\frac{dp}{\rho}+l_v \quad (6\text{-}15)$$

Here $l_v=\dot{E}_v/\dot{m}$ is the energy dissipation per unit mass. This equation has been called the **engineering Bernoulli equation.** For an incompressible flow, Eq. (6-15) becomes

$$\frac{p_1}{\rho}+\alpha_1\frac{V_1^2}{2}+gz_1+\delta W_S=\frac{p_2}{\rho}+\alpha_2\frac{V_2^2}{2}+gz_2+l_v \quad (6\text{-}16)$$

The Bernoulli equation can be written for incompressible, inviscid flow along a streamline, where no shaft work is done.

$$\frac{p_1}{\rho}+\frac{V_1^2}{2}+gz_1=\frac{p_2}{\rho}+\frac{V_2^2}{2}+gz_2 \quad (6\text{-}17)$$

Unlike the momentum equation (Eq. [6-11]), the Bernoulli equation is not easily generalized to multiple inlets or outlets.

Microscopic Balance Equations Partial differential balance equations express the conservation principles at a point in space. Equations for mass, momentum, total energy, and mechanical energy may be found in Whitaker (ibid.), Bird, Stewart, and Lightfoot (*Transport Phenomena,* Wiley, New York, 1960), and Slattery (*Momentum, Heat and Mass Transfer in Continua,* 2d ed., Krieger, Huntington, N.Y., 1981), for example. These references also present the equations in other useful coordinate systems besides the cartesian system. The coordinate systems are fixed in inertial reference frames. The two most used equations, for mass and momentum, are presented here.

Mass Balance, Continuity Equation The continuity equation, expressing conservation of mass, is written in cartesian coordinates as

$$\frac{\partial\rho}{\partial t}+\frac{\partial\rho v_x}{\partial x}+\frac{\partial\rho v_y}{\partial y}+\frac{\partial\rho v_z}{\partial z}=0 \quad (6\text{-}18)$$

In terms of the **substantial derivative,** D/Dt,

$$\frac{D\rho}{Dt}\equiv\frac{\partial\rho}{\partial t}+v_x\frac{\partial\rho}{\partial x}+v_y\frac{\partial\rho}{\partial y}+v_z\frac{\partial\rho}{\partial z}=-\rho\left(\frac{\partial v_x}{\partial x}+\frac{\partial v_y}{\partial y}+\frac{\partial v_z}{\partial z}\right) \quad (6\text{-}19)$$

The substantial derivative, also called the **material derivative,** is the rate of change in a Lagrangian reference frame, that is, following a material particle. In vector notation the continuity equation may be expressed as

$$\frac{D\rho}{Dt}=-\rho\nabla\cdot\mathbf{v} \quad (6\text{-}20)$$

For incompressible flow,

$$\nabla\cdot\mathbf{v}=\frac{\partial v_x}{\partial x}+\frac{\partial v_y}{\partial y}+\frac{\partial v_z}{\partial z}=0 \quad (6\text{-}21)$$

Stress Tensor The stress tensor is needed to completely describe the stress state for microscopic momentum balances in multidimensional flows. The components of the stress tensor σ_{ij} give the force in the j direction on a plane perpendicular to the i direction, using a sign convention defining a positive stress as one where the fluid with the greater i coordinate value exerts a force in the positive i direction on the fluid with the lesser i coordinate. Several references in fluid mechanics and continuum mechanics provide discussions, to various levels of detail, of stress in a fluid (Denn; Bird, Stewart, and Lightfoot; Schlichting; Fung [*A First Course in Continuum Mechanics,* 2d. ed., Prentice-Hall, Englewood Cliffs, N.J., 1977]; Truesdell and Toupin [in Flügge, *Handbuch der Physik,* vol. 3/1, Springer-Verlag, Berlin, 1960]; Slattery [*Momentum, Energy and Mass Transfer in Continua,* 2d ed., Krieger, Huntington, N.Y., 1981]).

The stress has an isotropic contribution due to fluid pressure and dilatation, and a **deviatoric** contribution due to viscous deformation effects. The deviatoric contribution for a Newtonian fluid is the three-dimensional generalization of Eq. (6-2):

$$\tau_{ij}=\mu D_{ij} \quad (6\text{-}22)$$

The total stress is

$$\sigma_{ij}=(-p+\lambda\nabla\cdot\mathbf{v})\delta_{ij}+\tau_{ij} \quad (6\text{-}23)$$

The identity tensor δ_{ij} is zero for $i \neq j$ and unity for $i = j$. The coefficient λ is a material property related to the **bulk viscosity,** $\kappa = \lambda + 2\mu/3$. There is considerable uncertainty about the value of κ. Traditionally, Stokes' hypothesis, $\kappa = 0$, has been invoked, but the validity of this hypothesis is doubtful (Slattery, ibid.). For incompressible flow, the value of bulk viscosity is immaterial as Eq. (6-23) reduces to

$$\sigma_{ij} = -p\delta_{ij} + \tau_{ij} \tag{6-24}$$

Similar generalizations to multidimensional flow are necessary for non-Newtonian constitutive equations.

Cauchy Momentum and Navier-Stokes Equations The differential equations for conservation of momentum are called the **Cauchy momentum equations.** These may be found in general form in most fluid mechanics texts (e.g., Slattery [ibid.]; Denn; Whitaker; and Schlichting). For the important special case of an incompressible Newtonian fluid with constant viscosity, substitution of Eqs. (6-22) and (6-24) lead to the **Navier-Stokes equations,** whose three Cartesian components are

$$\rho\left(\frac{\partial v_x}{\partial t} + v_x\frac{\partial v_x}{\partial x} + v_y\frac{\partial v_x}{\partial y} + v_z\frac{\partial v_x}{\partial z}\right) = -\frac{\partial p}{\partial x} + \mu\left(\frac{\partial^2 v_x}{\partial x^2} + \frac{\partial^2 v_x}{\partial y^2} + \frac{\partial^2 v_x}{\partial z^2}\right) + \rho g_x \tag{6-25}$$

$$\rho\left(\frac{\partial v_y}{\partial t} + v_x\frac{\partial v_y}{\partial x} + v_y\frac{\partial v_y}{\partial y} + v_z\frac{\partial v_y}{\partial z}\right) = -\frac{\partial p}{\partial y} + \mu\left(\frac{\partial^2 v_y}{\partial x^2} + \frac{\partial^2 v_y}{\partial y^2} + \frac{\partial^2 v_y}{\partial z^2}\right) + \rho g_y \tag{6-26}$$

$$\rho\left(\frac{\partial v_z}{\partial t} + v_x\frac{\partial v_z}{\partial x} + v_y\frac{\partial v_z}{\partial y} + v_z\frac{\partial v_z}{\partial z}\right) = -\frac{\partial p}{\partial z} + \mu\left(\frac{\partial^2 v_z}{\partial x^2} + \frac{\partial^2 v_z}{\partial y^2} + \frac{\partial^2 v_z}{\partial z^2}\right) + \rho g_z \tag{6-27}$$

In vector notation,

$$\rho\frac{D\mathbf{v}}{Dt} = \frac{\partial \mathbf{v}}{\partial t} + (\mathbf{v}\cdot\nabla)\mathbf{v} = -\nabla p + \mu\nabla^2\mathbf{v} + \rho\mathbf{g} \tag{6-28}$$

The pressure and gravity terms may be combined by replacing the pressure p by the equivalent pressure $P = p + \rho gz$. The left-hand side terms of the Navier-Stokes equations are the **inertial terms,** while the terms including viscosity μ are the **viscous terms.** Limiting cases under which the Navier-Stokes equations may be simplified include **creeping flows** in which the inertial terms are neglected, **potential flows** (inviscid or irrotational flows) in which the viscous terms are neglected, and **boundary layer** and **lubrication** flows in which certain terms are neglected based on scaling arguments. Creeping flows are described by Happel and Brenner (*Low Reynolds Number Hydrodynamics,* Prentice-Hall, Englewood Cliffs, N.J., 1965); potential flows by Lamb (*Hydrodynamics,* 6th ed., Dover, New York, 1945) and Milne-Thompson (*Theoretical Hydrodynamics,* 5th ed., Macmillan, New York, 1968); boundary layer theory by Schlichting (*Boundary Layer Theory,* 8th ed., McGraw-Hill, New York, 1987), and lubrication theory by Batchelor (*An Introduction to Fluid Dynamics,* Cambridge University, Cambridge, 1967) and Denn (*Process Fluid Mechanics,* Prentice-Hall, Englewood Cliffs, N.J., 1980).

Because the Navier-Stokes equations are first-order in pressure and second-order in velocity, their solution requires one pressure boundary condition and two velocity boundary conditions (for each velocity component) to completely specify the solution. The **no slip** condition, which requires that the fluid velocity equal the velocity of any bounding solid surface, occurs in most problems. Specification of velocity is a type of boundary condition sometimes called a *Dirichlet condition.* Often boundary conditions involve stresses, and thus velocity gradients, rather than the velocities themselves. Specification of velocity derivatives is a *Neumann boundary condition.* For example, at the boundary between a viscous liquid and a gas, it is often assumed that the liquid shear stresses are zero. In numerical solution of the Navier-Stokes equations, Dirichlet and Neumann, or **essential** and **natural,** boundary conditions may be satisfied by different means.

Fluid statics, discussed in Sec. 10 of the *Handbook* in reference to pressure measurement, is the branch of fluid mechanics in which the fluid velocity is either zero or is uniform and constant relative to an inertial reference frame. With velocity gradients equal to zero, the momentum equation reduces to a simple expression for the pressure field, $\nabla p = \rho\mathbf{g}$. Letting z be directed vertically upward, so that $g_z = -g$ where g is the gravitational acceleration (9.806 m²/s), the pressure field is given by

$$dp/dz = -\rho g \tag{6-29}$$

This equation applies to any incompressible or compressible static fluid. For an incompressible liquid, pressure varies linearly with depth. For compressible gases, p is obtained by integration accounting for the variation of ρ with z.

The **force exerted on a submerged planar surface** of area A is given by $F = p_c A$ where p_c is the pressure at the geometrical **centroid** of the surface. The **center of pressure,** the point of application of the net force, is always lower than the centroid. For details see, for example, Shames, where may also be found discussion of forces on **curved surfaces, buoyancy,** and **stability of floating bodies.**

Examples Four examples follow, illustrating the application of the conservation equations to obtain useful information about fluid flows.

Example 1: Force Exerted on a Reducing Bend An incompressible fluid flows through a reducing elbow (Fig. 6-5) situated in a horizontal plane. The inlet velocity V_1 is given and the pressures p_1 and p_2 are measured. Selecting the inlet and outlet surfaces 1 and 2 as shown, the continuity equation Eq. (6-9) can be used to find the exit velocity $V_2 = V_1A_1/A_2$. The mass flow rate is obtained by $\dot{m} = \rho V_1 A_1$.

Assume that the velocity profile is nearly uniform so that β is approximately unity. The force exerted on the fluid by the bend has x and y components; these can be found from Eq. (6-11). The x component gives

$$F_x = \dot{m}(V_{2x} - V_{1x}) + p_1A_{1x} + p_2A_{2x}$$

while the y component gives

$$F_y = \dot{m}(V_{2y} - V_{1y}) + p_1A_{1y} + p_2A_{2y}$$

The velocity components are $V_{1x} = V_1$, $V_{1y} = 0$, $V_{2x} = V_2\cos\theta$, and $V_{2y} = V_2\sin\theta$. The area vector components are $A_{1x} = -A_1$, $A_{1y} = 0$, $A_{2x} = A_2\cos\theta$, and $A_{2y} = A_2\sin\theta$. Therefore, the force components may be calculated from

$$F_x = \dot{m}(V_2\cos\theta - V_1) - p_1A_1 + p_2A_2\cos\theta$$

$$F_y = \dot{m}V_2\sin\theta + p_2A_2\sin\theta$$

The force acting on the fluid is **F;** the equal and opposite force exerted by the fluid on the bend is **−F.**

Example 2: Simplified Ejector Figure 6-6 shows a very simplified sketch of an ejector, a device that uses a high velocity primary fluid to pump another (secondary) fluid. The continuity and momentum equations may be

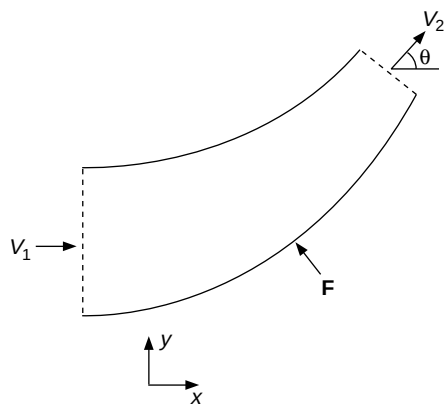

FIG. 6-5 Force at a reducing bend. **F** is the force exerted by the bend on the fluid. The force exerted by the fluid on the bend is **−F.**

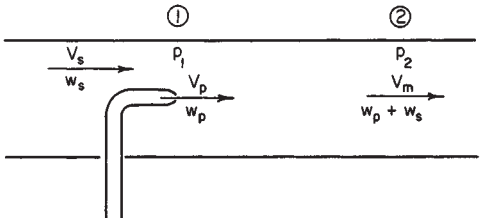

FIG. 6-6 Draft-tube ejector.

applied on the control volume with inlet and outlet surfaces 1 and 2 as indicated in the figure. The cross-sectional area is uniform, $A_1 = A_2 = A$. Let the mass flow rates and velocities of the primary and secondary fluids be $\dot{m}_p$, $\dot{m}_s$, V_p and V_s. Assume for simplicity that the density is uniform. Conservation of mass gives $\dot{m}_2 = \dot{m}_p + \dot{m}_s$. The exit velocity is $V_2 = \dot{m}_2/(\rho A)$. The principle momentum exchange in the ejector occurs between the two fluids. Relative to this exchange, the force exerted by the walls of the device are found to be small. Therefore, the force term F is neglected from the momentum equation. Written in the flow direction, assuming uniform velocity profiles, and using the extension of Eq. (6-11) for multiple inlets, it gives the pressure rise developed by the device:

$$(p_2 - p_1)A = (\dot{m}_p + \dot{m}_s)V_2 - \dot{m}_p V_p - \dot{m}_s V_s$$

Application of the momentum equation to ejectors of other types is discussed in Lapple (*Fluid and Particle Dynamics,* University of Delaware, Newark, 1951) and in Sec. 10 of the *Handbook.*

Example 3: Venturi Flowmeter An incompressible fluid flows through the venturi flowmeter in Fig. 6-7. An equation is needed to relate the flow rate Q to the pressure drop measured by the manometer. This problem can be solved using the mechanical energy balance. In a well-made venturi, viscous losses are negligible, the pressure drop is entirely the result of acceleration into the throat, and the flow rate predicted neglecting losses is quite accurate. The inlet area is A and the throat area is a.

With control surfaces at 1 and 2 as shown in the figure, Eq. (6-17) in the absence of losses and shaft work gives

$$\frac{p_1}{\rho} + \frac{V_1^2}{2} = \frac{p_2}{\rho} + \frac{V_2^2}{2}$$

The continuity equation gives $V_2 = V_1 A/a$, and $V_1 = Q/A$. The pressure drop measured by the manometer is $p_1 - p_2 = (\rho_m - \rho)g\Delta z$. Substituting these relations into the energy balance and rearranging, the desired expression for the flow rate is found.

$$Q = \frac{1}{A}\sqrt{\frac{2(\rho_m - \rho)g\Delta z}{\rho[(A/a)^2 - 1]}}$$

Example 4: Plane Poiseuille Flow An incompressible Newtonian fluid flows at a steady rate in the x direction between two very large flat plates, as shown in Fig. 6-8. The flow is laminar. The velocity profile is to be found. This example is found in most fluid mechanics textbooks; the solution presented here closely follows Denn.

This problem requires use of the microscopic balance equations because the velocity is to be determined as a function of position. The boundary conditions for this flow result from the no-slip condition. All three velocity components must be zero at the plate surfaces, $y = H/2$ and $y = -H/2$.

Assume that the flow is **fully developed,** that is, all velocity derivatives vanish in the x direction. Since the flow field is infinite in the z direction, all velocity derivatives should be zero in the z direction. Therefore, velocity components are a function of y alone. It is also assumed that there is no flow in the z direction, so $v_z = 0$. The continuity equation Eq. (6-21), with $v_z = 0$ and $\partial v_x/\partial x = 0$, reduces to

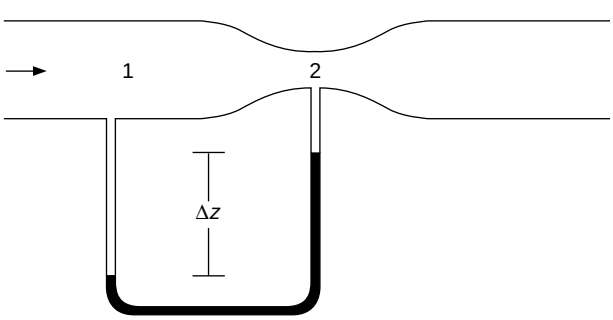

FIG. 6-7 Venturi flowmeter.

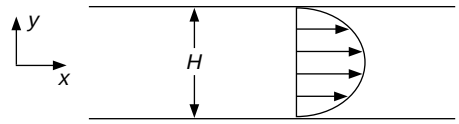

FIG. 6-8 Plane Poiseuille flow.

$$\frac{dv_y}{dy} = 0.$$

Since $v_y = 0$ at $y = \pm H/2$, the continuity equation integrates to $v_y = 0$. This is a direct result of the assumption of fully developed flow.

The Navier-Stokes equations are greatly simplified when it is noted that $v_y = v_z = 0$ and $\partial v_x/\partial x = \partial v_x/\partial z = \partial v_x/\partial t = 0$. The three components are written in terms of the equivalent pressure P:

$$0 = -\frac{\partial P}{\partial x} + \mu\frac{\partial^2 v_x}{\partial y^2}$$

$$0 = -\frac{\partial P}{\partial y}$$

$$0 = -\frac{\partial P}{\partial z}$$

The latter two equations require that P is a function only of x, and therefore $\partial P/\partial x = dP/dx$. Inspection of the first equation shows one term which is a function only of x and one which is only a function of y. This requires that both terms are constant. The pressure gradient $-dP/dx$ is constant. The x-component equation becomes

$$\frac{d^2 v_x}{dy^2} = \frac{1}{\mu}\frac{dP}{dx}$$

Two integrations of the x-component equation give

$$v_x = \frac{1}{2\mu}\frac{dP}{dx}y^2 + C_1 y + C_2$$

where the constants of integration C_1 and C_2 are evaluated from the boundary conditions $v_x = 0$ at $y = \pm H/2$. The result is

$$v_x = \frac{H^2}{8\mu}\left(-\frac{dP}{dx}\right)\left[1 - \left(\frac{2y}{H}\right)^2\right]$$

This is a **parabolic** velocity distribution. The average velocity $V = (1/H)\int_{-H/2}^{H/2} v_x\,dy$ is

$$V = \frac{H^2}{12\mu}\left(-\frac{dP}{dx}\right)$$

This flow is one-dimensional, as there is only one nonzero velocity component, v_x, which, along with the pressure, varies in only one coordinate direction.

INCOMPRESSIBLE FLOW IN PIPES AND CHANNELS

Mechanical Energy Balance The mechanical energy balance, Eq. (6-16), for **fully developed** incompressible flow in a straight circular pipe of constant diameter D reduces to

$$\frac{p_1}{\rho} + gz_1 = \frac{p_2}{\rho} + gz_2 + l_v \qquad (6\text{-}30)$$

In terms of the equivalent pressure, $P \equiv p + \rho gz$,

$$P_1 - P_2 = \rho l_v \qquad (6\text{-}31)$$

The pressure drop due to frictional losses l_v is proportional to pipe length L for fully developed flow and may be denoted as the (positive) quantity $\Delta P \equiv P_1 - P_2$.

Friction Factor and Reynolds Number For a Newtonian fluid in a smooth pipe, dimensional analysis relates the frictional pressure drop per unit length $\Delta P/L$ to the pipe diameter D, density ρ, and average velocity V through two dimensionless groups, the **Fanning friction factor** f and the **Reynolds number** Re.

$$f \equiv \frac{D\Delta P}{2\rho V^2 L} \tag{6-32}$$

$$\mathrm{Re} \equiv \frac{DV\rho}{\mu} \tag{6-33}$$

For smooth pipe, the friction factor is a function only of the Reynolds number. In rough pipe, the relative roughness ϵ/D also affects the friction factor. Figure 6-9 plots f as a function of Re and ϵ/D. Values of ϵ for various materials are given in Table 6-1. The Fanning friction factor should not be confused with the Darcy friction factor used by Moody (*Trans. ASME,* **66,** 671 [1944]), which is four times greater. Using the momentum equation, the stress at the wall of the pipe may be expressed in terms of the friction factor:

$$\tau_w = f\,\frac{\rho V^2}{2} \tag{6-34}$$

Laminar and Turbulent Flow Below a **critical Reynolds number** of about 2,100, the flow is laminar; over the range $2{,}100 < \mathrm{Re} < 5{,}000$ there is a transition to turbulent flow. For laminar flow, the Hagen-Poiseuille equation

$$f = \frac{16}{\mathrm{Re}}, \qquad \mathrm{Re} \le 2{,}100 \tag{6-35}$$

may be derived from the Navier-Stokes equation and is in excellent agreement with experimental data. It may be rewritten in terms of volumetric flow rate, $Q = V\pi D^2/4$, as

$$Q = \frac{\pi \Delta P D^4}{128 \mu L}, \qquad \mathrm{Re} \le 2{,}100 \tag{6-36}$$

TABLE 6-1 Values of Surface Roughness for Various Materials*

Material	Surface roughness ε, mm
Drawn tubing (brass, lead, glass, and the like)	0.00152
Commercial steel or wrought iron	0.0457
Asphalted cast iron	0.122
Galvanized iron	0.152
Cast iron	0.259
Wood stove	0.183–0.914
Concrete	0.305–3.05
Riveted steel	0.914–9.14

* From Moody, *Trans. Am. Soc. Mech. Eng.,* **66,** 671–684 (1944); *Mech. Eng.,* **69,** 1005–1006 (1947). Additional values of ε for various types or conditions of concrete wrought-iron, welded steel, riveted steel, and corrugated-metal pipes are given in Brater and King, *Handbook of Hydraulics,* 6th ed., McGraw-Hill, New York, 1976, pp. 6-12–6-13. To convert millimeters to feet, multiply by 3.281×10^{-3}.

For turbulent flow in smooth tubes, the Blasius equation gives the friction factor accurately for a wide range of Reynolds numbers.

$$f = \frac{0.079}{\mathrm{Re}^{0.25}}, \qquad 4{,}000 < \mathrm{Re} < 10^5 \tag{6-37}$$

The Colebrook formula (Colebrook, *J. Inst. Civ. Eng.* [*London*], **11,** 133–156 [1938–39]) gives a good approximation for the f-Re-(ϵ/D) data for rough pipes over the entire turbulent flow range:

$$\frac{1}{\sqrt{f}} = -4 \log\left[\frac{\epsilon}{3.7D} + \frac{1.256}{\mathrm{Re}\sqrt{f}}\right] \qquad \mathrm{Re} > 4{,}000 \tag{6-38}$$

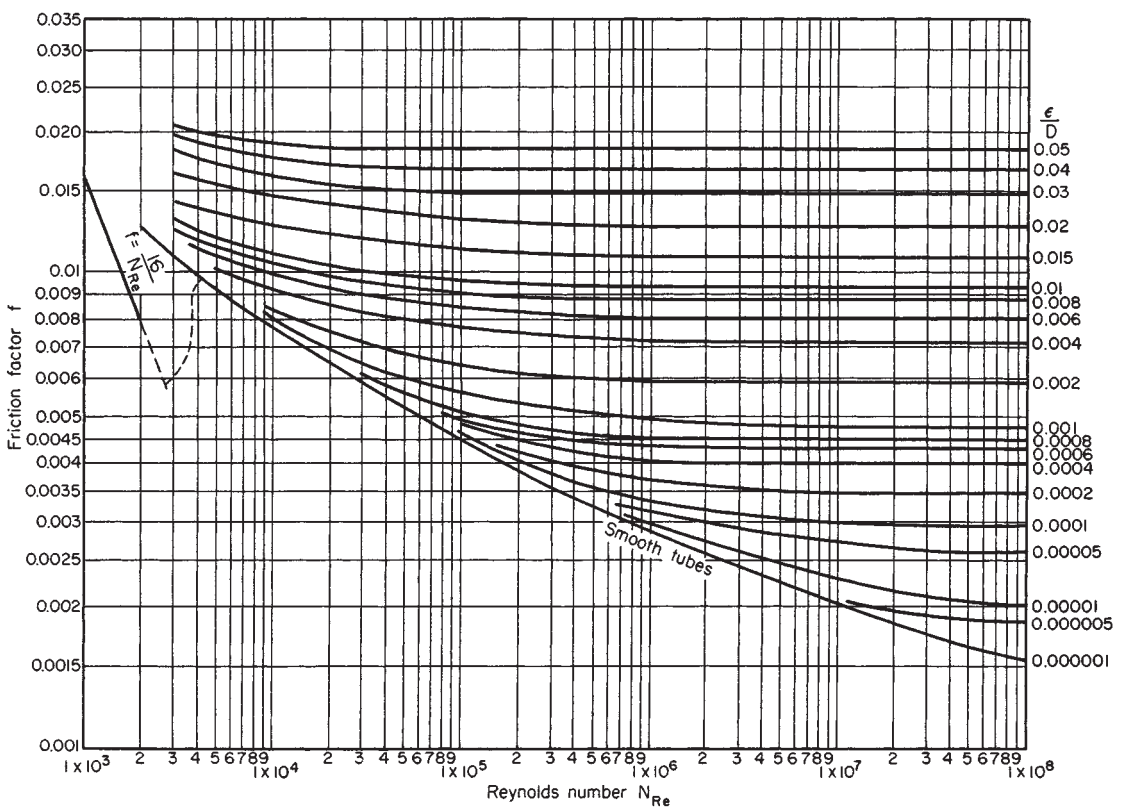

FIG. 6-9 Fanning Friction Factors. Reynolds number $\mathrm{Re} = DV\rho/\mu$, where D = pipe diameter, V = velocity, ρ = fluid density, and μ = fluid viscosity. (*Based on Moody,* Trans. ASME, ***66,*** *671 [1944].*)

An equation by Churchill (*Chem. Eng.*, **84**[24], 91–92 [Nov. 7, 1977]) for both smooth and rough tubes offers the advantage of being explicit in f:

$$\frac{1}{\sqrt{f}} = -4 \log \left[\frac{0.27\epsilon}{D} + (7/\mathrm{Re})^{0.9} \right] \qquad \mathrm{Re} > 4{,}000 \qquad (6\text{-}39)$$

In laminar flow, f is independent of ϵ/D. In turbulent flow, the friction factor for rough pipe follows the smooth tube curve for a range of Reynolds numbers (hydraulically smooth flow). For greater Reynolds numbers, f deviates from the smooth pipe curve, eventually becoming independent of Re. This region, often called *complete turbulence*, is frequently encountered in commercial pipe flows. The Reynolds number above which f becomes essentially independent of Re is (Davies, *Turbulence Phenomena*, Academic, New York, 1972, p. 37)

$$\mathrm{Re} = \frac{20[3.2 - 2.46 \ln (\epsilon/D)]}{(\epsilon/D)} \qquad (6\text{-}40)$$

Roughness may also affect the transition from laminar to turbulent flow (Schlichting).

Common pipe flow problems include calculation of pressure drop given the flow rate (or velocity) and calculation of flow rate (or velocity) given pressure drop. When flow rate is given, the Reynolds number is first calculated to determine the flow regime, so that the appropriate relations between f and Re (or pressure drop and velocity or flow rate) are used. When pressure drop is given and the velocity is unknown, the Reynolds number and flow regime cannot be immediately determined. It is necessary to assume the flow regime and then verify by checking Re afterward. With experience, the initial guess for the flow regime will usually prove correct. When solving Eq. (6-38) for velocity when pressure drop is given, it is useful to note that the right-hand side is independent of velocity since $\mathrm{Re}\sqrt{f} = (D^{3/2}/\mu)\sqrt{\rho \Delta P/(2L)}$.

As Fig. 6-9 suggests, the friction factor is uncertain in the transition range $2{,}100 < \mathrm{Re} < 4{,}000$ and a conservative choice should be made for design purposes.

Velocity Profiles In laminar flow, the solution of the Navier-Stokes equation, corresponding to the Hagen-Poiseuille equation, gives the velocity v as a function of radial position r in a circular pipe of radius R in terms of the average velocity $V = Q/A$. The **parabolic** profile, with centerline velocity twice the average velocity, is shown in Fig. 6-10.

$$v = 2V\left(1 - \frac{r^2}{R^2}\right) \qquad (6\text{-}41)$$

In turbulent flow, the velocity profile is much more blunt, with most of the velocity gradient being in a region near the wall, described by a **universal** velocity profile. It is characterized by a **viscous sublayer,** a **turbulent core,** and a **buffer zone** in between.

Viscous sublayer

$$u_+ = y_+ \qquad \text{for} \qquad y_+ < 5 \qquad (6\text{-}42)$$

Buffer zone

$$u_+ = 5.00 \ln y_+ - 3.05 \qquad \text{for} \qquad 5 < y_+ < 30 \qquad (6\text{-}43)$$

Turbulent core

$$u_+ = 2.5 \ln y_+ + 5.5 \qquad \text{for} \qquad y_+ > 30 \qquad (6\text{-}44)$$

Here, $u_+ = v/u_*$ is the dimensionless, time-averaged axial velocity, $u_* = \sqrt{\tau_w/\rho}$ is the **friction velocity** and $\tau_w = f\rho V^2/2$ is the wall stress. The friction velocity is of the order of the root mean square velocity fluctuation perpendicular to the wall in the turbulent core. The dimensionless distance from the wall is $y_+ = yu_*\rho/\mu$. The universal velocity profile is valid in the wall region for any cross-sectional channel shape. For incompressible flow in constant diameter circular pipes, $\tau_w = \Delta P/4L$ where ΔP is the pressure drop in length L. In circular pipes, Eq. (6-44) gives a surprisingly good fit to experimental results over the entire cross section of the pipe, even though it is based on assumptions which are valid only near the pipe wall.

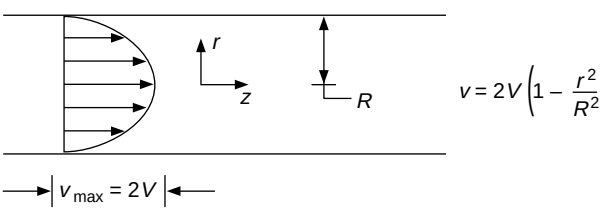

FIG. 6-10 Parabolic velocity profile for laminar flow in a pipe, with average velocity V.

For rough pipes, the velocity profile in the turbulent core is given by

$$u_+ = 2.5 \ln y/\epsilon + 8.5 \qquad \text{for} \qquad y_+ > 30 \qquad (6\text{-}45)$$

when the dimensionless roughness $\epsilon_+ = \epsilon u_* \rho/\mu$ is greater than 5 to 10; for smaller ϵ_+, the velocity profile in the turbulent core is unaffected by roughness.

For velocity profiles in the transition region, see Patel and Head (*J. Fluid Mech.*, **38,** part 1, 181–201 [1969]) where profiles over the range $1{,}500 < \mathrm{Re} < 10{,}000$ are reported.

Entrance and Exit Effects In the entrance region of a pipe, some distance is required for the flow to adjust from upstream conditions to the fully developed flow pattern. This distance depends on the Reynolds number and on the flow conditions upstream. For a uniform velocity profile at the pipe entrance, the computed length in laminar flow required for the centerline velocity to reach 99 percent of its fully developed value is (Dombrowski, Foumeny, Ookawara and Riza, *Can. J. Chem. Engr.*, **71,** 472–476 [1993])

$$L_{\mathrm{ent}}/D = 0.370 \exp(-0.148\mathrm{Re}) + 0.0550\mathrm{Re} + 0.260 \qquad (6\text{-}46)$$

In turbulent flow, the entrance length is about

$$L_{\mathrm{ent}}/D = 40 \qquad (6\text{-}47)$$

The frictional losses in the entrance region are larger than those for the same length of fully developed flow. (See the subsection, "Frictional Losses in Pipeline Elements," following.) At the pipe exit, the velocity profile also undergoes rearrangement, but the exit length is much shorter than the entrance length. At low Re, it is about one pipe radius. At $\mathrm{Re} > 100$, the exit length is essentially 0.

Residence Time Distribution For laminar Newtonian pipe flow, the cumulative residence time distribution $F(\theta)$ is given by

$$F(\theta) = 0 \qquad \text{for} \qquad \theta < \frac{\theta_{\mathrm{avg}}}{2}$$

$$F(\theta) = 1 - \frac{1}{4}\left(\frac{\theta_{\mathrm{avg}}}{\theta}\right)^2 \qquad \text{for} \qquad \theta \geq \frac{\theta_{\mathrm{avg}}}{2} \qquad (6\text{-}48)$$

where $F(\theta)$ is the fraction of material which resides in the pipe for less than time θ and θ_{avg} is the average residence time, $\theta = V/L$.

The residence time distribution in long transfer lines may be made narrower (more uniform) with the use of **flow inverters** or **static mixing elements.** These devices exchange fluid between the wall and central regions. Variations on the concept may be used to provide effective mixing of the fluid. See Godfrey ("Static Mixers," in Harnby, Edwards, and Nienow, *Mixing in the Process Industries*, 2d ed., Butterworth Heinemann, Oxford, 1992); Gretta and Smith (*Trans. ASME J. Fluids Eng.*, **115,** 255–263 [1993]); Kemblowski and Pustelnik (*Chem. Eng. Sci.*, **43,** 473–478 [1988]).

A theoretically derived equation for flow in helical pipe coils by Ruthven (*Chem. Eng. Sci.*, **26,** 1113–1121 [1971]; **33,** 628–629 [1978]) is given by

$$F(\theta) = 1 - \left(\frac{1}{4}\right)\left[\frac{\theta_{\mathrm{avg}}}{\theta}\right]^{2.81} \qquad \text{for} \qquad 0.5 < \frac{\theta_{\mathrm{avg}}}{\theta} < 1.63 \qquad (6\text{-}49)$$

and was substantially confirmed by Trivedi and Vasudeva (*Chem. Eng. Sci.*, **29,** 2291–2295 [1974]) for $0.6 < \mathrm{De} < 6$ and $0.0036 < D/D_c < 0.097$ where $\mathrm{De} = \mathrm{Re}\sqrt{D/D_c}$ is the Dean number and D_c is the diameter of curvature of the coil. Measurements by Saxena and Nigam (*Chem. Eng. Sci.*, **34,** 425–426 [1979]) indicate that such a distribution will hold for $\mathrm{De} > 1$. The residence time distribution for helical coils is narrower than for straight circular pipes, due to the secondary flow which exchanges fluid between the wall and center regions.

In turbulent flow, axial mixing is usually described in terms of turbulent diffusion or dispersion coefficients, from which cumulative residence time distribution functions can be computed. Davies (*Turbulence Phenomena,* Academic, New York, 1972, p. 93), gives $D_L = 1.01 v \mathrm{Re}^{0.875}$ for the longitudinal dispersion coefficient. Levenspiel (*Chemical Reaction Engineering,* 2d ed., Wiley, New York, 1972, pp. 253–278) discusses the relations among various residence time distribution functions, and the relation between dispersion coefficient and residence time distribution.

Noncircular Channels Calculation of frictional pressure drop in noncircular channels depends on whether the flow is laminar or turbulent, and on whether the channel is full or open. For **turbulent flow** in **ducts running full,** the **hydraulic diameter** D_H should be substituted for D in the friction factor and Reynolds number definitions, Eqs. (6-32) and (6-33). The hydraulic diameter is defined as **four times the channel cross-sectional area divided by the wetted perimeter.** For example, the hydraulic diameter for a circular pipe is $D_H = D$, for an annulus of inner diameter d and outer diameter D, $D_H = D - d$, for a rectangular duct of sides a, b, $D_H = ab/[2(a+b)]$. The **hydraulic radius** R_H is defined as **one-fourth** of the hydraulic diameter.

With the hydraulic diameter subsitituted for D in f and Re, Eqs. (6-37) through (6-40) are good approximations. Note that V appearing in f and Re is the actual average velocity $V = Q/A$; for noncircular pipes; it is **not** $Q/(\pi D_H^2/4)$. The pressure drop should be calculated from the friction factor for noncircular pipes. Equations relating Q to ΔP and D for circular pipes **may not be used** for noncircular pipes with D replaced by D_H because $V \neq Q/(\pi D_H^2/4)$.

Turbulent flow in noncircular channels is generally accompanied by secondary flows perpendicular to the axial flow direction (Schlichting). These flows may cause the pressure drop to be slightly greater than that computed using the hydraulic diameter method. For data on pressure drop in annuli, see Brighton and Jones (*J. Basic Eng.,* **86,** 835–842 [1964]); Okiishi and Serovy (*J. Basic Eng.,* **89,** 823–836 [1967]); and Lawn and Elliot (*J. Mech. Eng. Sci.,* **14,** 195–204 [1972]). For rectangular ducts of large aspect ratio, Dean (*J. Fluids Eng.,* **100,** 215–233 [1978]) found that the numerator of the exponent in the Blasius equation (6-37) should be increased to 0.0868. Jones (*J. Fluids Eng.,* **98,** 173–181 [1976]) presents a method to improve the estimation of friction factors for rectangular ducts using a modification of the hydraulic diameter–based Reynolds number.

The hydraulic diameter method does not work well for **laminar flow** because the shape affects the flow resistance in a way that cannot be expressed as a function only of the ratio of cross-sectional area to wetted perimeter. For some shapes, the Navier-Stokes equations have been integrated to yield relations between flow rate and pressure drop. These relations may be expressed in terms of **equivalent diameters** D_E defined to make the relations reduce to the second form of the Hagen-Poiseulle equation, Eq. (6-36); that is, $D_E \equiv (128 Q\mu L/\pi\Delta P)^{1/4}$. **Equivalent diameters are not the same as hydraulic diameters.** Equivalent diameters yield the correct relation between flow rate and pressure drop when substituted into Eq. (6-36), but not Eq. (6-35) because $V \neq Q/(\pi D_E/4)$. Equivalent diameter D_E is not to be used in the friction factor and Reynolds number; $f \neq 16/\mathrm{Re}$ using the equivalent diameters defined in the following. This situation is, by arbitrary definition, opposite to that for the hydraulic diameter D_H used for turbulent flow.

Ellipse, semiaxes a and b (Lamb, *Hydrodynamics,* 6th ed., Dover, New York, 1945, p. 587):

$$D_E = \left(\frac{32a^3b^3}{a^2+b^2}\right)^{1/4} \tag{6-50}$$

Rectangle, width a, height b (Owen, *Trans. Am. Soc. Civ. Eng.,* **119,** 1157–1175 [1954]):

$$D_E = \left(\frac{128ab^3}{\pi K}\right)^{1/4} \tag{6-51}$$

$a/b =$	1	1.5	2	3	4	5	10	∞
$K =$	28.45	20.43	17.49	15.19	14.24	13.73	12.81	12

Annulus, inner diameter D_1 outer diameter D_2 (Lamb, op. cit., p. 587):

$$D_E = \left\{(D_2^2 - D_1^2)\left[D_2^2 + D_1^2 - \frac{D_2^2 - D_1^2}{\ln(D_2/D_1)}\right]\right\}^{1/4} \tag{6-52}$$

For isosceles triangles and regular polygons, see Sparrow (*AIChE J.,* **8,** 599–605 [1962]), Carlson and Irvine (*J. Heat Transfer,* **83,** 441–444 [1961]), Cheng (*Proc. Third Int. Heat Transfer Conf.,* New York, **1,** 64–76 [1966]), and Shih (*Can. J. Chem. Eng.,* **45,** 285–294 [1967]).

The critical Reynolds number for **transition from laminar to turbulent flow** in noncircular channels varies with channel shape. In rectangular ducts, $1{,}900 < \mathrm{Re}_c < 2{,}800$ (Hanks and Ruo, *Ind. Eng. Chem. Fundam.,* **5,** 558–561 [1966]). In triangular ducts, $1{,}600 < \mathrm{Re}_c < 1{,}800$ (Cope and Hanks, *Ind. Eng. Chem. Fundam.,* **11,** 106–117 [1972]; Bandopadhayay and Hinwood, *J. Fluid Mech.,* **59,** 775–783 [1973]).

Nonisothermal Flow For nonisothermal flow of **liquids,** the friction factor may be increased if the liquid is being cooled or decreased if the liquid is being heated, because of the effect of temperature on viscosity near the wall. In shell and tube heat-exchanger design, the recommended practice is to first estimate f using the bulk mean liquid temperature over the tube length. Then, in laminar flow, the result is divided by $(\mu_a/\mu_w)^{0.23}$ in the case of cooling or $(\mu_a/\mu_w)^{0.38}$ in the case of heating. For turbulent flow, f is divided by $(\mu_a/\mu_w)^{0.11}$ in the case of cooling or $(\mu_a/\mu_w)^{0.17}$ in case of heating. Here, μ_a is the viscosity at the average bulk temperature and μ_w is the viscosity at the average wall temperature (Seider and Tate, *Ind. Eng. Chem.,* **28,** 1429–1435 [1936]). In the case of rough commercial pipes, rather than heat-exchanger tubing, it is common for flow to be in the "complete" turbulence regime where f is independent of Re. In such cases, the friction factor should not be corrected for wall temperature. If the liquid density varies with temperature, the average bulk density should be used to calculate the pressure drop from the friction factor. In addition, a (usually small) correction may be applied for acceleration effects by adding the term $G^2[(1/\rho_2) - (1/\rho_1)]$ from the mechanical energy balance to the pressure drop $\Delta P = P_1 - P_2$, where G is the mass velocity. This acceleration results from small compressibility effects associated with temperature-dependent density. Christiansen and Gordon (*AIChE J.,* **15,** 504–507 [1969]) present equations and charts for frictional loss in laminar nonisothermal flow of Newtonian and non-Newtonian liquids heated or cooled with constant wall temperature.

Frictional dissipation of mechanical energy can result in significant heating of fluids, particularly for very viscous liquids in small channels. Under adiabatic conditions, the bulk liquid temperature rise is given by $\Delta T = \Delta P/C_v\rho$ for incompressible flow through a channel of constant cross-sectional area. For flow of polymers, this amounts to about 4°C per 10 MPa pressure drop, while for hydrocarbon liquids it is about 6°C per 10 MPa. The temperature rise in laminar flow is highly nonuniform, being concentrated near the pipe wall where most of the dissipation occurs. This may result in significant viscosity reduction near the wall, and greatly increased flow or reduced pressure drop, and a flattened velocity profile. Compensation should generally be made for the heat effect when ΔP exceeds 1.4 MPa (203 psi) for adiabatic walls or 3.5 MPa (508 psi) for isothermal walls (Gerard, Steidler, and Appeldoorn, *Ind. Eng. Chem. Fundam.,* **4,** 332–339 [1969]).

Open Channel Flow For flow in **open channels,** the data are largely based on experiments with water in turbulent flow, in channels of sufficient roughness that there is no Reynolds number effect. The hydraulic radius approach may be used to estimate a friction factor with which to compute friction losses. Under conditions of **uniform flow** where liquid depth and cross-sectional area do not vary significantly with position in the flow direction, there is a balance between gravitational forces and wall stress, or equivalently between frictional losses and potential energy change. The mechanical energy balance reduces to $l_v = g(z_1 - z_2)$. In terms of the friction factor and hydraulic diameter or hydraulic radius,

$$l_v = \frac{2fV^2L}{D_H} = \frac{fV^2L}{2R_H} = g(z_1 - z_2) \tag{6-53}$$

The hydraulic radius is the cross-sectional area divided by the wetted perimeter, where the wetted perimeter *does not include the free sur-*

face. Letting $S = \sin\theta$ = channel slope (elevation loss per unit length of channel, θ = angle between channel and horizontal), Eq. (6-53) reduces to

$$V = \sqrt{\frac{2gSR_H}{f}} \tag{6-54}$$

The most often used friction correlation for open channel flows is due to Manning (*Trans. Inst. Civ. Engrs. Ireland,* **20,** 161 [1891]) and is equivalent to

$$f = \frac{29n^2}{R_H^{1/3}} \tag{6-55}$$

where n is the channel roughness, with dimensions of $(\text{length})^{1/6}$. Table 6-2 gives roughness values for several channel types.

For gradual changes in channel cross section and liquid depth, and for slopes less than 10°, the momentum equation for a rectangular channel of width b and liquid depth h may be written as a differential equation in the flow direction x.

$$\frac{dh}{dx}(1 - \text{Fr}) - \text{Fr}\left(\frac{h}{b}\right)\frac{db}{dx} = S - \frac{fV^2(b + 2h)}{2gbh} \tag{6-56}$$

For a given fixed flow rate $Q = Vbh$, and channel width profile $b(x)$, Eq. (6-56) may be integrated to determine the liquid depth profile $h(x)$. The dimensionless Froude number is $\text{Fr} = V^2/gh$. When $\text{Fr} = 1$, the flow is **critical,** when $\text{Fr} < 1$, the flow is **subcritical,** and when $\text{Fr} > 1$, the flow is **supercritical.** Surface disturbances move at a wave velocity $c = \sqrt{gh}$; they cannot propagate upstream in supercritical flows. The **specific energy** E_{sp} is nearly constant.

$$E_{sp} = h + \frac{V^2}{2g} \tag{6-57}$$

This equation is cubic in liquid depth. Below a minimum value of E_{sp} there are no real positive roots; above the minimum value there are two positive real roots. At this minimum value of E_{sp} the flow is critical; that is, $\text{Fr} = 1$, $V = \sqrt{gh}$, and $E_{sp} = (3/2)h$. Near critical flow conditions, wave motion and sudden depth changes called **hydraulic jumps** are likely. Chow (*Open Channel Hydraulics,* McGraw-Hill, New York, 1959), discusses the numerous surface profile shapes which may exist in nonuniform open channel flows.

For flow over a sharp-crested weir of width b and height L, from a liquid depth H, the flow rate is given approximately by

$$Q = \frac{2}{3}C_d b\sqrt{2g}(H - L)^{3/2} \tag{6-58}$$

where $C_d \approx 0.6$ is a discharge coefficient. Flow through notched weirs is described under flow meters in Sec. 10 of the *Handbook.*

TABLE 6-2 Average Values of *n* for Manning Formula, Eq. (6-55)

Surface	n, $\text{m}^{1/6}$	n, $\text{ft}^{1/6}$
Cast-iron pipe, fair condition	0.014	0.011
Riveted steel pipe	0.017	0.014
Vitrified sewer pipe	0.013	0.011
Concrete pipe	0.015	0.012
Wood-stave pipe	0.012	0.010
Planed-plank flume	0.012	0.010
Semicircular metal flumes, smooth	0.013	0.011
Semicircular metal flumes, corrugated	0.028	0.023
Canals and ditches		
Earth, straight and uniform	0.023	0.019
Winding sluggish canals	0.025	0.021
Dredged earth channels	0.028	0.023
Natural-stream channels		
Clean, straight bank, full stage	0.030	0.025
Winding, some pools and shoals	0.040	0.033
Same, but with stony sections	0.055	0.045
Sluggish reaches, very deep pools, rather weedy	0.070	0.057

SOURCE: Brater and King, *Handbook of Hydraulics,* 6th ed., McGraw-Hill, New York, 1976, p. 7–22. For detailed information, see Chow, *Open-Channel Hydraulics,* McGraw-Hill, New York, 1959, pp. 110–123.

Non-Newtonian Flow For **isothermal laminar flow** of time-independent non-Newtonian liquids, integration of the Cauchy momentum equations yields the fully developed velocity profile and flow rate–pressure drop relations. For the **Bingham plastic** fluid described by Eq. (6-3), in a pipe of diameter D and a pressure drop per unit length $\Delta P/L$, the flow rate is given by

$$Q = \frac{\pi D^3 \tau_w}{32\mu_\infty}\left[1 - \frac{4\tau_y}{3\tau_w} + \frac{\tau_y^4}{3\tau_w^4}\right] \tag{6-59}$$

where the wall stress is $\tau_w = D\Delta P/(4L)$. The velocity profile consists of a central nondeforming plug of radius $r_p = 2\tau_y/(\Delta P/L)$ and an annular deforming region. The velocity profile in the annular region is given by

$$v_z = \frac{1}{\mu_\infty}\left[\frac{\Delta P}{4L}(R^2 - r^2) - \tau_y(R - r)\right], \qquad r_P \le r \le R \tag{6-60}$$

where r is the radial coordinate and R is the pipe radius. The velocity of the central, nondeforming plug is obtained by setting $r = r_P$ in Eq. (6-60). When Q is given and Eq. (6-59) is to be solved for τ_w and the pressure drop, multiple positive roots for the pressure drop may be found. The root corresponding to $\tau_w < \tau_y$ is physically unrealizable, as it corresponds to $r_p > R$ and the pressure drop is insufficient to overcome the yield stress.

For a **power law fluid,** Eq. (6-4), with constant properties K and n, the flow rate is given by

$$Q = \pi\left(\frac{\Delta P}{2KL}\right)^{1/n}\left(\frac{n}{1 + 3n}\right)R^{(1+3n)/n} \tag{6-61}$$

and the velocity profile by

$$v_z = \left(\frac{\Delta P}{2KL}\right)^{1/n}\left(\frac{n}{1 + n}\right)[R^{(1+n)/n} - r^{(1+n)/n}] \tag{6-62}$$

Similar relations for other non-Newtonian fluids may be found in Govier and Aziz and in Bird, Armstrong, and Hassager (*Dynamics of Polymeric Liquids,* vol. 1: *Fluid Mechanics,* Wiley, New York, 1977).

For steady-state laminar flow of any time-independent viscous fluid, at average velocity V in a pipe of diameter D, the Rabinowitsch-Mooney relations give a general relationship for the shear rate at the pipe wall.

$$\dot\gamma_w = \frac{8V}{D}\left(\frac{1 + 3n'}{4n'}\right) \tag{6-63}$$

where n' is the slope of a plot of $D\Delta P/(4L)$ versus $8V/D$ on logarithmic coordinates,

$$n' = \frac{d\ln[D\Delta P/(4L)]}{d\ln(8V/D)} \tag{6-64}$$

By plotting capillary viscometry data this way, they can be used directly for pressure drop design calculations, or to construct the rheogram for the fluid. For pressure drop calculation, the flow rate and diameter determine the velocity, from which $8V/D$ is calculated and $D\Delta P/(4L)$ read from the plot. For a Newtonian fluid, $n' = 1$ and the shear rate at the wall is $\dot\gamma = 8V/D$. For a power law fluid, $n' = n$. To construct a rheogram, n' is obtained from the slope of the experimental plot at a given value of $8V/D$. The shear rate at the wall is given by Eq. (6-63) and the corresponding shear stress at the wall is $\tau_w = D\Delta P/(4L)$ read from the plot. By varying the value of $8V/D$, the shear rate versus shear stress plot can be constructed.

The generalized approach of Metzner and Reed (*AIChE J.,* **1,** 434 [1955]) for time-independent non-Newtonian fluids defines a modified Reynolds number as

$$\text{Re}_{MR} \equiv \frac{D^{n'}V^{2-n'}\rho}{K'8^{n'-1}} \tag{6-65}$$

where K' satisfies

$$\frac{D\Delta P}{4L} = K'\left(\frac{8V}{D}\right)^{n'} \tag{6-66}$$

With this definition, $f = 16/\text{Re}_{MR}$ is automatically satisfied at the value of $8V/D$ where K' and n' are evaluated. Equation (6-66) may be obtained by integration of Eq. (6-64) only when n' is a constant, as, for

example, the cases of Newtonian and power law fluids. For Newtonian fluids, $K' = \mu$ and $n' = 1$; for power law fluids, $K' = K[(1 + 3n)/(4n)]^n$ and $n' = n$. For Bingham plastics, K' and n' are variable, given as a function of τ_w (Metzner, *Ind. Eng. Chem.*, **49,** 1429–1432 [1957]).

$$K = \tau_w^{1-n'}\left[\frac{\mu_\infty}{1 - 4\tau_y/3\tau_w + (\tau_y/\tau_w)^4/3}\right]^{n'} \tag{6-67}$$

$$n' = \frac{1 - 4\tau_y/(3\tau_w) + (\tau_y/\tau_w)^4/3}{1 - (\tau_y/\tau_w)^4} \tag{6-68}$$

For laminar flow of power law fluids in channels of noncircular cross section, see Schecter (*AIChE J.*, **7,** 445–448 [1961]), Wheeler and Wissler (*AIChE J.*, **11,** 207–212 [1965]), Bird, Armstrong, and Hassager (*Dynamics of Polymeric Liquids*, vol. 1: *Fluid Mechanics*, Wiley, New York, 1977), and Skelland (*Non-Newtonian Flow and Heat Transfer*, Wiley, New York, 1967).

Steady state, fully developed laminar flows of viscoelastic fluids in straight, constant-diameter pipes show no effects of viscoelasticity. The viscous component of the constitutive equation may be used to develop the flow rate–pressure drop relations, which apply downstream of the entrance region after viscoelastic effects have disappeared. A similar situation exists for time-dependent fluids.

The **transition to turbulent flow** begins at Re_{MR} in the range of 2,000 to 2,500 (Metzner and Reed, *AIChE J.*, **1,** 434 [1955]). For Bingham plastic materials, K' and n' must be evaluated for the τ_w condition in question in order to determine Re_{MR} and establish whether the flow is laminar. An alternative method for Bingham plastics is by Hanks (Hanks, *AIChE J.*, **9,** 306 [1963]; **14,** 691 [1968]; Hanks and Pratt, *Soc. Petrol. Engrs. J.*, **7,** 342 [1967]; and Govier and Aziz, pp. 213–215). The transition from laminar to turbulent flow is influenced by **viscoelastic** properties (Metzner and Park, *J. Fluid Mech.*, **20,** 291 [1964]) with the critical value of Re_{MR} increased to beyond 10,000 for some materials.

For **turbulent flow of non-Newtonian fluids,** the design chart of Dodge and Metzner (*AIChE J.*, **5,** 189 [1959]), Fig. 6-11, is most widely used. For Bingham plastic materials in turbulent flow, it is generally assumed that stresses greatly exceed the yield stress, so that the friction factor–Reynolds number relationship for Newtonian fluids applies, with μ_∞ substituted for μ. This is equivalent to setting $n' = 1$ and $\tau_y/\tau_w = 0$ in the Dodge-Metzner method, so that $Re_{MR} = DV\rho/\mu_\infty$. Wilson and Thomas (*Can. J. Chem. Eng.*, **63,** 539–546 [1985]) give friction factor equations for turbulent flow of power law fluids and Bingham plastic fluids.

Power law fluids:

$$\frac{1}{\sqrt{f}} = \frac{1}{\sqrt{f_N}} + 8.2\,\frac{1-n}{1+n} + 1.77\ln\left(\frac{1+n}{2}\right) \tag{6-69}$$

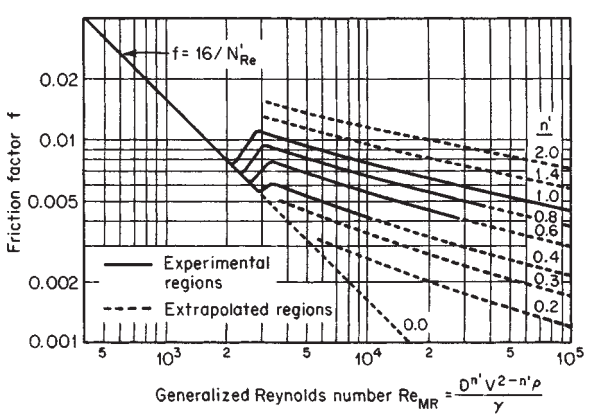

FIG. 6-11 Fanning friction factor for non-Newtonian flow. (*From Dodge and Metzner,* Am. Inst. Chem. Eng. J., **5,** *189 [1959].*)

where f_N is the friction factor for Newtonian fluid evaluated at $Re = DV\rho/\mu_{eff}$ where the effective viscosity is

$$\mu_{eff} = K\left(\frac{3n+1}{4n}\right)^{n-1}\left(\frac{8V}{D}\right)^{n-1} \tag{6-70}$$

Bingham fluids:

$$\frac{1}{\sqrt{f}} = \frac{1}{\sqrt{f_N}} + 1.77\ln\left(\frac{(1-\xi)^2}{1+\xi}\right) + \xi(10 + 0.884\xi) \tag{6-71}$$

where f_N is evaluated at $Re = DV\rho/\mu_\infty$ and $\xi = \tau_y/\tau_w$. Iteration is required to use this equation since $\tau_w = f\rho V^2/2$.

Drag reduction in turbulent flow can be achieved by adding soluble high molecular weight polymers in extremely low concentration to Newtonian liquids. The reduction in friction is generally believed to be associated with the viscoelastic nature of the solutions effective in the wall region. For a given polymer, there is a minimum molecular weight necessary to initiate drag reduction at a given flow rate, and a critical concentration above which drag reduction will not occur (Kim, Little and Ting, *J. Colloid Interface Sci.*, **47,** 530–535 [1974]). Drag reduction is reviewed by Hoyt (*J. Basic Eng.*, **94,** 258–285 [1972]); Little, et al. (*Ind. Eng. Chem. Fundam.*, **14,** 283–296 [1975]) and Virk (*AIChE J.*, **21,** 625–656 [1975]). At maximum possible drag reduction in smooth pipes,

$$\frac{1}{\sqrt{f}} = -19\log\left(\frac{50.73}{Re\sqrt{f}}\right) \tag{6-72}$$

or, approximately,

$$f = \frac{0.58}{Re^{0.58}} \tag{6-73}$$

for $4{,}000 < Re < 40{,}000$. The actual drag reduction depends on the polymer system. For further details, see Virk (ibid.).

Economic Pipe Diameter, Turbulent Flow The economic optimum pipe diameter may be computed so that the last increment of investment reduces the operating cost enough to produce the required minimum return on investment. For long cross-country pipelines, alloy pipes of appreciable length and complexity, or pipelines with control valves, detailed analyses of investment and operating costs should be made. Peters and Timmerhaus (*Plant Design and Economics for Chemical Engineers,* 4th ed., McGraw-Hill, New York, 1991) provide a detailed method for determining the economic optimum size. For pipelines of the lengths usually encountered in chemical plants and petroleum refineries, simplified selection charts are often adequate. In many cases there is an economic optimum velocity that is nearly independent of diameter, which may be used to estimate the economic diameter from the flow rate. For low-viscosity liquids in schedule 40 steel pipe, economic optimum velocity is typically in the range of 1.8 to 2.4 m/s (5.9 to 7.9 ft/s). For gases with density ranging from 0.2 to 20 kg/m^3 (0.013 to 1.25 lbm/ft^3), the economic optimum velocity is about 40 m/s to 9 m/s (131 to 30 ft/s). Charts and rough guidelines for economic optimum size do not apply to multiphase flows.

Economic Pipe Diameter, Laminar Flow Pipelines for the transport of high-viscosity liquids are seldom designed purely on the basis of economics. More often, the size is dictated by operability considerations such as available pressure drop, shear rate, or residence time distribution. Peters and Timmerhaus (ibid., Chap. 10) provide an economic pipe diameter chart for laminar flow. For non-Newtonian fluids, see Skelland (*Non-Newtonian Flow and Heat Transfer,* Chap. 7, Wiley, New York, 1967).

Vacuum Flow When gas flows under high vacuum conditions or through very small openings, the continuum hypothesis is no longer appropriate if the channel dimension is not very large compared to the mean free path of the gas. When the mean free path is comparable to the channel dimension, flow is dominated by collisions of molecules with the wall, rather than by collisions between molecules. An approximate expression based on Brown, et al. (*J. Appl. Phys.*, **17,** 802–813 [1946]) for the mean free path is

$$\lambda = \left(\frac{2\mu}{p}\right)\sqrt{\frac{8RT}{\pi M_w}} \tag{6-74}$$

The Knudsen number Kn is the ratio of the mean free path to the channel dimension. For pipe flow, $\mathrm{Kn} = \lambda/D$. **Molecular flow** is characterized by Kn > 1.0; continuum viscous (laminar or turbulent) flow is characterized by Kn < 0.01. **Transition** or **slip** flow applies over the range 0.01 < Kn < 1.0.

Vacuum flow is usually described with flow variables different from those used for normal pressures, which often leads to confusion. **Pumping speed** S is the actual volumetric flow rate of gas through a flow cross section. **Throughput** Q is the product of pumping speed and absolute pressure. In the SI system, Q has units of $\mathrm{Pa} \cdot \mathrm{m}^3/\mathrm{s}$.

$$Q = Sp \tag{6-75}$$

The mass flow rate w is related to the throughput using the ideal gas law.

$$w = \frac{M_w}{RT} Q \tag{6-76}$$

Throughput is therefore proportional to mass flow rate. For a given mass flow rate, throughput is independent of pressure. The relation between throughput and pressure drop $\Delta p = p_1 - p_2$ across a flow element is written in terms of the **conductance** C. **Resistance** is the reciprocal of conductance. Conductance has dimensions of volume per time.

$$Q = C\Delta p \tag{6-77}$$

The conductance of a series of flow elements is given by

$$\frac{1}{C} = \frac{1}{C_1} + \frac{1}{C_2} + \frac{1}{C_3} + \cdots \tag{6-78}$$

while for elements in parallel,

$$C = C_1 + C_2 + C_3 + \cdots \tag{6-79}$$

For a vacuum pump of speed S_p withdrawing from a vacuum vessel through a connecting line of conductance C, the pumping speed at the vessel is

$$S = \frac{S_p C}{S_p + C} \tag{6-80}$$

Molecular Flow Under molecular flow conditions, conductance is independent of pressure. It is proportional to $\sqrt{T/M_w}$, with the proportionality constant a function of geometry. For fully developed pipe flow,

$$C = \frac{\pi D^3}{8L} \sqrt{\frac{RT}{M_w}} \tag{6-81}$$

For an orifice of area A,

$$C = 0.40A \sqrt{\frac{RT}{M_w}} \tag{6-82}$$

Conductance equations for several other geometries are given by Ryans and Roper (*Process Vacuum System Design and Operation*, Chap. 2, McGraw-Hill, New York, 1986). For a circular annulus of outer and inner diameters D_1 and D_2 and length L, the method of Guthrie and Wakerling (*Vacuum Equipment and Techniques*, McGraw-Hill, New York, 1949) may be written

$$C = 0.42K \frac{(D_1 - D_2)^2 (D_1 + D_2)}{L} \sqrt{\frac{RT}{M_w}} \tag{6-83}$$

where K is a dimensionless constant with values given in Table 6-3.

For a short pipe of circular cross section, the conductance as calculated for an orifice from Eq. (6-82) is multiplied by a correction factor K which may be approximated as (Kennard, *Kinetic Theory of Gases*, McGraw-Hill, New York, 1938, pp. 306–308)

$$K = \frac{1}{1 + (L/D)} \qquad \text{for} \quad 0 \le L/D \le 0.75 \tag{6-84}$$

$$K = \frac{1 + 0.8(L/D)}{1 + 1.90(L/D) + 0.6(L/D)^2} \qquad \text{for} \quad L/D > 0.75 \tag{6-85}$$

For $L/D > 100$, the error in neglecting the end correction by using the fully developed pipe flow equation (6-81) is less than 2 percent. For rectangular channels, see Normand (*Ind. Eng. Chem.*, **40,** 783–787 [1948]).

Yu and Sparrow (*J. Basic Eng.*, **70,** 405–410 [1970]) give a theoretically derived chart for slot seals with or without a sheet located in or passing through the seal, giving mass flow rate as a function of the ratio of seal plate thickness to gap opening.

Slip Flow In the transition region between molecular flow and continuum viscous flow, the conductance for fully developed pipe flow is most easily obtained by the method of Brown, et al. (*J. Appl. Phys.*, **17,** 802–813 [1946]), which uses the parameter

$$X = \sqrt{\frac{8}{\pi}} \left(\frac{\lambda}{D}\right) = \left(\frac{2\mu}{p_m D}\right) \sqrt{\frac{RT}{M}} \tag{6-86}$$

where p_m is the arithmetic mean absolute pressure. A correction factor F, read from Fig. 6-12 as a function of X, is applied to the conductance for viscous flow.

$$C = F \frac{\pi D^4 p_m}{128 \mu L} \tag{6-87}$$

For slip flow through **square channels,** see Milligan and Wilkerson (*J. Eng. Ind.*, **95,** 370–372 [1973]). For slip flow through **annuli,** see Maegley and Berman (*Phys. Fluids*, **15,** 780–785 [1972]).

The **pump-down time** θ for evacuating a vessel in the absence of air in-leakage is given approximately by

$$\theta = \left(\frac{V_t}{S_0}\right) \ln \left(\frac{p_1 - p_0}{p_2 - p_0}\right) \tag{6-88}$$

where V_t = volume of vessel plus volume of piping between vessel and pump; S_0 = system speed as given by Eq. (6-80), assumed independent of pressure; p_1 = initial vessel pressure; p_2 = final vessel pressure; and p_0 = lowest pump intake pressure attainable with the pump in question. See Dushman and Lafferty (*Scientific Foundations of Vacuum Technique*, 2d ed., Wiley, New York, 1962).

The amount of inerts which has to be removed by a pumping system after the pump-down stage depends on the in-leakage of air at the various fittings, connections, and so on. Air leakage is often correlated with system volume and pressure, but this approach introduces uncer-

TABLE 6-3 Constants for Circular Annuli

D_2/D_1	K	D_2/D_1	K
0	1.00	0.707	1.254
0.259	1.072	0.866	1.430
0.500	1.154	0.966	1.675

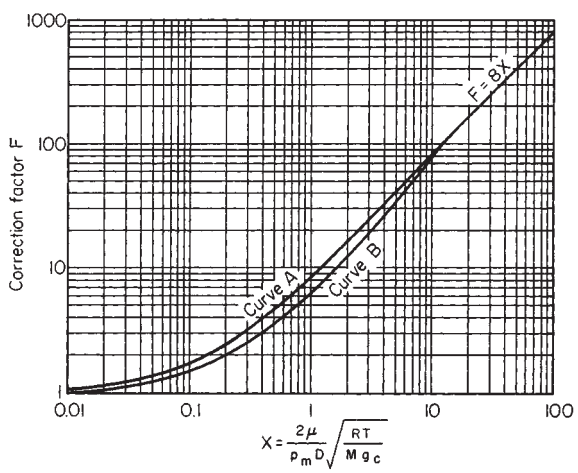

FIG. 6-12 Correction factor for Poiseuille's equation at low pressures. Curve *A:* experimental curve for glass capillaries and smooth metal tubes. (*From Brown, et al.,* J. Appl. Phys., **17,** 802 [1946].) Curve *B:* experimental curve for iron pipe (*From Riggle, Courtesy of E. I. du Pont de Nemours & Co.*)

tainty because the number and size of leaks does not necessily correlate with system volume, and leakage is sensitive to maintenance quality. Ryans and Roper (*Process Vacuum System Design and Operation,* McGraw-Hill, New York, 1986) present a thorough discussion of air leakage.

FRICTIONAL LOSSES IN PIPELINE ELEMENTS

The viscous or frictional loss term in the mechanical energy balance for most cases is obtained experimentally. For many common fittings found in piping systems, such as expansions, contractions, elbows and valves, data are available to estimate the losses. Substitution into the energy balance then allows calculation of pressure drop. A common error is to assume that pressure drop and frictional losses are equivalent. Equation (6-16) shows that in addition to frictional losses, other factors such as shaft work and velocity or elevation change influence pressure drop.

Losses l_v for incompressible flow in sections of straight pipe of constant diameter may be calculated as previously described using the Fanning friction factor:

$$l_v = \frac{\Delta P}{\rho} = \frac{2fV^2L}{D} \tag{6-89}$$

where ΔP = drop in equivalent pressure, $P = p + \rho gz$, with p = pressure, ρ = fluid density, g = acceleration of gravity, and z = elevation. Losses in the fittings of a piping network are frequently termed *minor losses* or *miscellaneous losses.* These descriptions are misleading because in process piping fitting losses are often much greater than the losses in straight piping sections.

Equivalent Length and Velocity Head Methods Two methods are in common use for estimating fitting loss. One, the **equivalent length** method, reports the losses in a piping element as the length of straight pipe which would have the same loss. For turbulent flows, the equivalent length is usually reported as a number of diameters of pipe of the same size as the fitting connection; L_e/D is given as a fixed quantity, independent of D. This approach tends to be most accurate for a single fitting size and loses accuracy with deviation from this size. For laminar flows, L_e/D correlations normally have a size dependence through a Reynolds number term.

The other method is the **velocity head** method. The term $V^2/2g$ has dimensions of length and is commonly called a *velocity head.* Application of the Bernoulli equation to the problem of frictionless discharge at velocity V through a nozzle at the bottom of a column of liquid of height H shows that $H = V^2/2g$. Thus H is the liquid head corresponding to the velocity V. Use of the velocity head to scale pressure drops has wide application in fluid mechanics. Examination of the Navier-Stokes equations suggests that when the inertial terms dominate the viscous terms, pressure gradients are expected to be proportional to ρV^2 where V is a characteristic velocity of the flow.

In the velocity head method, the losses are reported as a number of velocity heads K. Then, the engineering Bernoulli equation for an incompressible fluid can be written

$$p_1 - p_2 = \alpha_2 \frac{\rho V_2^2}{2} - \alpha_1 \frac{\rho V_1^2}{2} + \rho g(z_2 - z_1) + K \frac{\rho V^2}{2} \tag{6-90}$$

where V is the reference velocity upon which the velocity head loss coefficient K is based. For a section of straight pipe, $K = 4fL/D$.

Contraction and Entrance Losses For a **sudden contraction** at a sharp-edged entrance to a pipe or sudden reduction in cross-sectional area of a channel, as shown in Fig. 6-13*a*, the loss coefficient based on the downstream velocity V_2 is given for **turbulent flow** in Crane Co. Tech Paper 410 (1980) approximately by

$$K = 0.5\left(1 - \frac{A_2}{A_1}\right) \tag{6-91}$$

Example 5: Entrance Loss Water, $\rho = 1000$ kg/m^3, flows from a large vessel through a sharp-edged entrance into a pipe at a velocity in the pipe of 2 m/s. The flow is turbulent. Estimate the pressure drop from the vessel into the pipe.

With $A_2/A_1 \sim 0$, the viscous loss coefficient is $K = 0.5$ from Eq. (6-91). The mechanical energy balance, Eq. (6-16) with $V_1 = 0$ and $z_2 - z_1 = 0$ and assuming uniform flow ($\alpha_2 = 1$) becomes

$$p_1 - p_2 = \frac{\rho V_2^2}{2} + 0.5\,\frac{\rho V_2^2}{2} = 4{,}000 + 2{,}000 = 6{,}000 \text{ Pa}$$

Note that the total pressure drop consists of 0.5 velocity heads of frictional loss contribution, and 1 velocity head of velocity change contribution. The frictional contribution is a permanent loss of mechanical energy by viscous dissipation. The acceleration contribution is reversible; if the fluid were subsequently decelerated in a frictionless diffuser, a 4,000 Pa pressure rise would occur.

For a **trumpet-shaped** rounded entrance, with a radius of rounding greater than about 15 percent of the pipe diameter (Fig. 6-13*b*), the turbulent flow loss coefficient K is only about 0.1 (Vennard and Street, *Elementary Fluid Mechanics,* 5th ed., Wiley, New York, 1975, pp. 420–421). Rounding of the inlet prevents formation of the **vena contracta,** thereby reducing the resistance to flow.

For **laminar flow** the losses in sudden contraction may be estimated for area ratios $A_2/A_1 < 0.2$ by an equivalent additional pipe length L_e given by

$$L_e/D = 0.3 + 0.04\text{Re} \tag{6-92}$$

where D is the diameter of the smaller pipe and Re is the Reynolds number in the smaller pipe. For laminar flow in the entrance to rectangular ducts, see Shah (*J. Fluids Eng.,* **100,** 177–179 [1978]) and Roscoe (*Philos. Mag.,* **40,** 338–351 [1949]). For creeping flow, Re < 1, of power law fluids, the entrance loss is approximately $L_e/D = 0.3/n$ (Boger, Gupta, and Tanner, *J. Non-Newtonian Fluid Mech.,* **4,** 239–248 [1978]). For viscoelastic fluid flow in circular channels with sudden contraction, a toroidal vortex forms upstream of the contraction plane. Such flows are reviewed by Boger (*Ann. Review Fluid Mech.,* **19,** 157–182 [1987]).

For creeping flow through **conical converging channels,** inertial acceleration terms are negligible and the viscous pressure drop $\Delta p = \rho l_v$ may be computed by integration of the differential form of the Hagen-Poiseuille equation Eq. (6-36), provided the angle of convergence is small. The result for a power law fluid is

$$\Delta p = K\left(\frac{3n+1}{4n}\right)^n \left(\frac{8V_2}{D_2}\right)^n \left\{\frac{1}{6n\tan(\alpha/2)}\left[1 - \left(\frac{D_2}{D_1}\right)^{3n}\right]\right\} \tag{6-93}$$

where D_1 = inlet diameter
D_2 = exit diameter
V_2 = velocity at the exit
α = total included angle

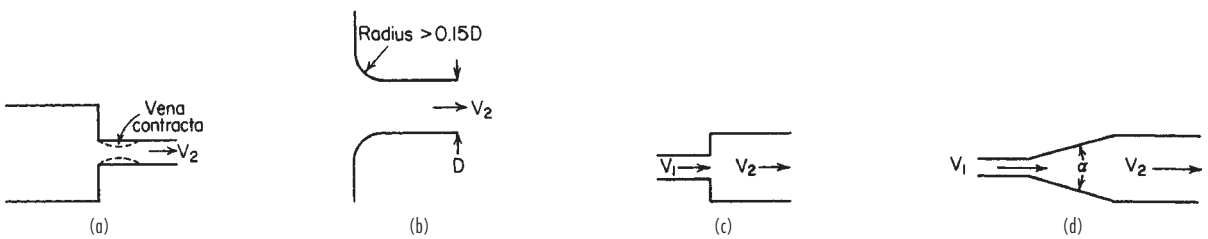

FIG. 6-13 Contractions and enlargements: (*a*) sudden contraction, (*b*) rounded contraction, (*c*) sudden enlargement, and (*d*) uniformly diverging duct.

Equation (6-93) agrees with experimental data (Kemblowski and Kiljanski, *Chem. Eng. J.* (*Lausanne*), **9,** 141–151 [1975]) for $\alpha < 11°$. For Newtonian liquids, Eq. (6-93) simplifies to

$$\Delta p = \mu \left(\frac{8V_2}{D_2}\right)\left\{\frac{1}{6\tan(\alpha/2)}\left[1-\left(\frac{D_2}{D_1}\right)^3\right]\right\} \qquad (6\text{-}94)$$

For creeping flow through rectangular or two-dimensional converging channels, the differential form of the Hagen-Poiseulle equation with equivalent diameter given by Eq. (6-49) may be used, provided the convergence is gradual.

Expansion and Exit Losses For ducts of any cross section, the frictional loss for a **sudden enlargement** (Fig. 6-13*c*) with turbulent flow is given by the Borda-Carnot equation:

$$l_v = \frac{V_1^2 - V_2^2}{2} = \frac{V_1^2}{2}\left(1-\frac{A_1}{A_2}\right)^2 \qquad (6\text{-}95)$$

where V_1 = velocity in the smaller duct
V_2 = velocity in the larger duct
A_1 = cross-sectional area of the smaller duct
A_2 = cross-sectional area of the larger duct

Equation (6-95) is valid for incompressible flow. For compressible flows, see Benedict, Wyler, Dudek, and Gleed (*J. Eng. Power,* **98,** 327–334 [1976]). For an infinite expansion, $A_1/A_2 = 0$, Eq. (6-95) shows that the **exit loss** from a pipe is 1 velocity head. This result is easily deduced from the mechanical energy balance Eq. (6-90), noting that $p_1 = p_2$. This exit loss is due to the dissipation of the discharged jet; there is no pressure drop at the exit.

For creeping Newtonian flow (Re < 1), the frictional loss due to a sudden enlargement should be obtained from the same equation for a sudden contraction (Eq. [6-92]). Note, however, that Boger, Gupta, and Tanner (ibid.) give an exit friction equivalent length of 0.12 diameter, increasing for power law fluids as the exponent decreases. For laminar flows at higher Reynolds numbers, the pressure drop is twice that given by Eq. (6-95). This results from the velocity profile factor α in the mechanical energy balance being 2.0 for the parabolic laminar velocity profile.

If the transition from a small to a large duct of any cross-sectional shape is accomplished by a **uniformly diverging duct** (see Fig. 6-13*d*) with a straight axis, the total frictional pressure drop can be computed by integrating the differential form of Eq. (6-89), $dl_v/dx = 2fV^2/D$ over the length of the expansion, provided the total angle α between the diverging walls is less than 7°. For angles between 7 and 45°, the loss coefficient may be estimated as 2.6 sin $(\alpha/2)$ times the loss coefficient for a sudden expansion; see Hooper (*Chem. Eng.,* Nov. 7, 1988). Gibson (*Hydraulics and Its Applications,* 5th ed., Constable, London 1952, p. 93) recommends multiplying the sudden enlargement loss by 0.13 for $5° < \alpha < 7.5°$ and by $0.0110\alpha^{1.22}$ for $7.5° < \alpha < 35°$. For angles greater than 35 to 45°, the losses are normally considered equal to those for a sudden expansion, although in some cases the losses may be greater. Expanding flow through standard pipe reducers should be treated as sudden expansions.

Trumpet-shaped enlargements for **turbulent flow** designed for constant decrease in velocity head per unit length were found by Gibson (ibid., p. 95) to give 20 to 60 percent less frictional loss than straight taper pipes of the same length.

A special feature of expansion flows occurs when **viscoelastic** liquids are extruded through a die at a low Reynolds number. The extrudate may expand to a diameter several times greater than the die diameter, whereas for a Newtonian fluid the diameter expands only 10 percent. This phenomenon, called **die swell,** is most pronounced with short dies (Graessley, Glasscock, and Crawley, *Trans. Soc. Rheol.,* **14,** 519–544 [1970]). For velocity distribution measurements near the die exit, see Goulden and MacSporran (*J. Non-Newtonian Fluid Mech.,* **1,** 183–198 [1976]) and Whipple and Hill (*AIChE J.,* **24,** 664–671 [1978]). At high flow rates, the extrudate becomes distorted, suffering **melt fracture** at wall shear stresses greater than 10^5 N/m^2. This phenomenon is reviewed by Denn (*Ann. Review Fluid Mech.,* **22,** 13–34 [1990]). Ramamurthy (*J. Rheol.,* **30,** 337–357 [1986]) has found a dependence of apparent stick-slip behavior in melt fracture to be dependent on the material of construction of the die.

Fittings and Valves For **turbulent flow,** the frictional loss for fittings and valves can be expressed by the equivalent length or velocity head methods. As fitting size is varied, K values are relatively more constant than L_e/D values, but since fittings generally do not achieve geometric similarity between sizes, K values tend to decrease with increasing fitting size. Table 6-4 gives K values for many types of fittings and valves.

Manufacturers of valves, especially control valves, express valve capacity in terms of a flow coefficient C_v, which gives the flow rate through the valve in gal/min of water at 60°F under a pressure drop of 1 lbf/in^2. It is related to K by

$$C_v = \frac{C_1 d^2}{\sqrt{K}} \qquad (6\text{-}96)$$

where C_1 is a dimensional constant equal to 29.9 and d is the diameter of the valve connections in inches.

For **laminar flow,** data for the frictional loss of valves and fittings are meager. (Beck and Miller, *J. Am. Soc. Nav. Eng.,* **56,** 62–83 [1944]; Beck, ibid., **56,** 235–271, 366–388, 389–395 [1944]; De Craene, *Heat. Piping Air Cond.,* **27**[10], 90–95 [1955]; Karr and Schutz, *J. Am. Soc. Nav. Eng.,* **52,** 239–256 [1940]; and Kittredge and Rowley, *Trans. ASME,* **79,** 1759–1766 [1957]). The data of Kittredge and Rowley indicate that K is constant for Reynolds numbers above 500 to 2,000, but increases rapidly as Re decreases below 500. Typical values for K for laminar flow Reynolds numbers are shown in Table 6-5.

Methods to calculate losses for **tee and wye junctions** for dividing and combining flow are given by Miller (*Internal Flow Systems,* 2d ed., Chap. 13, BHRA, Cranfield, 1990), including effects of Reynolds number, angle between legs, area ratio, and radius. Junctions with more than three legs are also discussed. The sources of data for the loss coefficient charts are Blaisdell and Manson (*U.S. Dept. Agric. Res. Serv. Tech. Bull.* 1283 [August 1963]) for combining flow and Gardel (*Bull. Tech. Suisses Romande,* **85**[9], 123–130 [1957]; **85**[10], 143–148 [1957]) together with additional unpublished data for dividing flow.

Miller (*Internal Flow Systems,* 2d ed., Chap. 13, BHRA, Cranfield, 1990) gives the most complete information on losses in **bends and curved pipes.** For turbulent flow in circular cross-section bends of constant area, as shown in Fig. 6-14*a*, a more accurate estimate of the loss coefficient K than that given in Table 6-4 is

$$K = K^* C_{\mathrm{Re}} C_o C_f \qquad (6\text{-}97)$$

where K^*, given in Fig. 6-14*b*, is the loss coefficient for a smooth-walled bend at a Reynolds number of 10^6. The Reynolds number correction factor C_{Re} is given in Fig. 6-14*c*. For $0.7 < r/D < 1$ or for $K^* < 0.4$, use the C_{Re} value for $r/D = 1$. Otherwise, if $r/D < 1$, obtain C_{Re} from

$$C_{\mathrm{Re}} = \frac{K^*}{K^* + 0.2(1 - C_{\mathrm{Re},\, r/D\,=\,1})} \qquad (6\text{-}98)$$

The correction C_o (Fig. 6-14*d*) accounts for the extra losses due to developing flow in the outlet tangent of the pipe, of length L_o. The total loss for the bend plus outlet pipe includes the bend loss K plus the straight pipe frictional loss in the outlet pipe $4fL_o/D$. Note that $C_o = 1$ for L_o/D greater than the termination of the curves on Fig. 6-14*d*, which indicate the distance at which fully developed flow in the outlet pipe is reached. Finally, the roughness correction is

$$C_f = \frac{f_{\mathrm{rough}}}{f_{\mathrm{smooth}}} \qquad (6\text{-}99)$$

where f_{rough} is the friction factor for a pipe of diameter D with the roughness of the bend, at the bend inlet Reynolds number. Similarly, f_{smooth} is the friction factor for smooth pipe. For $\mathrm{Re} > 10^6$ and $r/D \geq 1$, use the value of C_f for $\mathrm{Re} = 10^6$.

Example 6: Losses with Fittings and Valves It is desired to calculate the liquid level in the vessel shown in Fig. 6-15 required to produce a discharge velocity of 2 m/s. The fluid is water at 20°C with $\rho = 1{,}000$ kg/m^3 and $\mu = 0.001$ Pa · s, and the butterfly valve is at $\theta = 10°$. The pipe is 2-in Schedule 40, with an inner diameter of 0.0525 m. The pipe roughness is 0.046 mm. Assuming the flow is turbulent and taking the velocity profile factor $\alpha = 1$, the engineering Bernoulli equation Eq. (6-16), written between surfaces 1 and 2, where the

TABLE 6-4 Additional Frictional Loss for Turbulent Flow through Fittings and Valves[a]

Type of fitting or valve	Additional friction loss, equivalent no. of velocity heads, K
45° ell, standard[b,c,d,e,f]	0.35
45° ell, long radius[c]	0.2
90° ell, standard[b,c,e,f,g,h]	0.75
Long radius[b,c,d,e]	0.45
Square or miter[h]	1.3
180° bend, close return[b,c,e]	1.5
Tee, standard, along run, branch blanked off[e]	0.4
Used as ell, entering run[g,i]	1.0
Used as ell, entering branch[e,g,i]	1.0
Branching flow[i,j,k]	1[l]
Coupling[e,e]	0.04
Union[e]	0.04
Gate valve,[b,e,m] open	0.17
¾ open[n]	0.9
½ open[n]	4.5
¼ open[n]	24.0
Diaphragm valve,[a] open	2.3
¾ open[n]	2.6
½ open[n]	4.3
¼ open[n]	21.0
Globe valve,[e,m]	
Bevel seat, open	6.0
½ open[n]	9.5
Composition seat, open	6.0
½ open[n]	8.5
Plug disk, open	9.0
¾ open[n]	13.0
½ open[n]	36.0
¼ open[n]	112.0
Angle valve,[b,e] open	2.0
Y or blowoff valve,[b,m] open	3.0
Plug cock[p]	
$\theta = 5°$	0.05
$\theta = 10°$	0.29
$\theta = 20°$	1.56
$\theta = 40°$	17.3
$\theta = 60°$	206.0
Butterfly valve[p]	
$\theta = 5°$	0.24
$\theta = 10°$	0.52
$\theta = 20°$	1.54
$\theta = 40°$	10.8
$\theta = 60°$	118.0
Check valve,[b,e,m] swing	2.0[q]
Disk	10.0[q]
Ball	70.0[q]
Foot valve[e]	15.0
Water meter,[h] disk	7.0[r]
Piston	15.0[r]
Rotary (star-shaped disk)	10.0[r]
Turbine-wheel	6.0[r]

[a] Lapple, *Chem. Eng.,* **56**(5), 96–104 (1949), general survey reference.
[b] "Flow of Fluids through Valves, Fittings, and Pipe," Tech. Pap. 410, Crane Co., 1969.
[c] Freeman, *Experiments upon the Flow of Water in Pipes and Pipe Fittings,* American Society of Mechanical Engineers, New York, 1941.
[d] Giesecke, *J. Am. Soc. Heat. Vent. Eng.,* **32,** 461 (1926).
[e] *Pipe Friction Manual,* 3d ed., Hydraulic Institute, New York, 1961.
[f] Ito, *J. Basic Eng.,* **82,** 131–143 (1960).
[g] Giesecke and Badgett, *Heat. Piping Air Cond.,* **4**(6), 443–447 (1932).
[h] Schoder and Dawson, *Hydraulics,* 2d ed., McGraw-Hill, New York, 1934, p. 213.
[i] Hoopes, Isakoff, Clarke, and Drew, *Chem. Eng. Prog.,* **44,** 691–696 (1948).
[j] Gilman, *Heat. Piping Air Cond.,* **27**(4), 141–147 (1955).
[k] McNown, *Proc. Am. Soc. Civ. Eng.,* **79,** Separate 258, 1–22 (1953); discussion, ibid., **80,** Separate 396, 19–45 (1954). For the effect of branch spacing on junction losses in dividing flow, see Hecker, Nystrom, and Qureshi, *Proc. Am. Soc. Civ. Eng., J. Hydraul. Div.,* **103**(HY3), 265–279 (1977).
[l] This is pressure drop (including friction loss) between run and branch, based on velocity in the mainstream before branching. Actual value depends on the flow split, ranging from 0.5 to 1.3 if mainstream enters run and from 0.7 to 1.5 if mainstream enters branch.
[m] Lansford, *Loss of Head in Flow of Fluids through Various Types of 1½-in. Valves,* Univ. Eng. Exp. Sta. Bull. Ser. 340, 1943.

pressures are both atmospheric and the fluid velocities are 0 and $V = 2$ m/s, respectively, and there is no shaft work, simplifies to

$$gZ = \frac{V^2}{2} + l_v$$

Contributing to l_v are losses for the entrance to the pipe, the three sections of straight pipe, the butterfly valve, and the 90° bend. Note that no exit loss is used because the discharged jet is outside the control volume. Instead, the $V^2/2$ term accounts for the kinetic energy of the discharging stream. The Reynolds number in the pipe is

$$\mathrm{Re} = \frac{DV\rho}{\mu} = \frac{0.0525 \times 2 \times 1000}{0.001} = 1.05 \times 10^5$$

From Fig. 6-9 or Eq. (6-38), at $\epsilon/D = 0.046 \times 10^{-3}/0.0525 = 0.00088$, the friction factor is about 0.0054. The straight pipe losses are then

$$l_{v(\mathrm{sp})} = \left(\frac{4fL}{D}\right)\frac{V^2}{2} = \left(\frac{4 \times 0.0054 \times (1+1+1)}{0.0525}\right)\frac{V^2}{2} = 1.23\,\frac{V^2}{2}$$

The losses from Table 6-4 in terms of velocity heads K are $K = 0.5$ for the sudden contraction and $K = 0.52$ for the butterfly valve. For the 90° standard radius ($r/D = 1$), the table gives $K = 0.75$. The method of Eq. (6-94), using Fig. 6-14, gives

$$K = K^*C_{\mathrm{Re}}C_oC_f = 0.24 \times 1.24 \times 1.0 \times \left(\frac{0.0054}{0.0044}\right) = 0.37$$

This value is more accurate than the value in Table 6-4. The value $f_{\mathrm{smooth}} = 0.0044$ is obtainable either from Eq. (6-37) or Fig. 6-9.

The total losses are then

$$l_v = (1.23 + 0.5 + 0.52 + 0.37)\frac{V^2}{2} = 2.62\,\frac{V^2}{2}$$

and the liquid level Z is

$$Z = \frac{1}{g}\left(\frac{V^2}{2} + 2.62\,\frac{V^2}{2}\right) = 3.62\,\frac{V^2}{2g} = \frac{3.62 \times 2^2}{2 \times 9.81} = 0.73 \text{ m}$$

Curved Pipes and Coils For flow through curved pipe or coil, a secondary circulation perpendicular to the main flow called the **Dean effect** occurs. This circulation increases the friction relative to straight pipe flow and stabilizes laminar flow, delaying the transition Reynolds number to about

$$\mathrm{Re}_{\mathrm{crit}} = 2{,}100\left(1 + 12\sqrt{\frac{D}{D_c}}\right) \qquad (6\text{-}100)$$

where D_c is the coil diameter. Equation (6-100) is valid for $10 < D_c/D < 250$. The **Dean number** is defined as

$$\mathrm{De} = \frac{\mathrm{Re}}{(D_c/D)^{1/2}} \qquad (6\text{-}101)$$

In laminar flow, the friction factor for curved pipe f_c may be expressed in terms of the straight pipe friction factor $f = 16/\mathrm{Re}$ as (Hart, *Chem. Eng. Sci.,* **43,** 775–783 [1988])

TABLE 6-5 Additional Frictional Loss for Laminar Flow through Fittings and Valves

Type of fitting or valve	Additional frictional loss expressed as K			
	Re = 1,000	500	100	50
90° ell, short radius	0.9	1.0	7.5	16
Gate valve	1.2	1.7	9.9	24
Globe valve, composition disk	11	12	20	30
Plug	12	14	19	27
Angle valve	8	8.5	11	19
Check valve, swing	4	4.5	17	55

SOURCE: From curves by Kittredge and Rowley, *Trans. Am. Soc. Mech. Eng.,* **79,** 1759–1766 (1957).

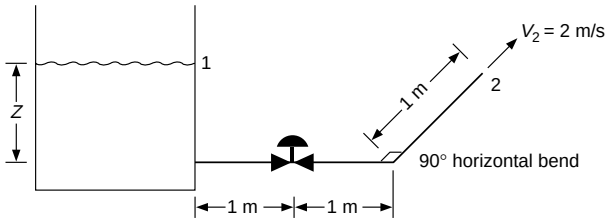

FIG. 6-15 Tank discharge example.

$$\frac{f_c}{f} = 1 + 0.090\left(\frac{\mathrm{De}^{1.5}}{70 + \mathrm{De}}\right) \tag{6-102}$$

For turbulent flow, equations by Ito (*J. Basic Eng,* **81,** 123 [1959]) and Srinivasan, Nandapurkar, and Holland (*Chem. Eng.* [*London*] no. 218, CE113-CE119 [May 1968]) may be used, with probable accuracy of ±15 percent. Their equations are similar to

$$f_c = \frac{0.079}{\mathrm{Re}^{0.25}} + \frac{0.0073}{\sqrt{(D_c/D)}} \tag{6-103}$$

The pressure drop for flow in **spirals** is discussed by Srinivasan, et al. (loc. cit.) and Ali and Seshadri (*Ind. Eng. Chem. Process Des. Dev.,* **10,** 328–332 [1971]). For friction loss in laminar flow through **semicircular ducts,** see Masliyah and Nandakumar (*AIChE J.,* **25,** 478–487 [1979]); for curved channels of **square cross section,** see Cheng, Lin, and Ou (*J. Fluids Eng.,* **98,** 41–48 [1976]).

For **non-Newtonian** (**power law**) **fluids** in coiled tubes, Mashelkar and Devarajan (*Trans. Inst. Chem. Eng.* (*London*), **54,** 108–114 [1976]) propose the correlation

$$f_c = (9.07 - 9.44n + 4.37n^2)(D/D_c)^{0.5}(\mathrm{De}')^{-0.768 + 0.122n} \tag{6-104}$$

where De′ is a modified Dean number given by

$$\mathrm{De}' = \frac{1}{8}\left(\frac{6n+2}{n}\right)^n \mathrm{Re}_{\mathrm{MR}}\sqrt{\frac{D}{D_c}} \tag{6-105}$$

where $\mathrm{Re}_{\mathrm{MR}}$ is the Metzner-Reed Reynolds number, Eq. (6-65). This correlation was tested for the range De′ = 70 to 400, D/D_c = 0.01 to 0.135, and n = 0.35 to 1. See also Oliver and Asghar (*Trans. Inst. Chem. Eng.* [*London*], **53,** 181–186 [1975]).

Screens The pressure drop for incompressible flow across a screen of fractional free area α may be computed from

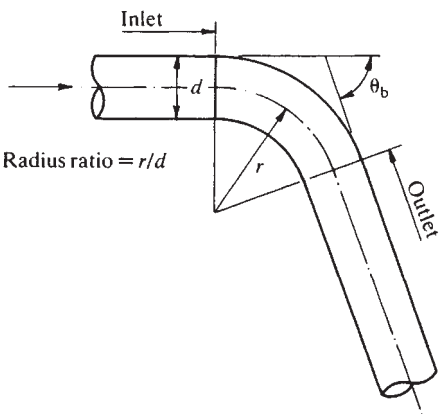

(a)

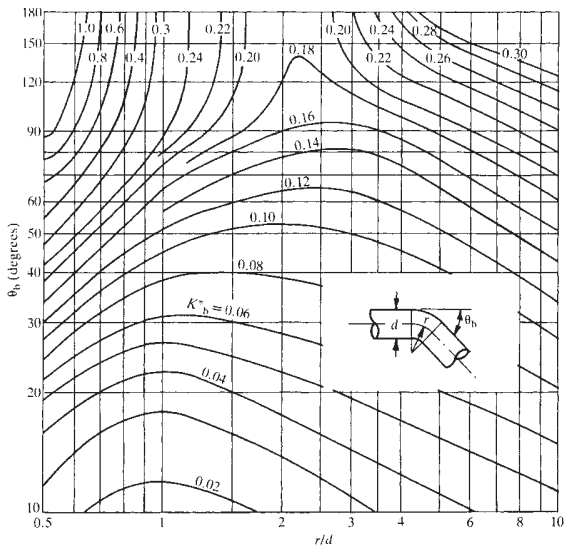

(b)

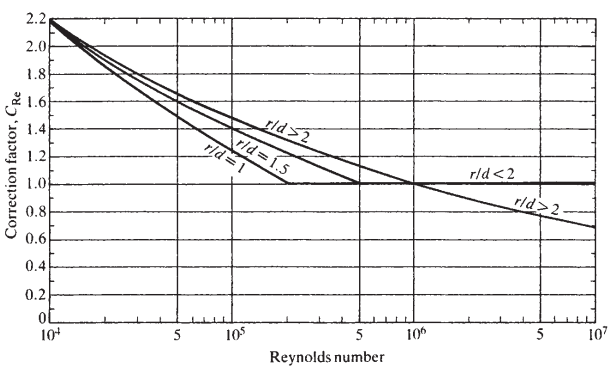

(c)

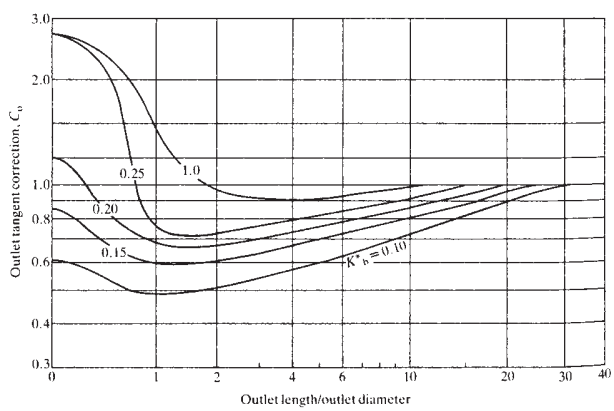

(d)

FIG. 6-14 Loss coefficients for flow in bends and curved pipes: (*a*) flow geometry, (*b*) loss coefficient for a smooth-walled bend at Re = 10^6, (*c*) Re correction factor, (*d*) outlet pipe correction factor (*From D. S. Miller,* Internal Flow Systems, 2*d. ed., BHRA, Cranfield, U.K., 1990.*)

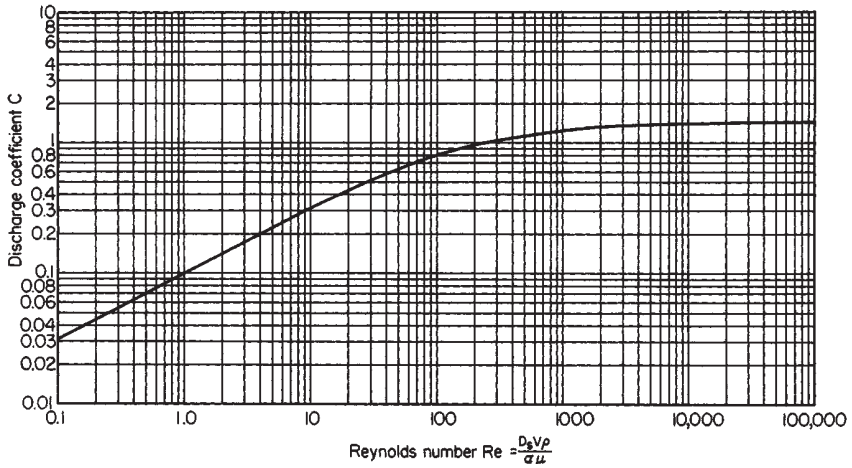

FIG. 6-16 Screen discharge coefficients, plain square-mesh screens. (*Courtesy of E. I. du Pont de Nemours & Co.*)

$$\Delta p = K\frac{\rho V^2}{2} \tag{6-106}$$

where ρ = fluid density
V = superficial velocity based upon the gross area of the screen
K = velocity head loss

$$K = \left(\frac{1}{C^2}\right)\left(\frac{1-\alpha^2}{\alpha^2}\right) \tag{6-107}$$

The discharge coefficient for the screen C with aperture D_s is given as a function of screen Reynolds number $\mathrm{Re} = D_s(V/\alpha)\rho/\mu$ in Fig. 6-16 for **plain square-mesh screens,** $\alpha = 0.14$ to 0.79. This curve fits most of the data within ±20 percent. In the laminar flow region, Re < 20, the discharge coefficient can be computed from

$$C = 0.1\sqrt{\mathrm{Re}} \tag{6-108}$$

Coefficients greater than 1.0 in Fig. 6-16 probably indicate partial pressure recovery downstream of the minimum aperture, due to rounding of the wires.

Grootenhuis (*Proc. Inst. Mech. Eng.* [*London*], **A168,** 837–846 [1954]) presents data which indicate that for a series of screens, the total pressure drop equals the number of screens times the pressure drop for one screen, and is not affected by the spacing between screens or their orientation with respect to one another, and presents a correlation for frictional losses across plain square-mesh screens and sintered gauzes. Armour and Cannon (*AIChE J.,* **14,** 415–420 [1968]) give a correlation based on a packed bed model for plain, twill, and "dutch" weaves. For losses through monofilament fabrics see Pedersen (*Filtr. Sep.,* **11,** 586–589 [1975]). For screens **inclined at an angle** θ, use the normal velocity component V'

$$V' = V\cos\theta \tag{6-109}$$

(Carothers and Baines, *J. Fluids Eng.,* **97,** 116–117 [1975]) in place of V in Eq. (6-106). This applies for Re > 500, $C = 1.26$, $\alpha \le 0.97$ and $0 < \theta < 45°$, for square-mesh screens and diamond-mesh netting. Screens inclined at an angle to the flow direction also experience a tangential stress.

For **non-Newtonian** fluids in slow flow, friction loss across a square-woven or full-twill-woven screen can be estimated by considering the screen as a set of parallel tubes, each of diameter equal to the average minimal opening between adjacent wires, and length twice the diameter, without entrance effects (Carley and Smith, *Polym. Eng. Sci.,* **18,** 408–415 [1978]). For screen stacks, the losses of individual screens should be summed.

JET BEHAVIOR

A **free jet,** upon leaving an outlet, will entrain the surrounding fluid, expand, and decelerate. To a first approximation, total momentum is conserved as jet momentum is transferred to the entrained fluid. For practical purposes, a jet is considered free when its cross-sectional area is less than one-fifth of the total cross-sectional flow area of the region through which the jet is flowing (Elrod, *Heat. Piping Air Cond.,* **26**(3), 149–155 [1954]), and the surrounding fluid is the same as the jet fluid. A **turbulent jet** in this discussion is considered to be a free jet with Reynolds number greater than 2,000. Additional discussion on the relation between Reynolds number and turbulence in jets is given by Elrod (ibid.). Abramowicz (*The Theory of Turbulent Jets,* MIT Press, Cambridge, 1963) provides a thorough discourse on the theory of turbulent jets. Hussein, et al. (*J. Fluid Mech.,* **258,** 31–75 [1994]) give extensive velocity data for a free jet, as well as an extensive discussion of free jet experimentation and comparison of data with momentum conservation equations.

A turbulent free jet is normally considered to consist of four flow regions (Tuve, *Heat. Piping Air Cond.,* **25**(1), 181–191 [1953]; Davies, *Turbulence Phenomena,* Academic, New York, 1972) as shown in Fig. 6-17:

1. Region of flow establishment—a short region whose length is about 6.4 nozzle diameters. The fluid in the conical core of the same length has a velocity about the same as the initial discharge velocity. The termination of this *potential core* occurs when the growing mixing or boundary layer between the jet and the surroundings reaches the centerline of the jet.
2. A transition region that extends to about 8 nozzle diameters.
3. Region of established flow—the principal region of the jet. In this region, the velocity profile transverse to the jet is self-preserving when normalized by the centerline velocity.

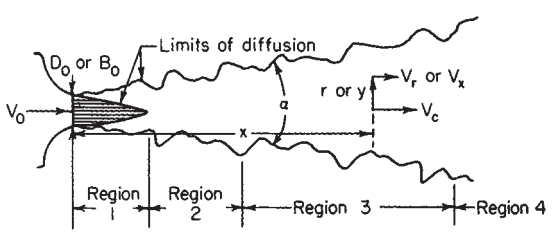

FIG. 6-17 Configuration of a turbulent free jet.

TABLE 6-6 Turbulent Free-Jet Characteristics
Where Both Jet Fluid and Entrained Fluid Are Air

Rounded-inlet circular jet

Longitudinal distribution of velocity along jet center line°†

$$\frac{V_c}{V_0} = K\frac{D_0}{x} \qquad \text{for } 7 < \frac{x}{D_0} < 100$$

$K = 5$ for $V_0 = 2.5$ to 5.0 m/s
$K = 6.2$ for $V_0 = 10$ to 50 m/s

Radial distribution of longitudinal velocity†

$$\log\left(\frac{V_c}{V_r}\right) = 40\left(\frac{r}{x}\right)^2 \qquad \text{for } 7 < \frac{x}{D_0} < 100$$

Jet angle°†

$$\alpha \simeq 20° \qquad \text{for } \frac{x}{D_0} < 100$$

Entrainment of surrounding fluid‡

$$\frac{q}{q_0} = 0.32\,\frac{x}{D_0} \qquad \text{for } 7 < \frac{x}{D_0} < 100$$

Rounded-inlet, infinitely wide slot jet

Longitudinal distribution of velocity along jet centerline‡

$$\frac{V_c}{V_0} = 2.28\left(\frac{B_0}{x}\right)^{0.5} \qquad \text{for } 5 < \frac{x}{B_0} < 2{,}000 \text{ and } V_0 = 12 \text{ to } 55 \text{ m/s}$$

Transverse distribution of longitudinal velocity‡

$$\log\left(\frac{V_c}{V_x}\right) = 18.4\left(\frac{y}{x}\right)^2 \qquad \text{for } 5 < \frac{x}{B_0} < 2{,}000$$

Jet angle‡

α is slightly larger than that for a circular jet

Entrainment of surrounding fluid‡

$$\frac{q}{q_0} = 0.62\left(\frac{x}{B_0}\right)^{0.5} \qquad \text{for } 5 < \frac{x}{B_0} < 2{,}000$$

°Nottage, Slaby, and Gojsza, *Heat, Piping Air Cond.*, **24**(1), 165–176 (1952).
†Tuve, *Heat, Piping Air Cond.*, **25**(1), 181–191 (1953).
‡Albertson, Dai, Jensen, and Rouse, *Trans. Am. Soc. Civ. Eng.*, **115,** 639–664 (1950), and Discussion, ibid., **115,** 665–697 (1950).

4. A terminal region where the residual centerline velocity reduces rapidly within a short distance. For air jets, the residual velocity will reduce to less than 0.3 m/s, (1.0 ft/s) usually considered still air.

Several references quote a length of 100 nozzle diameters for the length of the established flow region. However, this length is dependent on initial velocity and Reynolds number.

Table 6-6 gives characteristics of **rounded-inlet circular jets** and **rounded-inlet infinitely wide slot jets** (aspect ratio > 15). The information in the table is for a homogeneous, incompressible air system under isothermal conditions. The table uses the following nomenclature:

B_0 = slot height
D_0 = circular nozzle opening
q = total jet flow at distance x
q_0 = initial jet flow rate
r = radius from circular jet centerline
y = transverse distance from slot jet centerline
V_c = centerline velocity
V_r = circular jet velocity at r
V_y = velocity at y

Witze (*Am. Inst. Aeronaut. Astronaut. J.*, **12,** 417–418 [1974]) gives equations for the centerline velocity decay of different types of subsonic and supersonic circular free jets. Entrainment of surrounding fluid in the region of flow establishment is lower than in the region of established flow (see Hill, *J. Fluid Mech.*, **51,** 773–779 [1972]). Data of Donald and Singer (*Trans. Inst. Chem. Eng.* [*London*], **37,** 255–267 [1959]) indicate that jet angle and the coefficients given in Table 6-6 depend upon the fluids; for a water system, the jet angle for a circular jet is 14° and the entrainment ratio is about 70 percent of that for an air system. Most likely these variations are due to Reynolds number effects which are not taken into account in Table 6-6. Rushton (*AIChE J.*, **26,** 1038–1041 [1980]) examined available published results for circular jets and found that the centerline velocity decay is given by

$$\frac{V_c}{V_0} = 1.41\mathrm{Re}^{0.135}\left(\frac{D_0}{x}\right) \tag{6-110}$$

where $\mathrm{Re} = D_0V_0\rho/\mu$ is the initial jet Reynolds number. This result corresponds to a jet angle tan $\alpha/2$ proportional to $\mathrm{Re}^{-0.135}$.

Characteristics of **rectangular jets** of various aspect ratios are given by Elrod (*Heat., Piping, Air Cond.*, **26**[3], 149–155 [1954]). For **slot jets discharging into a moving fluid,** see Weinstein, Osterle, and Forstall (*J. Appl. Mech.*, **23,** 437–443 [1967]). **Coaxial jets** are discussed by Forstall and Shapiro (*J. Appl. Mech.*, **17,** 399–408 [1950]), and **double concentric jets** by Chigier and Beer (*J. Basic Eng.*, **86,** 797–804 [1964]). **Axisymmetric confined jets** are described by Barchilon and Curtet (*J. Basic Eng.*, **777–787** [1964]). **Restrained** turbulent jets of liquid discharging into air are described by Davies (*Turbulence Phenomena,* Academic, New York, 1972). These jets are inherently unstable and break up into drops after some distance. Lienhard and Day (*J. Basic Eng. Trans. AIME*, p. 515 [September 1970]) discuss the breakup of superheated liquid jets which flash upon discharge.

Density gradients affect the spread of a single-phase jet. A jet of lower density than the surroundings spreads more rapidly than a jet of the same density as the surroundings, and, conversely, a denser jet spreads less rapidly. Additional details are given by Keagy and Weller (*Proc. Heat Transfer Fluid Mech. Inst., ASME*, pp. 89–98, June 22–24 [1949]) and Cleeves and Boelter (*Chem. Eng. Prog.*, **43,** 123–134 [1947]).

Few experimental data exist on **laminar jets** (see Gutfinger and Shinnar, *AIChE J.*, **10,** 631–639 [1964]). Theoretical analysis for velocity distributions and entrainment ratios are available in Schlichting and in Morton (*Phys. Fluids*, **10,** 2120–2127 [1967]).

Theoretical analyses of jet flows for power law **non-Newtonian fluids** are given by Vlachopoulos and Stournaras (*AIChE J.*, **21,** 385–388 [1975]), Mitwally (*J. Fluids Eng.*, **100,** 363 [1978]), and Sridhar and Rankin (*J. Fluids Eng.*, **100,** 500 [1978]).

FLOW THROUGH ORIFICES

Section 10 of this *Handbook* describes the use of orifice meters for flow measurement. In addition, **orifices** are commonly found within pipelines as flow-restricting devices, in perforated pipe distributing and return manifolds, and in perforated plates. Incompressible flow through an orifice in a pipeline as shown in Fig. 6-18, is commonly described by the following equation for flow rate Q in terms of pressure drop across the orifice Δp, the orifice area A_o, the pipe cross-sectional area A, and the density ρ.

$$Q = C_oA_o\sqrt{\frac{2\Delta p/\rho}{[1-(A_o/A)^2]}} \tag{6-111}$$

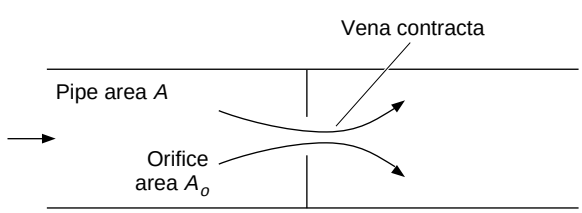

FIG. 6-18 Flow through an orifice.

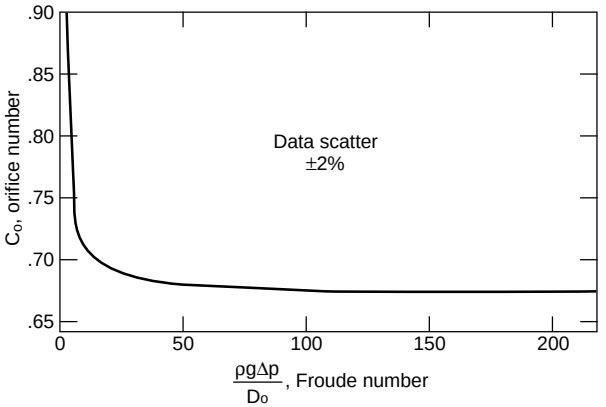

FIG. 6-19 Orifice coefficient vs. Froude number. (*Courtesy E. I. duPont de Nemours & Co.*)

The velocity of approach term $[1 - (A_o/A)^2]$ accounts for the kinetic energy approaching the orifice, while the **orifice coefficient** or **discharge coefficient** C_o accounts for the **vena contracta** effect which causes the fluid to accelerate to velocity greater than Q/A_o. The downstream pressure measurement corresponding to Δp in Eq. (6-111) is taken at the vena contracta. Downstream of the vena contracta, the velocity decelerates and some pressure recovery may be expected. Any pressure recovery is completed about 4 to 8 pipe diameters downstream of the orifice. As an approximation, the pressure recovery, expressed as a fraction of the orifice pressure drop, is approximately equal to the area ratio A_o/A. When the orifice discharges into a large chamber, instead of being installed within a pipe, there is negligible pressure recovery. Equation (6-111) may also be used for flow across a perforated plate with open area A_o and total area A.

The orifice coefficient has a value of about 0.62 at large Reynolds numbers ($\mathrm{Re} = D_o V_o \rho/\mu > 20{,}000$), although values ranging from 0.60 to 0.70 are frequently used. At lower Reynolds numbers, the orifice coefficient varies with both Re and with the area or diameter ratio. See Sec. 10 for more details.

When liquids discharge vertically downward from orifices into gas, gravity increases the discharge coefficient. Figure 6-19 shows this effect, giving the discharge coefficient in terms of a modified Froude number, $\mathrm{Fr} = \rho g \Delta p/D_o$.

The orifice coefficient deviates from its value for sharp-edged orifices when the orifice wall thickness exceeds about 75 percent of the orifice diameter. Some pressure recovery occurs within the orifice and the orifice coefficient increases. Pressure drop across **segmental orifices** is roughly 10 percent greater than that for concentric circular orifices of the same open area.

COMPRESSIBLE FLOW

Flows are typically considered **compressible** when the density varies by more than 5 to 10 percent. In practice compressible flows are normally limited to gases, supercritical fluids, and multiphase flows containing gases. Liquid flows are normally considered incompressible, except for certain calculations involved in **hydraulic transient** analysis (see following) where compressibility effects are important even for nearly incompressible liquids with extremely small density variations. Textbooks on compressible gas flow include Shapiro (*Dynamics and Thermodynamics of Compressible Fluid Flow,* vol. I and II, Ronald Press, New York [1953]) and Zucrow and Hofmann (*Gas Dynamics,* vol. I and II, Wiley, New York [1976]).

In chemical process applications, one-dimensional gas flows through nozzles or orifices and in pipelines are the most important applications of compressible flow. Multidimensional external flows are of interest mainly in aerodynamic applications.

Mach Number and Speed of Sound The **Mach number** $M = V/c$ is the ratio of fluid velocity, V, to the **speed of sound** or **acoustic velocity,** c. The speed of sound is the propagation velocity of infinitesimal pressure disturbances and is derived from a momentum balance. The compression caused by the pressure wave is adiabatic and frictionless, and therefore isentropic.

$$c = \sqrt{\left(\frac{\partial p}{\partial \rho}\right)_s} \tag{6-112}$$

The derivative of pressure p with respect to density ρ is taken at constant entropy s. For an ideal gas,

$$\left(\frac{\partial p}{\partial \rho}\right)_s = \frac{kRT}{M_w}$$

where k = ratio of specific heats, C_p/C_v
R = universal gas constant (8,314 J/kgmol K)
T = absolute temperature
M_w = molecular weight

Hence for an ideal gas,

$$c = \sqrt{\frac{kRT}{M_w}} \tag{6-113}$$

Most often, the Mach number is calculated using the speed of sound evaluated at the local pressure and temperature. When $M = 1$, the flow is **critical** or **sonic** and the velocity equals the local speed of sound. For **subsonic** flow $M < 1$ while **supersonic** flows have $M > 1$. Compressibility effects are important when the Mach number exceeds 0.1 to 0.2. A common error is to assume that compressibility effects are always negligible when the Mach number is small. The proper assessment of whether compressibility is important should be based on relative density changes, not on Mach number.

Isothermal Gas Flow in Pipes and Channels Isothermal compressible flow is often encountered in long transport lines, where there is sufficient heat transfer to maintain constant temperature. Velocities and Mach numbers are usually small, yet compressibility effects are important when the total pressure drop is a large fraction of the absolute pressure. For an ideal gas with $\rho = pM_w/RT$, integration of the differential form of the momentum or mechanical energy balance equations, assuming a constant friction factor f over a length L of a channel of constant cross section and hydraulic diameter D_H, yields,

$$p_1^2 - p_2^2 = G^2 \frac{RT}{M_w}\left[\frac{4fL}{D_H} + 2\ln\left(\frac{p_1}{p_2}\right)\right] \tag{6-114}$$

where the mass velocity $G = w/A = \rho V$ is the mass flow rate per unit cross-sectional area of the channel. The logarithmic term on the right-hand side accounts for the pressure change caused by acceleration of gas as its density decreases, while the first term is equivalent to the calculation of frictional losses using the density evaluated at the average pressure $(p_1 + p_2)/2$.

Solution of Eq. (6-114) for G and differentiation with respect to p_2 reveals a maximum mass flux $G_{\max} = p_2\sqrt{M_w/(RT)}$ and a corresponding exit velocity $V_{2,\max} = \sqrt{RT/M_w}$ and exit Mach number $M_2 = 1/\sqrt{k}$. This apparent **choking** condition, though often cited, is not physically meaningful for isothermal flow because at such high velocities, and high rates of expansion, isothermal conditions are not maintained.

Adiabatic Frictionless Nozzle Flow In process plant pipelines, compressible flows are usually more nearly adiabatic than isothermal. Solutions for adiabatic flows through frictionless nozzles and in channels with constant cross section and constant friction factor are readily available.

Figure 6-20 illustrates adiabatic discharge of a **perfect** gas through a frictionless nozzle from a large chamber where velocity is effectively zero. A perfect gas obeys the ideal gas law $\rho = pM_w/RT$ and also has constant specific heat. The subscript 0 refers to the **stagnation** conditions in the chamber. More generally, stagnation conditions refer to the conditions which would obtained by isentropically decelerating a gas flow to zero velocity. The minimum area section, or *throat,* of the nozzle is at the nozzle exit. The flow through the nozzle is isentropic

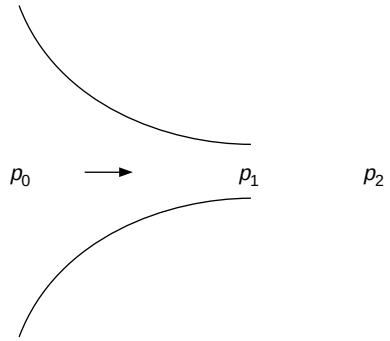

FIG. 6-20 Isentropic flow through a nozzle.

because it is frictionless (reversible) and adiabatic. In terms of the exit Mach number M_1 and the upstream stagnation conditions, the flow conditions at the nozzle exit are given by

$$\frac{p_0}{p_1} = \left(1 + \frac{k-1}{2} M_1^2\right)^{k/(k-1)} \tag{6-115}$$

$$\frac{T_0}{T_1} = 1 + \frac{k-1}{2} M_1^2 \tag{6-116}$$

$$\frac{\rho_0}{\rho_1} = \left(1 + \frac{k-1}{2} M_1^2\right)^{1/(k-1)} \tag{6-117}$$

The mass velocity $G = w/A$, where w is the mass flow rate and A is the nozzle exit area, at the nozzle exit is given by

$$G = p_0 \sqrt{\frac{kM_w}{RT_0}} \frac{M_1}{\left(1 + \frac{k-1}{2} M_1^2\right)^{(k+1)/2(k-1)}} \tag{6-118}$$

These equations are consistent with the isentropic relations for a perfect gas $p/p_0 = (\rho/\rho_0)^k$, $T/T_0 = (p/p_0)^{(k-1)/k}$. Equation (6-116) is valid for adiabatic flows with or without friction; it does not require isentropic flow. However, Eqs. (6-115) and (6-117) do require isentropic flow.

The exit Mach number M_1 may not exceed unity. At $M_1 = 1$, the flow is said to be **choked, sonic,** or **critical.** When the flow is choked, the pressure at the exit is greater than the pressure of the surroundings into which the gas flow discharges. The pressure drops from the exit pressure to the pressure of the surroundings in a series of shocks which are highly nonisentropic. Sonic flow conditions are denoted by *; sonic exit conditions are found by substituting $M_1 = M_1^* = 1$ into Eqs. (6-115) to (6-118).

$$\frac{p^*}{p_0} = \left(\frac{2}{k+1}\right)^{k/(k-1)} \tag{6-119}$$

$$\frac{T^*}{T_0} = \frac{2}{k+1} \tag{6-120}$$

$$\frac{\rho^*}{\rho_0} = \left(\frac{2}{k+1}\right)^{1/(k-1)} \tag{6-121}$$

$$G^* = p_0 \sqrt{\left(\frac{2}{k+1}\right)^{(k+1)/(k-1)} \left(\frac{kM_w}{RT_0}\right)} \tag{6-122}$$

Note that under choked conditions, the exit velocity is $V = V^* = c^* = \sqrt{kRT^*/M_w}$, not $\sqrt{kRT_0/M_w}$. Sonic velocity must be evaluated at the exit temperature. For air, with $k = 1.4$, the critical pressure ratio p^*/p_0 is 0.5285 and the critical temperature ratio $T^*/T_0 = 0.8333$. Thus, for air discharging from 300 K, the temperature drops by 50 K (90 R). This large temperature decrease results from the conversion of internal energy into kinetic energy and is reversible. As the discharged jet decelerates in the external stagant gas, it recovers its initial enthalpy.

When it is desired to determine the discharge rate through a nozzle from upstream pressure p_0 to external pressure p_2, Equations (6-115) through (6-122) are best used as follows. The critical pressure is first determined from Eq. (6-119). If $p_2 > p^*$, then the flow is subsonic (subcritical, unchoked). Then $p_1 = p_2$ and M_1 may be obtained from Eq. (6-115). Substitution of M_1 into Eq. (6-118) then gives the desired mass velocity G. Eqs. (6-116) and (6-117) may be used to find the exit temperature and density. On the other hand, if $p_2 \le p^*$, then the flow is choked and $M_1 = 1$. Then $p_1 = p^*$, and the mass velocity is G^* obtained from Eq. (6-122). The exit temperature and density may be obtained from Eqs. (6-120) and (6-121).

When the flow is choked, $G = G^*$ is independent of external downstream pressure. Reducing the downstream pressure will not increase the flow. The mass flow rate under choking conditions is directly proportional to the upstream pressure.

Example 7: Flow through Frictionless Nozzle Air at p_0 and temperature $T_0 = 293$ K discharges through a frictionless nozzle to atmospheric pressure. Compute the discharge mass flux G, the pressure, temperature, Mach number, and velocity at the exit. Consider two cases: (1) $p_0 = 7 \times 10^5$ Pa absolute, and (2) $p_0 = 1.5 \times 10^5$ Pa absolute.

1. $p_0 = 7.0 \times 10^5$ Pa. For air with $k = 1.4$, the critical pressure ratio from Eq. (6-119) is $p^*/p_0 = 0.5285$ and $p^* = 0.5285 \times 7.0 \times 10^5 = 3.70 \times 10^5$ Pa. Since this is greater than the external atmospheric pressure $p_2 = 1.01 \times 10^5$ Pa, the flow is choked and the exit pressure is $p_1 = 3.70 \times 10^5$ Pa. The exit Mach number is 1.0, and the mass flux is equal to G^* given by Eq. (6-118).

$$G^* = 7.0 \times 10^5 \times \sqrt{\left(\frac{2}{1.4+1}\right)^{(1.4+1)/(1.4-1)} \left(\frac{1.4 \times 29}{8314 \times 293}\right)} = 1{,}650 \text{ kg/m}^2 \cdot \text{s}$$

The exit temperature, since the flow is choked, is

$$T^* = \left(\frac{T^*}{T_0}\right) T_0 = \left(\frac{2}{1.4+1}\right) \times 293 = 244 \text{ K}$$

The exit velocity is $V = Mc = c^* = \sqrt{kRT^*/M_w} = 313$ m/s.

2. $p_0 = 1.5 \times 10^5$ Pa. In this case $p^* = 0.79 \times 10^5$ Pa, which is less than p_2. Hence, $p_1 = p_2 = 1.01 \times 10^5$ Pa. The flow is unchoked (subsonic). Equation (6-115) is solved for the Mach number.

$$\frac{1.5 \times 10^5}{1.01 \times 10^5} = \left(1 + \frac{1.4-1}{2} M_1^2\right)^{1.4/(1.4-1)}$$

$$M_1 = 0.773$$

Substitution into Eq. (6-118) gives G.

$$G = 1.5 \times 10^5 \times \sqrt{\frac{1.4 \times 29}{8{,}314 \times 293}} \times \frac{0.773}{\left(1 + \left(\frac{1.4-1}{2}\right) \times 0.773^2\right)^{(1.4+1)/2(1.4-1)}} = 337 \text{ kg/m}^2 \cdot \text{s}$$

The exit temperature is found from Eq. (6-116) to be 261.6 K or −11.5°C. The exit velocity is

$$V = Mc = 0.773 \times \sqrt{\frac{1.4 \times 8314 \times 261.6}{29}} = 250 \text{ m/s}$$

Adiabatic Flow with Friction in a Duct of Constant Cross Section Integration of the differential forms of the continuity, momentum, and total energy equations for a perfect gas, assuming a constant friction factor, leads to a tedious set of simultaneous algebraic equations. These may be found in Shapiro (*Dynamics and Thermodynamics of Compressible Fluid Flow,* vol. I, Ronald Press, New York, 1953) or Zucrow and Hofmann (*Gas Dynamics,* vol. I, Wiley, New York, 1976). Lapple's (*Trans. AIChE.,* **39,** 395–432 [1943]) widely cited graphical presentation of the solution of these equations contained a subtle error, which was corrected by Levenspiel (*AIChE J.,* **23,** 402–403 [1977]). Levenspiel's graphical solutions are presented in Fig. 6-21. These charts refer to the physical situation illustrated in Fig. 6-22, where a perfect gas discharges from stagnation conditions in a large chamber through an isentropic nozzle followed by a duct of length L. The resistance parameter is $N = 4fL/D_H$, where f = Fanning friction factor and D_H = hydraulic diameter.

The exit Mach number M_2 may not exceed unity. $M_2 = 1$ corresponds to choked flow; sonic conditions may exist only at the pipe exit. The mass velocity G^* in the charts is the choked mass flux **for an isentropic nozzle** given by Eq. (6-118). For a pipe of finite length,

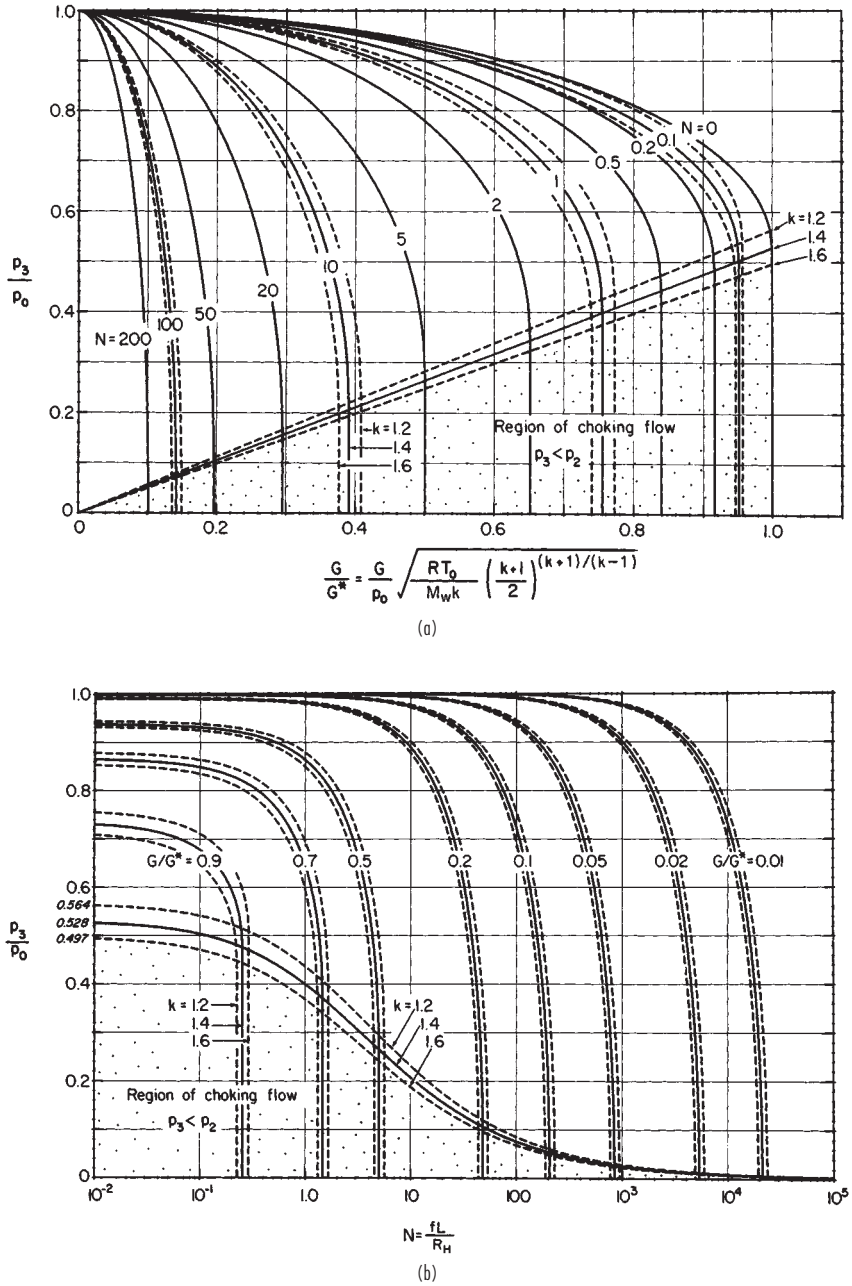

FIG. 6-21 Design charts for adiabatic flow of gases; (*a*) useful for finding the allowable pipe length for given flow rate; (*b*) useful for finding the discharge rate in a given piping system. (*From Levenspiel,* Am. Inst. Chem. Eng. J., ***23,*** *402* [*1977*].)

the mass flux is less than G^* under choking conditions. The curves in Fig. 6-21 become vertical at the choking point, where flow becomes independent of downstream pressure.

The equations for nozzle flow, Eqs. (6-114) through (6-118), remain valid for the nozzle section even in the presence of the discharge pipe. Equations (6-116) and (6-120), for the temperature variation, may also be used for the pipe, with M_2, p_2 replacing M_1, p_1 since they are valid for adiabatic flow, with or without friction.

The graphs in Fig. 6-21 are based on accurate calculations, but are

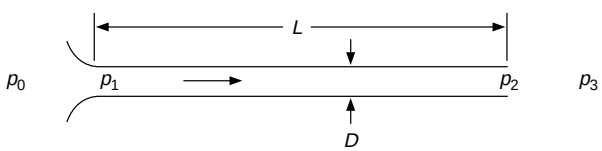

FIG. 6-22 Adiabatic compressible flow in a pipe with a well-rounded entrance.

difficult to interpolate precisely. While they are quite useful for rough estimates, precise calculations are best done using the equations for one-dimensional adiabatic flow with friction, which are suitable for computer programming. Let subscripts 1 and 2 denote two points along a pipe of diameter D, point 2 being downstream of point 1. From a given point in the pipe, where the Mach number is M, the additional length of pipe required to accelerate the flow to sonic velocity ($M = 1$) is denoted L_{max} and may be computed from

$$\frac{4fL_{max}}{D} = \frac{1 - M^2}{kM^2} + \frac{k+1}{2k} \ln \left(\frac{\frac{k+1}{2} M^2}{1 + \frac{k-1}{2} M^2} \right) \qquad (6\text{-}123)$$

With L = length of pipe between points 1 and 2, the change in Mach number may be computed from

$$\frac{4fL}{D} = \left(\frac{4fL_{max}}{D} \right)_1 - \left(\frac{4fL_{max}}{D} \right)_2 \qquad (6\text{-}124)$$

Eqs. (6-116) and (6-113), which are valid for adiabatic flow with friction, may be used to determine the temperature and speed of sound at points 1 and 2. Since the mass flux $G = \rho v = \rho c M$ is constant, and $\rho = PM_w/RT$, the pressure at point 2 (or 1) can be found from G and the pressure at point 1 (or 2).

The additional frictional losses due to pipeline fittings such as elbows may be added to the velocity head loss $N = 4fL/D_H$ using the same velocity head loss values as for incompressible flow. This works well for fittings which do not significantly reduce the channel cross-sectional area, but may cause large errors when the flow area is greatly reduced, as, for example, by restricting orifices. Compressible flow across restricting orifices is discussed in Sec. 10 of this *Handbook*. Similarly, elbows near the exit of a pipeline may choke the flow even though the Mach number is less than unity due to the nonuniform velocity profile in the elbow. For an abrupt contraction rather than rounded nozzle inlet, an additional 0.5 velocity head should be added to N. This is a reasonable approximation for G, but note that it allocates the additional losses to the pipeline, even though they are actually incurred in the entrance. It is an error to include one velocity head exit loss in N. The kinetic energy at the exit is already accounted for in the integration of the balance equations.

Example 8: Compressible Flow with Friction Losses Calculate the discharge rate of air to the atmosphere from a reservoir at 10^6 Pa gauge and 20°C through 10 m of straight 2-in Schedule 40 steel pipe (inside diameter = 0.0525 m), and 3 standard radius, flanged 90° elbows. Assume 0.5 velocity heads lost for the elbows.

For commercial steel pipe, with a roughness of 0.046 mm, the friction factor for fully rough flow is about 0.0047, from Eq. (6-38) or Fig. 6-9. It remains to be verified that the Reynolds number is sufficiently large to assume fully rough flow. Assuming an abrupt entrance with 0.5 velocity heads lost,

$$N = 4 \times 0.0047 \times \frac{10}{0.0525} + 0.5 + 3 \times 0.5 = 5.6$$

The pressure ratio p_3/p_0 is

$$\frac{1.01 \times 10^5}{(1 \times 10^6 + 1.01 \times 10^5)} = 0.092$$

From Fig. 6-21*b* at $N = 5.6$, $p_3/p_0 = 0.092$ and $k = 1.4$ for air, the flow is seen to be choked. At the choke point with $N = 5.6$ the critical pressure ratio p_2/p_0 is about 0.25 and G/G^* is about 0.48. Equation (6-122) gives

$$G^* = 1.101 \times 10^6 \times \sqrt{\left(\frac{2}{1.4+1} \right)^{(1.4+1)/(1.4-1)} \left(\frac{1.4 \times 29}{8{,}314 \times 293.15} \right)} = 2{,}600 \text{ kg/m}^2 \cdot \text{s}$$

Multiplying by $G/G^* = 0.48$ yields $G = 1{,}250$ kg/m$^2 \cdot$ s. The discharge rate is $w = GA = 1{,}250 \times \pi \times 0.0525^2/4 = 2.7$ kg/s.

Before accepting this solution, the Reynolds number should be checked. At the pipe exit, the temperature is given by Eq. (6-120) since the flow is choked. Thus, $T_2 = T^* = 244.6$ K. The viscosity of air at this temperature is about 1.6×10^{-5} Pa · s. Then

$$\text{Re} = \frac{DV\rho}{\mu} = \frac{DG}{\mu} = \frac{0.0525 \times 1{,}250}{1.6 \times 10^{-5}} = 4.1 \times 10^6$$

At the beginning of the pipe, the temperature is greater, giving greater viscosity and a Reynolds number of 3.6×10^6. Over the entire pipe length the Reynolds number is very large and the fully rough flow friction factor choice was indeed valid.

Once the mass flux G has been determined, Fig. 6-21*a* or 6-21*b* can be used to determine the pressure at any point along the pipe, simply by reducing $4fL/D_H$ and computing p_2 from the figures, given G, instead of the reverse. Charts for calculation between two points in a pipe with known flow and known pressure at either upstream or downstream locations have been presented by Loeb (*Chem. Eng.*, **76**[5], 179–184 [1969]) and for known downstream conditions by Powley (*Can. J. Chem. Eng.*, **36,** 241–245 [1958]).

Convergent/Divergent Nozzles (De Laval Nozzles) During frictionless adiabatic one-dimensional flow with changing cross-sectional area A the following relations are obeyed:

$$\frac{dA}{A} = \frac{dp}{\rho V^2}(1 - M^2) = \frac{1 - M^2}{M^2} \frac{d\rho}{\rho} = -(1 - M^2) \frac{dV}{V} \qquad (6\text{-}125)$$

Equation (6-125) implies that in converging channels, subsonic flows are accelerated and the pressure and density decrease. In diverging channels, subsonic flows are decelerated as the pressure and density increase. In subsonic flow, the converging channels act as nozzles and diverging channels as diffusers. In supersonic flows, the opposite is true. Diverging channels act as nozzles accelerating the flow, while converging channels act as diffusers decelerating the flow.

Figure 6-23 shows a converging/diverging nozzle. When p_2/p_0 is less than the critical pressure ratio (p^*/p_0), the flow will be subsonic in the converging portion of the nozzle, sonic at the throat, and supersonic in the diverging portion. At the throat, where the flow is critical and the velocity is sonic, the area is denoted A^*. The cross-sectional area and pressure vary with Mach number along the converging/diverging flow path according to the following equations for isentropic flow of a perfect gas:

$$\frac{A}{A^*} = \frac{1}{M} \left[\frac{2}{k+1} \left(1 + \frac{k-1}{2} M^2 \right) \right]^{(k+1)/2(k-1)} \qquad (6\text{-}126)$$

$$\frac{p_0}{p} = \left(1 + \frac{k-1}{2} M^2 \right)^{k/(k-1)} \qquad (6\text{-}127)$$

The temperature obeys the adiabatic flow equation for a perfect gas,

$$\frac{T_0}{T} = 1 + \frac{k-1}{2} M^2 \qquad (6\text{-}128)$$

Equation (6-128) does not require frictionless (isentropic) flow. The sonic mass flux through the throat is given by Eq. (6-122). With A set equal to the nozzle exit area, the exit Mach number, pressure, and temperature may be calculated. Only if the exit pressure equals the ambient discharge pressure is the ultimate expansion velocity reached in the nozzle. Expansion will be incomplete if the exit pressure exceeds the ambient discharge pressure; shocks will occur outside the nozzle. If the calculated exit pressure is less than the ambient discharge pressure, the nozzle is overexpanded and compression shocks within the expanding portion will result.

The shape of the converging section is a smooth trumpet shape similar to the simple converging nozzle. However, special shapes of the diverging section are required to produce the maximum supersonic exit velocity. Shocks result if the divergence is too rapid and excessive boundary layer friction occurs if the divergence is too shallow. See Liepmann and Roshko (*Elements of Gas Dynamics*, Wiley, New York, 1957, p. 284). If the nozzle is to be used as a thrust device, the diverg-

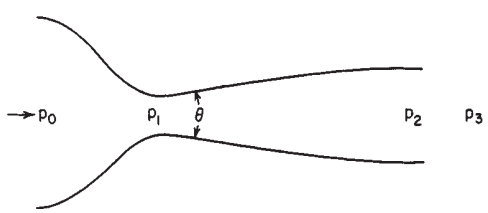

FIG. 6-23 Converging/diverging nozzle.

ing section can be conical with a total included angle of 30° (Sutton, *Rocket Propulsion Elements,* 2d ed., Wiley, New York, 1956). To obtain large exit Mach numbers, slot-shaped rather than axisymmetric nozzles are used.

MULTIPHASE FLOW

Multiphase flows, even when restricted to simple pipeline geometry, are in general quite complex, and several features may be identified which make them more complicated than single-phase flow. Flow pattern description is not merely an identification of laminar or turbulent flow. The relative quantities of the phases and the topology of the interfaces must be described. Because of phase density differences, vertical flow patterns are different from horizontal flow patterns, and horizontal flows are not generally axisymmetric. Even when phase equilibrium is achieved by good mixing in two-phase flow, the changing equilibrium state as pressure drops with distance, or as heat is added or lost, may require that interphase mass transfer, and changes in the relative amounts of the phases, be considered.

Wallis (*One-dimensional Two-phase Flow,* McGraw-Hill, New York, 1969) and Govier and Aziz present mass, momentum, mechanical energy, and total energy balance equations for two-phase flows. These equations are based on one-dimensional behavior for each phase. Such equations, for the most part, are used as a framework in which to interpret experimental data. Reliable prediction of multiphase flow behavior generally requires use of data or correlations. **Two-fluid modeling,** in which the full three-dimensional microscopic (partial differential) equations of motion are written for each phase, treating each as a continuum, occupying a volume fraction which is a continuous function of position, is a rapidly developing technique made possible by improved computational methods. For some relatively simple examples not requiring numerical computation, see Pearson (*Chem. Engr. Sci.,* **49,** 727–732 [1994]). Constitutive equations for two-fluid models are not yet sufficiently robust for accurate general-purpose two-phase flow computation, but may be quite good for particular classes of flows.

Liquids and Gases For cocurrent flow of liquids and gases in vertical (upflow), horizontal, and inclined pipes, a very large literature of experimental and theoretical work has been published, with less work on countercurrent and cocurrent vertical downflow. Much of the effort has been devoted to predicting flow patterns, pressure drop, and volume fractions of the phases, with emphasis on fully developed flow. In practice, many two-phase flows in process plants are not fully developed.

The most reliable methods for fully developed gas/liquid flows use **mechanistic models** to predict flow pattern, and use different pressure drop and void fraction estimation procedures for each flow pattern. Such methods are too lengthy to include here, and are well suited to incorporation into computer programs; commercial codes for gas/liquid pipeline flows are available. Some key references for mechanistic methods for flow pattern transitions and flow regime–specific pressure drop and void fraction methods include Taitel and Dukler (*AIChE J.,* **22,** 47–55 [1976]), Barnea, et al. (*Int. J. Multiphase Flow,* **6,** 217–225 [1980]), Barnea (*Int. J. Multiphase Flow,* **12,** 733–744 [1986]), Taitel, Barnea, and Dukler (*AIChE J.,* **26,** 345–354 [1980]), Wallis (*One-dimensional Two-phase Flow,* McGraw-Hill, New York, 1969), and Dukler and Hubbard (*Ind. Eng. Chem. Fundam.,* **14,** 337–347 [1975]). For preliminary or approximate calculations, **flow pattern maps** and flow regime–independent empirical correlations, are simpler and faster to use. Such methods for horizontal and vertical flows are provided in the following.

In **horizontal pipe,** flow patterns for fully developed flow have been reported in numerous studies. Transitions between flow patterns are gradual, and subjective owing to the visual interpretation of individual investigators. In some cases, statistical analysis of pressure fluctuations has been used to distinguish flow patterns. Figure 6-24 (Alves, *Chem. Eng. Progr.,* **50,** 449–456 [1954]) shows seven flow patterns for horizontal gas/liquid flow. **Bubble flow** is prevalent at high ratios of liquid to gas flow rates. The gas is dispersed as bubbles which move at velocity similar to the liquid and tend to concentrate near the top of the pipe at lower liquid velocities. **Plug flow** describes a pattern in which alternate plugs of gas and liquid move along the upper

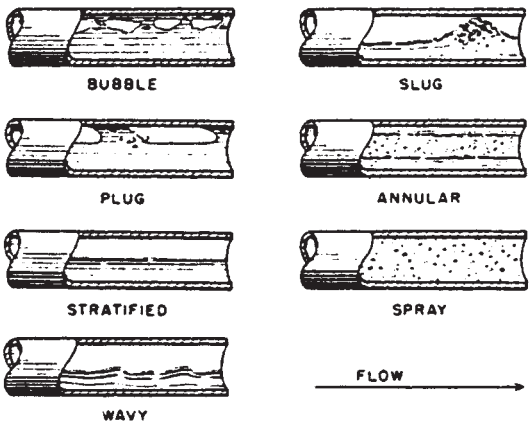

FIG. 6-24 Gas/liquid flow patterns in horizontal pipes. (*From Alves,* Chem. Eng. Progr., ***50,*** *449–456 [1954].*)

part of the pipe. In **stratified flow,** the liquid flows along the bottom of the pipe and the gas flows over a smooth liquid/gas interface. Similar to stratified flow, **wavy flow** occurs at greater gas velocities and has waves moving in the flow direction. When wave crests are sufficiently high to bridge the pipe, they form frothy slugs which move at much greater than the average liquid velocity. **Slug flow** can cause severe and sometimes dangerous vibrations in equipment because of impact of the high-velocity slugs against bends or other fittings. Slugs may also flood gas/liquid separation equipment.

In **annular flow,** liquid flows as a thin film along the pipe wall and gas flows in the core. Some liquid is entrained as droplets in the gas core. At very high gas velocities, nearly all the liquid is entrained as small droplets. This pattern is called **spray, dispersed,** or **mist flow.**

Approximate prediction of flow pattern may be quickly done using **flow pattern maps,** an example of which is shown in Fig. 6-25 (Baker, *Oil Gas J.,* **53**[12], 185–190, 192–195 [1954]). The Baker chart remains widely used; however, for critical calculations the mechanistic model methods referenced previously are generally preferred for their greater accuracy, especially for large pipe diameters and fluids with physical properties different from air/water at atmospheric pressure. In the chart,

$$\lambda = (\rho'_G \rho'_L)^{1/2} \tag{6-129}$$

$$\psi = \frac{1}{\sigma'} \left[\frac{\mu'_L}{(\rho'_L)^2} \right]^{1/3} \tag{6-130}$$

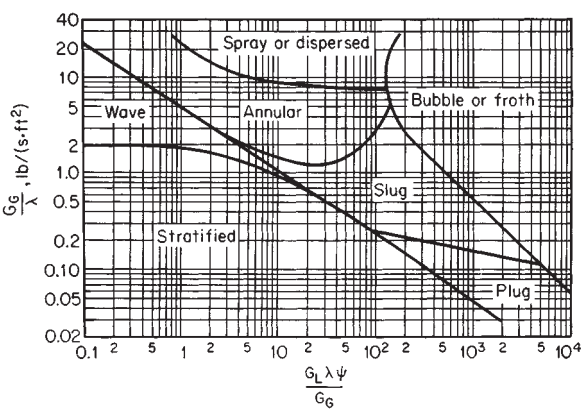

FIG. 6-25 Flow-pattern regions in cocurrent liquid/gas flow through horizontal pipes. To convert lbm/(ft² · s) to kg/(m² · s), multiply by 4.8824. (*From Baker,* Oil Gas J., ***53****[12], 185–190, 192, 195 [1954].*)

G_L and G_G are the liquid and gas mass velocities, μ'_L is the ratio of liquid viscosity to water viscosity, ρ'_G is the ratio of gas density to air density, ρ'_L is the ratio of liquid density to water density, and σ' is the ratio of liquid surface tension to water surface tension. The reference properties are at 20°C (68°F) and atmospheric pressure, water density 1,000 kg/m^3 (62.4 lbm/ft^3), air density 1.20 kg/m^3 (0.075 lbm/ft^3), water viscosity 0.001 Pa · s, (1.0 cp) and surface tension 0.073 N/m (0.0050 lbf/ft). The empirical parameters λ and ψ provide a crude accounting for physical properties. The Baker chart is dimensionally inconsistent since the dimensional quantity G_G/λ is plotted against a dimensionless one, $G_L\lambda\psi/G_G$, and so must be used with G_G in lbm/(ft^2 · s) units on the ordinate. To convert to kg/(m^2 · s), multiply by 4.8824.

Rapid approximate predictions of **pressure drop** for fully developed, incompressible horizontal gas/liquid flow may be made using the method of Lockhart and Martinelli (*Chem. Eng. Prog.*, **45,** 39–48 [1949]). First, the pressure drops that would be expected for each of the two phases as if flowing alone in single-phase flow are calculated. The Lockhart-Martinelli parameter X is defined in terms of the ratio of these pressure drops:

$$X = \left[\frac{(\Delta p/L)_L}{(\Delta p/L)_G}\right]^{1/2} \tag{6-131}$$

The two-phase pressure drop may be then be estimated from either of the single-phase pressure drops, using

$$\left(\frac{\Delta p}{L}\right)_{TP} = Y_L\left(\frac{\Delta p}{L}\right)_L \tag{6-132}$$

or

$$\left(\frac{\Delta p}{L}\right)_{TP} = Y_G\left(\frac{\Delta p}{L}\right)_G \tag{6-133}$$

where Y_L and Y_G are read from Fig. 6-26 as functions of X. The curve labels refer to the flow regime (laminar or turbulent) found for each of the phases flowing alone. The common turbulent-turbulent case is approximated well by

$$Y_L = 1 + \frac{20}{X} + \frac{1}{X^2} \tag{6-134}$$

Lockhart and Martinelli (ibid.) correlated pressure drop data from pipes 25 mm (1 in) in diameter or less within about ±50 percent. In general, the predictions are high for stratified, wavy, and slug flows and low for annular flow. The correlation can be applied to pipe diameters up to about 0.1 m (4 in) with about the same accuracy.

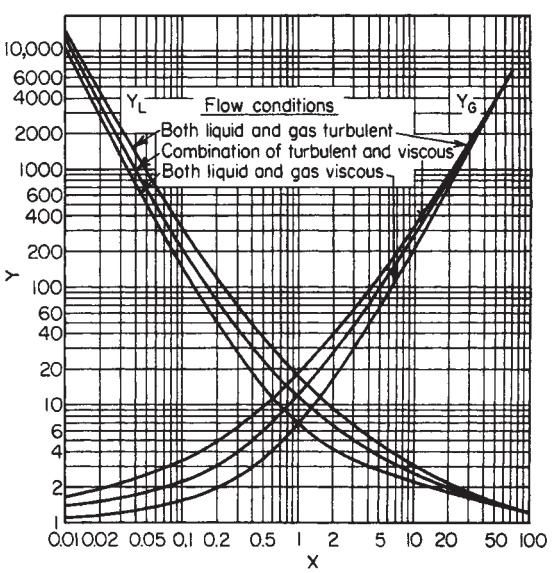

FIG. 6-26 Parameters for pressure drop in liquid/gas flow through horizontal pipes. (*Based on Lockhart and Martinelli,* Chem. Engr. Prog., ***45,*** *39 [1949].*)

The **volume fraction,** sometimes called **holdup,** of each phase in two-phase flow is generally not equal to its volumetric flow rate fraction, because of velocity differences, or **slip,** between the phases. For each phase, denoted by subscript i, the relations among superficial velocity V_i, in situ velocity v_i, volume fraction R_i, total volumetric flow rate Q_i, and pipe area A are

$$Q_i = V_i A = v_i R_i A \tag{6-135}$$

$$v_i = \frac{V_i}{R_i} \tag{6-136}$$

The **slip velocity** between gas and liquid is $v_s = v_G - v_L$. For two-phase gas/liquid flow, $R_L + R_G = 1$. A very common mistake in practice is to assume that in situ phase volume fractions are equal to input volume fractions.

For fully developed incompressible horizontal gas/liquid flow, a quick estimate for R_L may be obtained from Fig. 6-27, as a function of the Lockhart-Martinelli parameter X defined by Eq. (6-131). Indications are that liquid volume fractions may be overpredicted for liquids more viscous than water (Alves, *Chem. Eng. Prog.,* **50,** 449–456 [1954]), and underpredicted for pipes larger than 25 mm diameter (Baker, *Oil Gas J.,* **53**[12], 185–190, 192–195 [1954]).

A method for predicting pressure drop and volume fraction for **non-Newtonian fluids** in annular flow has been proposed by Eisenberg and Weinberger (*AIChE J.,* **25,** 240–245 [1979]). Das, Biswas, and Matra (*Can. J. Chem. Eng.,* **70,** 431–437 [1993]) studied holdup in both horizontal and vertical gas/liquid flow with non-Newtonian liquids. Farooqi and Richardson (*Trans Inst. Chem. Engrs.,* **60,** 292–305, 323–333 [1982]) developed correlations for holdup and pressure drop for gas/non-Newtonian liquid horizontal flow. They used a modified Lockhart-Martinelli parameter for non-Newtonian liquid holdup. They found that two-phase pressure drop may actually be less than the single-phase liquid pressure drop with shear thinning liquids in laminar flow.

Pressure drop data for a 1-in **feed tee** with the liquid entering the run and gas entering the branch are given by Alves (*Chem. Eng. Progr.,* **50,** 449–456 [1954]). Pressure drop and division of two-phase **annular flow in a tee** are discussed by Fouda and Rhodes (*Trans. Inst. Chem. Eng.* [*London*], **52,** 354–360 [1974]). Flow through tees can result in unexpected flow splitting. Further reading on gas/liquid flow through tees may be found in Mudde, Groen, and van den Akker (*Int. J. Multiphase Flow,* **19,** 563–573 [1993]); Issa and Oliveira (*Computers and Fluids,* **23,** 347–372 [1993]) and Azzopardi and Smith (*Int. J. Multiphase Flow,* **18,** 861–875 [1992]).

Results by Chenoweth and Martin (*Pet. Refiner,* **34**[10], 151–155 [1955]) indicate that single-phase data for **fittings** and **valves** can be used in their correlation for two-phase pressure drop. Smith, Murdock, and Applebaum (*J. Eng. Power,* **99,** 343–347 [1977]) evaluated existing correlations for two-phase flow of steam/water and other gas/liquid mixtures through sharp-edged **orifices** meeting ASTM standards for flow measurement. The correlation of Murdock (*J. Basic Eng.,* **84,** 419–433 [1962]) may be used for these orifices. See also Collins and Gacesa (*J. Basic Eng.,* **93,** 11–21 [1971]), for measurements with steam and water beyond the limits of this correlation.

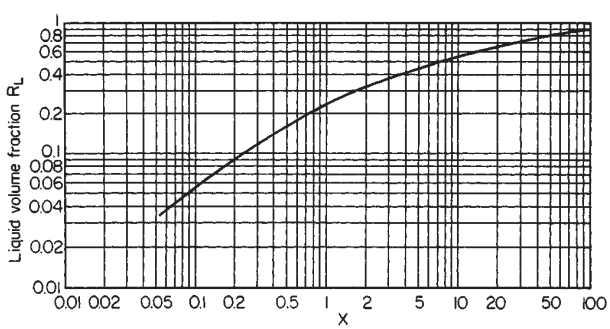

FIG. 6-27 Liquid volume fraction in liquid/gas flow through horizontal pipes. (*From Lockhart and Martinelli,* Eng. Prog., ***45,*** *39 [1949].*)

For pressure drop and holdup in **inclined pipe** with upward or downward flow, see Beggs and Brill (*J. Pet. Technol.*, **25,** 607–617 [1973]); the mechanistic model methods referenced above may also be applied to inclined pipes. Up to 10° from horizontal, upward pipe inclination has little effect on holdup (Gregory, *Can. J. Chem. Eng.*, **53,** 384–388 [1975]).

For fully developed incompressible **cocurrent upflow** of gases and liquids in **vertical pipes,** a variety of flow pattern terminologies and descriptions have appeared in the literature; some of these have been summarized and compared by Govier, Radford, and Dunn (*Can. J. Chem. Eng.*, **35,** 58–70 [1957]). One reasonable classification of patterns is illustrated in Fig. 6-28.

In **bubble flow,** gas is dispersed as bubbles throughout the liquid, but with some tendency to concentrate toward the center of the pipe. In **slug flow,** the gas forms large **Taylor bubbles** of diameter nearly equal to the pipe diameter. A thin film of liquid surrounds the Taylor bubble. Between the Taylor bubbles are liquid slugs containing some bubbles. **Froth** or **churn flow** is characterized by strong intermittency and intense mixing, with neither phase easily described as continuous or dispersed. There remains disagreement in the literature as to whether churn flow is a real fully developed flow pattern or is an indication of large entry length for developing slug flow (Zao and Dukler, *Int. J. Multiphase Flow,* **19,** 377–383 [1993]; Hewitt and Jayanti, *Int. J. Multiphase Flow,* **19,** 527–529 [1993]).

Ripple flow has an upward-moving wavy layer of liquid on the pipe wall; it may be thought of as a transition region to **annular, annular mist,** or **film flow,** in which gas flows in the core of the pipe while an annulus of liquid flows up the pipe wall. Some of the liquid is entrained as droplets in the gas core. **Mist flow** occurs when all the liquid is carried as fine drops in the gas phase; this pattern occurs at high gas velocities, typically 20 to 30 m/s (66 to 98 ft/s).

The correlation by Govier, et al. (*Can. J. Chem. Eng.*, **35,** 58–70 [1957]), Fig. 6-29, may be used for quick estimate of flow pattern.

Slip, or relative velocity between phases, occurs for vertical flow as well as for horizontal. No completely satisfactory, flow regime–independent correlation for volume fraction or holdup exists for vertical flow. Two frequently used flow regime–independent methods are those by Hughmark and Pressburg (*AIChE J.*, **7,** 677 [1961]) and Hughmark (*Chem. Eng. Prog.*, **58**[4], 62 [April 1962]). **Pressure drop** in **upflow** may be calculated by the procedure described in Hughmark (*Ind. Eng. Chem. Fundam.*, **2,** 315–321 [1963]). The mechanistic, flow regime–based methods are advisable for critical applications.

For **upflow** in **helically coiled tubes,** the flow pattern, pressure drop, and holdup can be predicted by the correlations of Banerjee, Rhodes, and Scott (*Can. J. Chem. Eng.*, **47,** 445–453 [1969]) and Akagawa, Sakaguchi, and Ueda (*Bull JSME,* **14,** 564–571 [1971]). Correlations for flow patterns in **downflow** in vertical pipe are given by Oshinowo and Charles (*Can. J. Chem. Eng.*, **52,** 25–35 [1974]) and Barnea, Shoham, and Taitel (*Chem. Eng. Sci.*, **37,** 741–744 [1982]). Use of **drift flux theory** for void fraction modeling in downflow is presented by Clark and Flemmer (*Chem. Eng. Sci.*, **39,** 170–173 [1984]). **Downward inclined** two-phase flow data and modeling are given by Barnea, Shoham, and Taitel (*Chem. Eng. Sci.*, **37,** 735–740 [1982]). Data for **downflow** in **helically coiled tubes** are presented by Casper (*Chem. Ing. Tech.*, **42,** 349–354 [1970]).

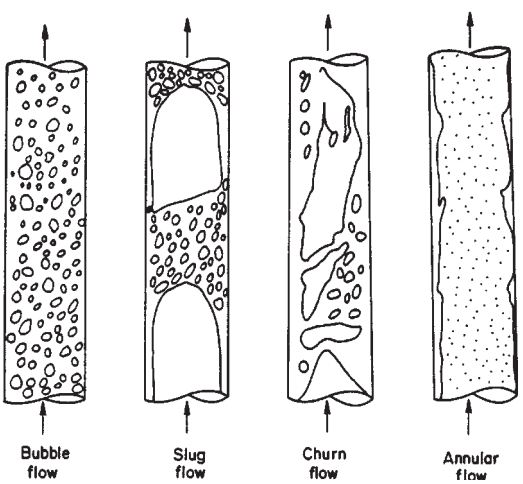

FIG. 6-28 Flow patterns in cocurrent upward vertical gas/liquid flow. (*From Taitel, Barnea, and Dukler,* AIChE J., **26,** 345–354 [1980]. *Reproduced by permission of the American Institute of Chemical Engineers © 1980 AIChE. All rights reserved.*)

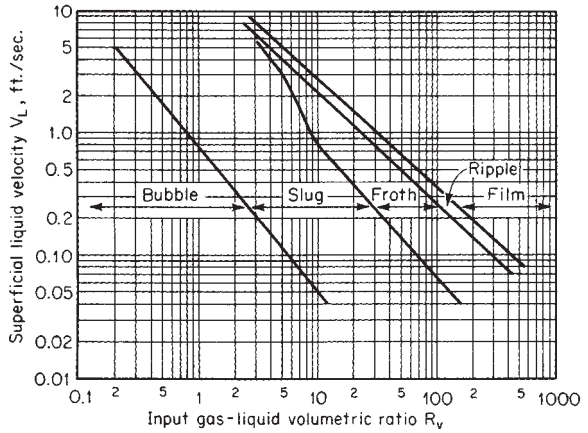

FIG. 6-29 Flow-pattern regions in cocurrent liquid/gas flow in upflow through vertical pipes. To convert ft/s to m/s, multiply by 0.3048. (*From Govier, Radford, and Dunn,* Can. J. Chem. Eng., **35,** 58–70 [1957].)

The entrance to a **drain** is flush with a horizontal surface, while the entrance to an **overflow** pipe is above the horizontal surface. When such pipes do not run full, considerable amounts of gas can be drawn down by the liquid. The amount of gas entrained is a function of pipe diameter, pipe length, and liquid flow rate, as well as the drainpipe outlet boundary condition. Extensive data on air entrainment and liquid head above the entrance as a function of water flow rate for pipe diameters from 43.9 to 148.3 mm (1.7 to 5.8 in) and lengths from about 1.22 to 5.18 m (4.0 to 17.0 ft) are reported by Kalinske (*Univ. Iowa Stud. Eng.*, Bull. 26, pp. 26–40 [1939–1940]). For heads greater than the critical, the pipes will run full with no entrainment. The critical head h for flow of water in drains and overflow pipes is given in Fig. 6-30. Kalinske's results show little effect of the height of protrusion of overflow pipes when the protrusion height is greater than about one pipe diameter. For conservative design, McDuffie (*AIChE J.*, **23,** 37–40 [1977]) recommends the following relation for minimum liquid height to prevent entrainment.

$$\mathrm{Fr} \le 1.6\left(\frac{h}{D}\right)^2 \tag{6-137}$$

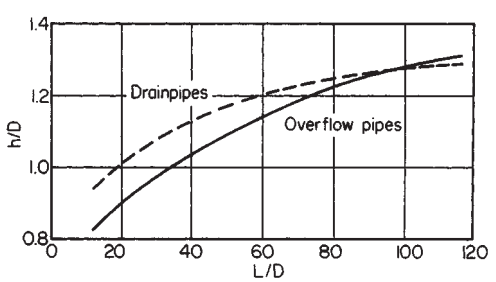

FIG. 6-30 Critical head for drain and overflow pipes. (*From Kalinske,* Univ. Iowa Stud. Eng., *Bull.* **26** *[1939–1940].*)

where the Froude number is defined by

$$\mathrm{Fr} \equiv \frac{V_L}{\sqrt{g(\rho_L - \rho_G)D/\rho_L}} \tag{6-138}$$

where g = acceleration due to gravity
V_L = liquid velocity in the drain pipe
ρ_L = liquid density
ρ_G = gas density
D = pipe inside diameter
h = liquid height

For additional information, see Simpson (*Chem. Eng.,* **75**(6), 192–214 [1968]). A critical Froude number of 0.31 to ensure vented flow is widely cited. Recent results (Thorpe, *3d Int. Conf. Multi-phase Flow,* The Hague, Netherlands, 18–20 May 1987, paper K2, and *4th Int. Conf. Multi-phase Flow,* Nice, France, 19–21 June 1989, paper K4) show hysteresis, with different critical Froude numbers for flooding and unflooding of drain pipes, and the influence of end effects. Wallis, Crowley, and Hagi (*Trans. ASME J. Fluids Eng.,* 405–413 [June 1977]) examine the conditions for horizontal discharge pipes to run full.

Flashing flow and **condensing flow** are two examples of multiphase flow with **phase change.** Flashing flow occurs when pressure drops below the bubble point pressure of a flowing liquid. A frequently used one-dimensional model for flashing flow through nozzles and pipes is the **homogeneous equilibrium model** which assumes that both phases move at the same in situ velocity, and maintain vapor/liquid equilibrium. It may be shown that a **critical flow** condition, analogous to sonic or critical flow during compressible gas flow, is given by the following expression for the mass flux G in terms of the derivative of pressure p with respect to mixture density ρ_m at constant entropy:

$$G_{\mathrm{crit}} = \rho_m \sqrt{\left(\frac{\partial p}{\partial \rho_m}\right)_s} \tag{6-139}$$

The corresponding acoustic velocity $\sqrt{(\partial p/\partial \rho_m)_s}$ is normally much less than the acoustic velocity for gas flow. The mixture density is given in terms of the individual phase densities and the **quality** (mass flow fraction vapor) x by

$$\frac{1}{\rho_m} = \frac{x}{\rho_G} + \frac{1-x}{\rho_L} \tag{6-140}$$

Choked and unchoked flow situations arise in pipes and nozzles in the same fashion for homogeneous equilibrium flashing flow as for gas flow. For nozzle flow from stagnation pressure p_0 to exit pressure p_1, the mass flux is given by

$$G^2 = -2\rho_{m1}^2 \int_{p_0}^{p_1} \frac{dp}{\rho_m} \tag{6-141}$$

The integration is carried out over an isentropic flash path: flashes at constant entropy must be carried out to evaluate ρ_m as a function of p. Experience shows that isenthalpic flashes provide good approximations unless the liquid mass fraction is very small. Choking occurs when G obtained by Eq. (6-141) goes through a maximum at a value of p_1 greater than the external discharge pressure. Equation (6-139) will also be satisfied at that point. In such a case the pressure at the nozzle exit equals the choking pressure and flashing shocks occur outside the nozzle exit.

For homogeneous flow in a pipe of diameter D, the differential form of the Bernoulli equation (6-15) rearranges to

$$\frac{dp}{\rho_m} + g\,dz + \frac{G^2}{\rho_m}\,d\frac{1}{\rho_m} + 2f\frac{dx'}{D}\frac{G^2}{\rho_m^2} = 0 \tag{6-142}$$

where x' is distance along the pipe. Integration over a length L of pipe assuming constant friction factor f yields

$$G^2 = \frac{-\int_{p_1}^{p_2} \rho_m\,dp - g\int_{z_1}^{z_2} \rho_m^2\,dz}{\ln(\rho_{m1}/\rho_{m2}) + 2fL/D} \tag{6-143}$$

Frictional pipe flow is not isentropic. Strictly speaking, the flashes must be carried out at constant $h + V^2/2 + gz$, where h is the enthalpy per unit mass of the two-phase flashing mixture. The flash calculations are fully coupled with the integration of the Bernoulli equation; the velocity V must be known at every pressure p to evaluate ρ_m. Computational routines, employing the thermodynamic and material balance features of flowsheet simulators, are the most practical way to carry out such flashing flow calculations, particularly when multicompent systems are involved. Significant simplification arises when the mass fraction liquid is large, for then the effect of the $V^2/2$ term on the flash splits may be neglected. If elevation effects are also negligible, the flash computations are decoupled from the Bernoulli equation integration. For many horizontal flashing flow calculations, this is satisfactory and the flash computatations may be carried out first, to find ρ_m as a function of p from p_1 to p_2, which may then be substituted into Eq. (6-143).

With flashes carried out along the appropriate thermodynamic paths, the formalism of Eqs. (6-139) through (6-143) applies to all homogeneous equilibrium compressible flows, including, for example, flashing flow, ideal gas flow, and nonideal gas flow. Equation (6-118), for example, is a special case of Eq. (6-141) where the quality $x = 1$ and the vapor phase is a perfect gas.

Various **nonequilibrium** and **slip flow** models have been proposed as improvements on the homogeneous equilibrium flow model. See, for example, Henry and Fauske (*Trans. ASME J. Heat Transfer,* 179–187 [May 1971]). Nonequilibrium and slip effects both increase computed mass flux for fixed pressure drop, compared to homogeneous equilibrium flow. For flow paths greater than about 100 mm, homogeneous equilibrium behavior appears to be the best assumption (Fischer, et al., *Emergency Relief System Design Using DIERS Technology,* AIChE, New York [1992]). For shorter flow paths, the best estimate may sometimes be given by linearly interpolating (as a function of length) between **frozen flow** (constant quality, no flashing) at 0 length and equilibrium flow at 100 mm.

In a series of papers by Leung and coworkers (*AIChE J.,* **32,** 1743–1746 [1986]; **33,** 524–527 [1987]; **34,** 688–691 [1988]; *J. Loss Prevention Proc. Ind.,* **2**[2], 78–86 [April 1989]; **3**(1), 27–32 [January 1990]; *Trans. ASME J. Heat Transfer,* **112,** 524–528, 528–530 [1990]; **113,** 269–272 [1991]) approximate techniques have been developed for homogeneous equilibrium calculations based on pseudo–equation of state methods for flashing mixtures.

Relatively less work has been done on **condensing flows.** Slip effects are more important for condensing than for flashing flows. Soliman, Schuster, and Berenson (*J. Heat Transfer,* **90,** 267–276 [1968]) give a model for condensing vapor in **horizontal pipe.** They assume the condensate flows as an annular ring. The Lockhart-Martinelli correlation is used for the frictional pressure drop. To this pressure drop is added an acceleration term based on homogeneous flow, equivalent to the $G^2 d(1/\rho_m)$ term in Eq. (6-142). Pressure drop is computed by integration of the incremental pressure changes along the length of pipe.

For **condensing vapor** in **vertical downflow,** in which the liquid flows as a thin annular film, the frictional contribution to the pressure drop may be estimated based on the gas flow alone, using the friction factor plotted in Fig. 6-31, where Re_G is the Reynolds number for the gas flowing alone (Bergelin, et al., *Proc. Heat Transfer Fluid Mech. Inst.,* ASME, June 22–24, 1949, pp. 19–28).

$$-\frac{dp}{dz} = \frac{2f'_G \rho_G V_G^2}{D} \tag{6-144}$$

To this should be added the $G_G^2 d(1/\rho_G)/dx$ term to account for velocity change effects.

Gases and Solids The flow of gases and solids in **horizontal** pipe is usually classified as either **dilute phase** or **dense phase** flow. Unfortunately, there is no clear dilineation between the two types of flow, and the *dense phase* description may take on more than one meaning, creating some confusion (Knowlton, et al., *Chem. Eng. Progr.,* **90**(4), 44–54 [April 1994]). For dilute phase flow, achieved at low solids-to-gas weight ratios (loadings), and high gas velocities, the solids may be fully suspended and fairly uniformly dispersed over the pipe cross section (homogeneous flow), particularly for low-density or small particle size solids. At lower gas velocities, the solids may bounce along the bottom of the pipe. With higher loadings and lower gas velocities, the particles may settle to the bottom of the pipe, form-

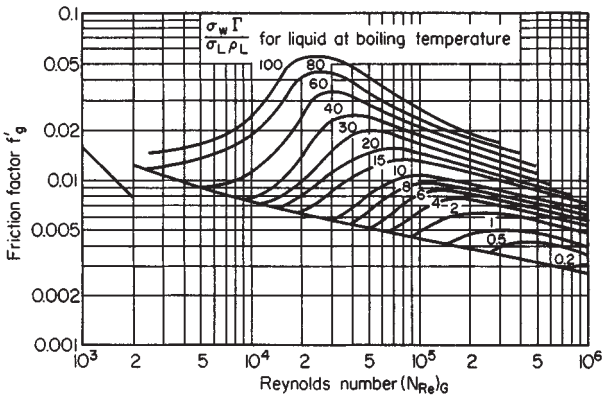

FIG. 6-31 Friction factors for condensing liquid/gas flow downward in vertical pipe. In this correlation $\Gamma/\rho L$ is in ft²/h. To convert ft²/h to m²/s, multiply by 0.00155. (*From Bergelin, et al.,* Proc. Heat Transfer Fluid Mech. Inst., *ASME, 1949, p. 19.*)

ing dunes, with the particles moving from dune to dune. In dense phase conveying, solids tend to concentrate in the lower portion of the pipe at high gas velocity. As gas velocity decreases, the solids may first form dense moving strands, followed by slugs. Discrete plugs of solids may be created intentionally by timed injection of solids, or the plugs may form spontaneously. Eventually the pipe may become blocked. For more information on flow patterns, see Coulson and Richardson (*Chemical Engineering,* vol. 2, 2d ed., Pergamon, New York, 1968, p. 583); Korn (*Chem. Eng.*, **57**[3], 108–111 [1950]); Patterson (*J. Eng. Power,* **81,** 43–54 [1959]); Wen and Simons (*AIChE J.,* **5,** 263–267 [1959]); and Knowlton, et al. (*Chem. Eng. Progr.,* **90**[4], 44–54 [April 1994]).

For the **minimum velocity** required to prevent formation of dunes or settled beds in **horizontal flow,** some data are given by Zenz (*Ind. Eng. Chem. Fundam.,* **3,** 65–75 [1964]), who presented a correlation for the minimum velocity required to keep particles from depositing on the bottom of the pipe. This rather tedious estimation procedure may also be found in Govier and Aziz, who provide additional references and discussion on transition velocities. In practice, the actual conveying velocities used in systems with loadings less than 10 are generally over 15 m/s, (49 ft/s) while for high loadings (>20) they are generally less than 7.5 m/s (24.6 ft/s) and are roughly twice the actual solids velocity (Wen and Simons, *AIChE J.,* **5,** 263–267 [1959]).

Total **pressure drop** for **horizontal gas/solid** flow includes acceleration effects at the entrance to the pipe and frictional effects beyond the entrance region. A great number of correlations for pressure gradient are available, none of which is applicable to all flow regimes. Govier and Aziz review many of these and provide recommendations on when to use them.

For **upflow** of gases and solids in **vertical pipes,** the **minimum conveying velocity** for low loadings may be estimated as twice the terminal settling velocity of the largest particles. Equations for terminal settling velocity are found in the "Particle Dynamics" subsection, following. **Choking** occurs as the velocity is dropped below the minimum conveying velocity and the solids are no longer transported, collapsing into solid plugs (Knowlton, et al., *Chem. Eng. Progr.,* **90**[4], 44–54 [April 1994]). See Smith (*Chem. Eng. Sci.,* **33,** 745–749 [1978]) for an equation to predict the onset of choking.

Total **pressure drop** for vertical upflow of gases and solids includes acceleration and frictional affects also found in horizontal flow, plus potential energy or hydrostatic effects. Govier and Aziz review many of the pressure drop calculation methods and provide recommendations for their use. See also Yang (*AIChE J.,* **24,** 548–552 [1978]).

Drag reduction has been reported for low loadings of small diameter particles (<60 μm diameter), ascribed to damping of turbulence near the wall (Rossettia and Pfeffer, *AIChE J.,* **18,** 31–39 [1972]).

For **dense phase** transport in **vertical pipes** of small diameter, see Sandy, Daubert, and Jones (*Chem. Eng. Prog.,* **66,** *Symp. Ser.,* 105, 133–142 [1970]).

The **flow of bulk solids through restrictions and bins** is discussed in symposium articles (*J. Eng. Ind.,* **91**[2] [1969]) and by Stepanoff (*Gravity Flow of Bulk Solids and Transportation of Solids in Suspension,* Wiley, New York, 1969). Some problems encountered in discharge from bins include (Knowlton, et al., *Chem. Eng. Progr.,* **90**[4], 44–54 [April 1994]) flow stoppage due to **ratholing** or **arching, segregation** of fine and coarse particles, **flooding** upon collapse of ratholes, and poor **residence time distribution** when **funnel flow** occurs.

Solid/liquid or **slurry** flow may be divided roughly into two categories based on settling behavior (see Etchells in Shamlou, *Processing of Solid-Liquid Suspensions,* Chap. 12, Butterworth-Heinemann, Oxford, 1993). **Nonsettling** slurries are made up of very fine, highly concentrated, or neutrally buoyant particles. These slurries are normally treated as pseudohomogeneous fluids. They may be quite viscous and are frequently non-Newtonian. Slurries of particles that tend to settle out rapidly are called **settling slurries** or **fast-settling slurries.** While in some cases positively buoyant solids are encountered, the present discussion will focus on solids which are more dense than the liquid.

For **horizontal flow** of **fast-settling slurries,** the following rough description may be made (Govier and Aziz). Ultrafine particles, 10 μm or smaller, are generally fully syspended and the particle distributions are not influenced by gravity. Fine particles 10 to 100 μm (3.3×10^{-5} to 33×10^{-5} ft) are usually fully suspended, but gravity causes concentration gradients. Medium-size particles, 100 to 1000 μm, may be fully suspended at high velocity, but often form a moving deposit on the bottom of the pipe. Coarse particles, 1,000 to 10,000 μm, (0.0033 to .033 ft), are seldom fully suspended and are usually conveyed as a moving deposit. Ultracoarse particles larger than 10,000 μm (0.033 ft) are not suspended at normal velocities unless they are unusually light.

Figure 6-32, taken from Govier and Aziz, schematically indicates four flow pattern regions superimposed on a plot of pressure gradient vs. mixture velocity $V_M = V_L + V_S = (Q_L + Q_S)/A$ where V_L and V_S are the superficial liquid and solid velocities, Q_L and Q_S are liquid and solid volumetric flow rates, and A is the pipe cross-sectional area. V_{M4} is the transition velocity above which a bed exists in the bottom of the pipe, part of which is stationary and part of which moves by **saltation,** with the upper particles tumbling and bouncing over one another, often with formation of dunes. With a broad particle-size distribution, the finer particles may be fully suspended. Near V_{M4}, the pressure gra-

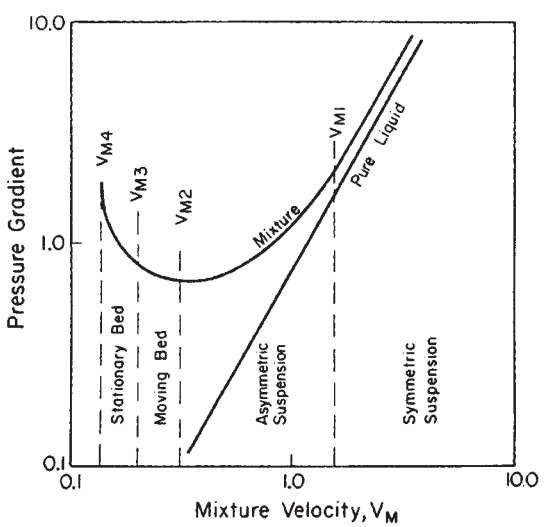

FIG. 6-32 Flow pattern regimes and pressure gradients in horizontal slurry flow. (*From Govier and Aziz,* The Flow of Complex Mixtures in Pipes, *Van Nostrand Reinhold, New York, 1972.*)

dient rapidly increases as V_M decreases. Above V_{M3}, the entire bed moves. Above V_{M2}, the solids are fully suspended; that is, there is no deposit, moving or stationary, on the bottom of the pipe. However, the concentration distribution of solids is asymmetric. This flow pattern is the most frequently used for fast-settling slurry transport. Typical mixture velocities are in the range of 1 to 3 m/s (3.3 to 9.8 ft/s). The minimum in the pressure gradient is found to be near V_{M2}. Above V_{M1}, the particles are symmetrically distributed, and the pressure gradient curve is nearly parallel to that for the liquid by itself.

The most important transition velocity, often regarded as the minimum transport or conveying velocity for settling slurries, is V_{M2}. The Durand equation (Durand, Minnesota Int. Hydraulics Conf., *Proc.*, 89, Int. Assoc. for Hydraulic Research [1953]; Durand and Condolios, *Proc. Colloq. On the Hyd. Transport of Solids in Pipes, Nat. Coal Board* [UK], Paper IV, 39–35 [1952]) gives the minimum transport velocity as

$$V_{M2} = F_L[2gD(s-1)]^{0.5} \tag{6-145}$$

where g = acceleration of gravity
D = pipe diameter
$s = \rho_S/\rho_L$ = ratio of solid to liquid density
F_L = a factor influenced by particle size and concentration

Probably F_L is a function of particle Reynolds number and concentration, but Fig. 6-33 gives Durand's empirical correlation for F_L as a function of particle diameter and the input, feed volume fraction solids, $C_S = Q_S/(Q_S + Q_L)$. The form of Eq. (6-145) may be derived from turbulence theory, as shown by Davies (*Chem. Eng. Sci.*, **42,** 1667–1670 [1987]).

No single correlation for **pressure drop** in horizontal solid/liquid flow has been found satisfactory for all particle sizes, densities, concentrations, and pipe sizes. However, with reference to Fig. 6-32, the following simplifications may be considered. The minimum pressure gradient occurs near V_{M2} and for conservative purposes it is generally desirable to exceed V_{M2}. When V_{M2} is exceeded, a rough guide for pressure drop is 25 percent greater than that calculated assuming that the slurry behaves as a psuedohomogeneous fluid with the density of the mixture and the viscosity of the liquid. Above the transition velocity to symmetric suspension, V_{M1}, the pressure drop closely approaches the pseudohomogeneous pressure drop. The following

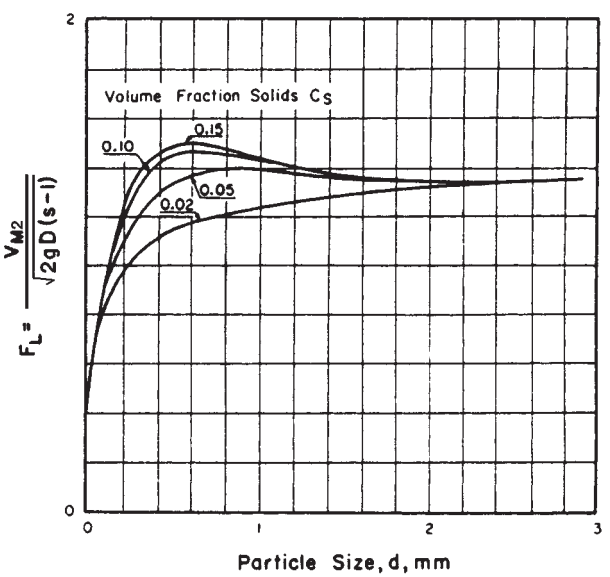

FIG. 6-33 Durand factor for minimum suspension velocity. (*From Govier and Aziz,* The Flow of Complex Mixtures in Pipes, *Van Nostrand Reinhold, New York, 1972.*)

correlation by Spells (*Trans. Inst. Chem. Eng.* [*London*], **33,** 79–84 [1955]) may be used for V_{M1}.

$$V_{M1}^2 = 0.075\left(\frac{DV_{M1}\rho_M}{\mu}\right)^{0.775} gD_S(s-1) \tag{6-146}$$

where D = pipe diameter
D_S = particle diameter (such that 85 percent by weight of particles are smaller than D_S
ρ_M = the slurry mixture density
μ = liquid viscosity
$s = \rho_S/\rho_L$ = ratio of solid to liquid density

Between V_{M2} and V_{M1} the concentration of solids gradually becomes more uniform in the vertical direction. This transition has been modeled by several authors as a concentration gradient where turbulent diffusion balances gravitational settling. See, for example, Karabelas (*AIChE J.*, **23,** 426–434 [1977]).

Published correlations for pressure drop are frequently very complicated and tedious to use, may not offer significant accuracy advantages over the simple guide given here, and many of them are applicable only for velocities above V_{M2}. One which does include the effect of sliding beds is due to Gaessler (Doctoral Dissertation, Technische Hochshule, Karlsruhe, Germany [1967]; reproduced by Govier and Aziz, pp. 668–669). Turian and Yuan (*AIChE J.*, **23,** 232–243 [1977]; see also Turian and Oroskar, *AIChE J.*, **24,** 1144 [1978]) segregated a large body of data into four flow regime groups and developed empirical correlations for predicting pressure drop in each flow regime.

Pressure drop data for the flow of **paper stock** in pipes are given in the data section of *Standards of the Hydraulic Institute* (Hydraulic Institute, 1965). The flow behavior of fiber suspensions is discussed by Bobkowicz and Gauvin (*Chem. Eng. Sci.*, **22,** 229–241 [1967]), Bugliarello and Daily (*TAPPI*, **44,** 881–893 [1961]), and Daily and Bugliarello (*TAPPI*, **44,** 497–512 [1961]).

In **vertical flow** of fast-settling slurries, the in situ concentration of solids with density greater than the liquid will exceed the feed concentration $C = Q_S/(Q_S + Q_L)$ for upflow and will be smaller than C for downflow. This results from slip between the phases. The **slip velocity,** the difference between the in situ average velocities of the two phases, is roughly equal to the terminal settling velocity of the solids in the liquid. Specification of the slip velocity for a pipe of a given diameter, along with the phase flow rates, allows calculation of in situ volume fractions, average velocities, and holdup ratios by simple material balances. Slip velocity may be affected by particle concentration and by turbulence conditions in the liquid. **Drift-flux theory,** a framework incorporating certain functional forms for empirical expressions for slip velocity, is described by Wallis (*One-Dimensional Two-Phase Flow*, McGraw-Hill, New York, 1969). **Minimum transport velocity** for upflow for design purposes is usually taken as twice the particle settling velocity. **Pressure drop** in vertical pipe flow includes the effects of kinetic and potential energy (elevation) changes and friction. Rose and Duckworth (*The Engineer*, **227**[5,903], 392 [1969]; **227**[5,904], 430 [1969]; **227**[5,905], 478 [1969]; see also Govier and Aziz, pp. 487–493) have developed a calculation procedure including all these effects, which may be applied not only to vertical solid/liquid flow, but also to gas/solid flow and to horizontal flow.

For fast-settling slurries, ensuring conveyance is usually the key design issue while pressure drop is somewhat less important. For **nonsettling slurries** conveyance is not an issue, because the particles do not separate from the liquid. Here, viscous and rheological behavior, which control pressure drop, take on critical importance.

Fine particles, often at high concentration, form nonsettling slurries for which useful design equations can be developed by treating them as homogeneous fluids. These fluids are usually very viscous and often non-Newtonian. Shear-thinning and Bingham plastic behavior are common; dilatancy is sometimes observed. Rheology of such fluids must in general be empirically determined, although theoretical results are available for some very limited circumstances. Further discussion of both fast-settling and nonsettling slurries may be found in Shook (in Shamlou, *Processing of Solid-Liquid Suspensions,* Chap. 11, Butterworth-Heinemann, Oxford, 1993).

FLUID DISTRIBUTION

Uniform fluid distribution is essential for efficient operation of chemical-processing equipment such as contactors, reactors, mixers, burners, heat exchangers, extrusion dies, and textile-spinning chimneys. To obtain optimum distribution, proper consideration must be given to flow behavior in the distributor, flow conditions upstream and downstream of the distributor, and the distribution requirements of the equipment. Even though the principles of fluid distribution have been well developed for more than three decades, they are frequently overlooked by equipment designers, and a significant fraction of process equipment needlessly suffers from maldistribution. In this subsection, guides for the design of various types of fluid distributors, taking into account only the flow behavior within the distributor, are given.

Perforated-Pipe Distributors The simple perforated pipe or sparger (Fig. 6-34) is a common type of distributor. As shown, the flow distribution is uniform; this is the case in which pressure recovery due to kinetic energy or momentum changes, frictional pressure drop along the length of the pipe, and pressure drop across the outlet holes have been properly considered. In typical turbulent flow applications, inertial effects associated with velocity changes may dominate frictional losses in determining the pressure distribution along the pipe, unless the length between orifices is large. Application of the momentum or mechanical energy equations in such a case shows that the pressure inside the pipe increases with distance from the entrance of the pipe. If the outlet holes are uniform in size and spacing, the discharge flow will be biased toward the closed end. Disturbances upstream of the distributor, such as pipe bends, may increase or decrease the flow to the holes at the beginning of the distributor. When frictional pressure drop dominates the inertial pressure recovery, the distribution is biased toward the feed end of the distributor.

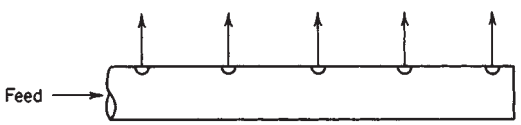

FIG. 6-34 Perforated-pipe distributor.

For turbulent flow, with roughly uniform distribution, assuming a constant friction factor, the combined effect of friction and inertial (momentum) pressure recovery is given by

$$\Delta p = \left(\frac{4fL}{3D} - 2K\right)\frac{\rho V_i^2}{2} \qquad \text{(discharge manifolds)} \qquad (6\text{-}147)$$

where Δp = net pressure drop over the length of the distributor
L = pipe length
D = pipe diameter
f = Fanning friction factor
V_i = distributor inlet velocity

The factor K would be 1 in the case of full momentum recovery, or 0.5 in the case of negligible viscous losses in the portion of flow which remains in the pipe after the flow divides at a takeoff point (Denn, pp. 126–127). Experimental data (Van der Hegge Zijnen, *Appl. Sci. Res.*, **A3,** 144–162 [1951–1953]; and Bailey, *J. Mech. Eng. Sci.*, **17,** 338–347 [1975]), while scattered, show that K is probably close to 0.5 for discharge manifolds. For inertially dominated flows, Δp will be negative. For **return manifolds** the recovery factor K is close to 1.0, and the pressure drop between the first hole and the exit is given by

$$\Delta p = \left(\frac{4fL}{3D} + 2K\right)\frac{\rho V_e^2}{2} \qquad \text{(return manifolds)} \qquad (6\text{-}148)$$

where V_e is the pipe exit velocity.

One means to obtain a desired uniform distribution is to make the average pressure drop across the holes Δp_o large compared to the pressure variation over the length of pipe Δp. Then, the relative variation in pressure drop across the various holes will be small, and so will be the variation in flow. When the area of an individual hole is small compared to the cross-sectional area of the pipe, hole pressure drop may be expressed in terms of the discharge coefficient C_o and the velocity across the hole V_o as

$$\Delta p_o = \frac{1}{C_o^2}\frac{\rho V_o^2}{2} \qquad (6\text{-}149)$$

Provided C_o is the same for all the holes, the *percent maldistribution*, defined as the percentage variation in flow between the first and last holes, may be estimated reasonably well for small maldistribution by (Senecal, *Ind. Eng. Chem.*, **49,** 993–997 [1957])

$$\text{Percent maldistribution} = 100\left(1 - \sqrt{\frac{\Delta p_o - |\Delta p|}{\Delta p_o}}\right) \qquad (6\text{-}150)$$

This equation shows that for 5 percent maldistribution, the pressure drop across the holes should be about 10 times the pressure drop over the length of the pipe. For discharge manifolds with $K = 0.5$ in Eq. (6-147), and with $4fL/3D \ll 1$, the pressure drop across the holes should be 10 times the inlet velocity head, $\rho V_i^2/2$ for 5 percent maldistribution. This leads to a simple design equation.

Discharge manifolds, $4fL/3D \ll 1$, 5% maldistribution:

$$\frac{V_o}{V_i} = \frac{A_p}{A_o} = \sqrt{10}C_o \qquad (6\text{-}151)$$

Here A_p = pipe cross-sectional area and A_o is the *total* hole area of the distributor. Use of large hole velocity to pipe velocity ratios promotes perpendicular discharge streams. In practice, there are many cases where the $4fL/3D$ term will be less than unity but not close to zero. In such cases, Eq. (6-151) will be conservative, while Eqs. (6-147), (6-149), and (6-150) will give more accurate design calculations. In cases where $4fL/(3D) > 2$, friction effects are large enough to render Eq. (6-151) nonconservative. When significant variations in f along the length of the distributor occur, calculations should be made by dividing the distributor into small enough sections that constant f may be assumed over each section.

For return manifolds with $K = 1.0$ and $4fL/(3D) \ll 1$, 5 percent maldistribution is achieved when hole pressure drop is 20 times the pipe exit velocity head.

Return manifolds, $4fL/3D \ll 1$, 5% maldistribution:

$$\frac{V_o}{V_e} = \frac{A_p}{A_o} = \sqrt{20}C_o \qquad (6\text{-}152)$$

When $4fL/3D$ is not negligible, Eq. (6-152) is not conservative and Eqs. (6-148), (6-149), and (6-150) should be used.

One common misconception is that good distribution is always provided by high pressure drop, so that increasing flow rate improves distribution by increasing pressure drop. Conversely, it is mistakenly believed that turndown of flow through a perforated pipe designed using Eqs. (6-151) and (6-152) will cause maldistribution. However, when the distribution is nearly uniform, decreasing the flow rate decreases Δp and Δp_o in the same proportion, and Eqs. (6-151) and (6-152) are still satisfied, preserving good distribution independent of flow rate, as long as friction losses remain small compared to inertial (velocity head change) effects. Conversely, increasing the flow rate through a distributor with severe maldistribution will not generally produce good distribution.

Often, the pressure drop required for design flow rate is unacceptably large for a distributor pipe designed for uniform velocity through uniformly sized and spaced orifices. Several measures may be taken in such situations. These include the following:

1. Taper the diameter of the distributor pipe so that the pipe velocity and velocity head remain constant along the pipe, thus substantially reducing pressure variation in the pipe.
2. Vary the hole size and/or the spacing between holes to compensate for the pressure variation along the pipe. This method may be sensitive to flow rate and a distributor optimized for one flow rate may suffer increased maldistribution as flow rate deviates from design rate.
3. Feed or withdraw from both ends, reducing the pipe flow velocity head and required hole pressure drop by a factor of 4.

The orifice discharge coefficient C_o is usually taken to be about 0.62. However, C_o is dependent on the ratio of hole diameter to pipe diameter, pipe wall thickness to hole diameter ratio, and pipe velocity to hole velocity ratio. As long as all these are small, the coefficient 0.62 is generally adequate.

Example 9: Pipe Distributor A 3-in schedule 40 (inside diameter 7.793 cm) pipe is to be used as a distributor for a flow of 0.010 m^3/s of water ($\rho = 1{,}000$ kg/m^3, $\mu = 0.001$ Pa · s). The pipe is 0.7 m long and is to have 10 holes of uniform diameter and spacing along the length of the pipe. The distributor pipe is submerged. Calculate the required hole size to limit maldistribution to 5 percent, and estimate the pressure drop across the distributor.

The inlet velocity computed from $V_i = Q/A = 4Q/(\pi D^2)$ is 2.10 m/s, and the inlet Reynolds number is

$$\mathrm{Re} = \frac{DV_i\rho}{\mu} = \frac{0.07793 \times 2.10 \times 1000}{0.001} = 1.64 \times 10^5$$

For commercial pipe with roughness $\epsilon = 0.046$ mm, the friction factor is about 0.0043. Approaching the last hole, the flow rate, velocity and Reynolds number are about one-tenth their inlet values. At Re = 16,400 the friction factor f is about 0.0070. Using an average value of $f = 0.0057$ over the length of the pipe, $4fL/3D$ is 0.068 and may reasonably be neglected so that Eq. (6-151) may be used. With $C_o = 0.62$,

$$\frac{V_o}{V_i} = \frac{A_p}{A_o} = \sqrt{10}C_o = \sqrt{10} \times 0.62 = 1.96$$

With pipe cross-sectional area $A_p = 0.00477$ m^2, the total hole area is 0.00477/1.96 = 0.00243 m^2. The area and diameter of each hole are then 0.00243/10 = 0.000243 m^2 and 1.76 cm. With $V_o/V_i = 1.96$, the hole velocity is 1.96 × 2.10 = 4.12 m/s and the pressure drop across the holes is obtained from Eq. (6-149).

$$\Delta p_o = \frac{1}{C_o^2}\frac{\rho V_o^2}{2} = \frac{1}{0.62^2} \times \frac{1000(4.12)^2}{2} = 22{,}100 \text{ Pa}$$

Since the hole pressure drop is 10 times the pressure variation in the pipe, the total pressure drop from the inlet of the distributor may be taken as approximately 22,100 Pa.

Further detailed information on pipe distributors may be found in Senecal (*Ind. Eng. Chem.*, **49,** 993–997 [1957]). Much of the information on tapered manifold design has appeared in the pulp and paper literature (Spengos and Kaiser, *TAPPI,* **46**[3], 195–200 [1963]; Madeley, *Paper Technology,* **9**[1], 35–39 [1968]; Mardon, et al., *TAPPI,* **46**[3], 172–187 [1963]; Mardon, et al., *Pulp and Paper Magazine of Canada,* **72**[11], 76–81 [November 1971]; Trufitt, *TAPPI,* **58**[11], 144–145 [1975]).

Slot Distributors These are generally used in sheeting dies for extrusion of films and coatings and in air knives for control of thickness of a material applied to a moving sheet. A simple slotted pipe for turbulent flow conditions may give severe maldistribution because of nonuniform discharge velocity, but also because this type of design does not readily give perpendicular discharge (Koestel and Tuve, *Heat. Piping Air Cond.,* **20**[1], 153–157 [1948]; Senecal, *Ind. Eng. Chem.,* **49,** 993–997 [1957]; Koestel and Young, *Heat. Piping Air Cond.,* **23**[7], 111–115 [1951]). For slots in tapered ducts where the duct cross-sectional area decreases linearly to zero at the far end, the discharge angle will be constant along the length of the duct (Koestel and Young, ibid.). One way to ensure an almost perpendicular discharge is to have the ratio of the area of the slot to the cross-sectional area of the pipe equal to or less than 0.1. As in the case of perforated-pipe distributors, pressure variation within the slot manifold and pressure drop across the slot must be carefully considered.

In practice, the following methods may be used to keep the diameter of the pipe to a minimum consistent with good performance (Senecal, *Ind. Eng. Chem.*, **49,** 993–997 [1957]):

1. Feed from both ends.
2. Modify the cross-sectional design (Fig. 6-35); the slot is thus farther away from the influence of feed-stream velocity.
3. Increase pressure drop across the slot; this can be accomplished by lengthening the lips (Fig. 6-35).
4. Use screens (Fig. 6-35) to increase overall pressure drop across the slot.

Design considerations for air knives are discussed by Senecal (ibid.). Design procedures for extrusion dies when the flow is laminar, as with highly viscous fluids, are presented by Bernhardt (*Processing of Thermoplastic Materials,* Rheinhold, New York, 1959, pp. 248–281).

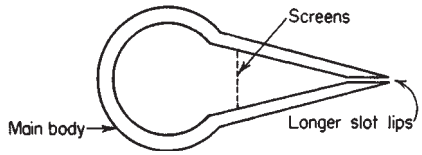

FIG. 6-35 Modified slot distributor.

Turning Vanes In applications such as ventilation, the discharge profile from slots can be improved by turning vanes. The tapered duct is the most amenable for turning vanes because the discharge angle remains constant. One way of installing the vanes is shown in Fig. 6-36. The vanes should have a depth twice the spacing (*Heating, Ventilating, Air Conditioning Guide,* vol. 38, American Society of Heating, Refrigerating and Air-Conditioning Engineers, 1960, pp. 282–283) and a curvature at the upstream end of the vanes of a circular arc which is tangent to the discharge angle θ of a slot without vanes and perpendicular at the downstream or discharge end of the vanes (Koestel and Young, *Heat. Piping Air Cond.,* **23**[7], 111–115 [1951]). Angle θ can be estimated from

$$\cot\theta = \frac{C_d A_s}{A_d} \tag{6-153}$$

where A_s = slot area
A_d = duct cross-sectional area at upstream end
C_d = discharge coefficient of slot

Vanes may be used to improve velocity distribution and reduce frictional loss in bends, when the ratio of bend turning radius to pipe diameter is less than 1.0. For a miter bend with low-velocity flows, simple circular arcs (Fig. 6-37) can be used, and with high-velocity flows, vanes of special airfoil shapes are required. For additional details and references, see Ower and Pankhurst (*The Measurement of Air Flow,* Pergamon, New York, 1977, p. 102); Pankhurst and Holder (*Wind-Tunnel Technique,* Pitman, London, 1952, pp. 92–93); Rouse (*Engineering Hydraulics,* Wiley, New York, 1950, pp. 399–401); and Jorgensen (*Fan Engineering,* 7th ed., Buffalo Forge Co., Buffalo, 1970, pp. 111, 117, 118).

Perforated Plates and Screens A nonuniform velocity profile in turbulent flow through channels or process equipment can be smoothed out to any desired degree by adding sufficient uniform resistance, such as perforated plates or screens across the flow channel, as shown in Fig. 6-38. Stoker (*Ind. Eng. Chem.,* **38,** 622–624 [1946]) provides the following equation for the effect of a uniform resistance on velocity profile:

$$\frac{V_{2,\max}}{V} = \sqrt{\frac{(V_{1,\max}/V)^2 + \alpha_2 - \alpha_1 + \alpha_2 K}{1 + K}} \tag{6-154}$$

Here, V is the area average velocity, K is the number of velocity heads of pressure drop provided by the uniform resistance, $\Delta p = K\rho V^2/2$, and α is the velocity profile factor used in the mechanical energy bal-

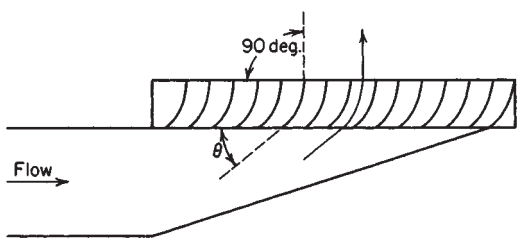

FIG. 6-36 Turning vanes in a slot distributor.

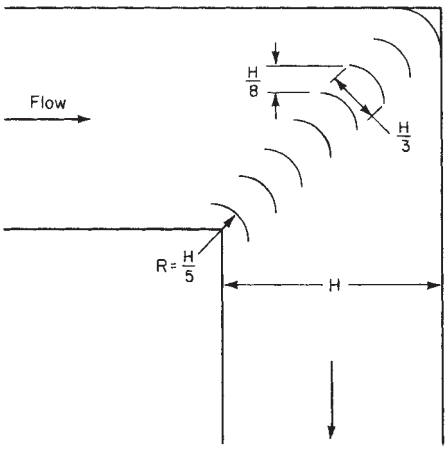

FIG. 6-37 Miter bend with vanes.

ance, Eq. (6-13). It is ratio of the area average of the cube of the velocity, to the cube of the area average velocity V. The shape of the exit velocity profile appears twice in Eq. (6-154), in $V_{2,max}/V$ and α_2. Typically, K is on the order of 10, and the desired exit velocity profile is fairly uniform so that $\alpha_2 \sim 1.0$ may be appropriate. Downstream of the resistance, the velocity profile will gradually reestablish the fully developed profile characteristic of the Reynolds number and channel shape. The screen or perforated plate open area required to produce the resistance K may be computed from Eqs. (6-107) or (6-111).

Screens and other flow restrictions may also be used to suppress stream swirl and turbulence (Loehrke and Nagib, *J. Fluids Eng.*, **98,** 342–353 [1976]). Contraction of the channel, as in a venturi, provides further reduction in turbulence level and flow nonuniformity.

Beds of Solids A suitable depth of solids can be used as a fluid distributor. As for other types of distribution devices, a pressure drop of 10 velocity heads is typically used, here based on the superficial velocity through the bed. There are several substantial disadvantages to use of particle beds for flow distribution. Heterogeneity of the bed may actually worsen rather than improve distribution. In general, uniform flow may be found only downstream of the point in the bed where sufficient pressure drop has occurred to produce uniform flow. Therefore, inefficiency results when the bed also serves reaction or mass transfer functions, as in catalysts, adsorbents, or tower packings for gas/liquid contacting, since portions of the bed are bypassed. In the case of trickle flow of liquid downward through column packings, inlet distribution is critical since the bed itself is relatively ineffective in distributing the liquid. Maldistribution of flow through packed beds also arises when the ratio of bed diameter to particle size is less than 10 to 30.

Other Flow Straightening Devices Other devices designed to produce uniform velocity or reduce swirl, sometimes with reduced pressure drop, are available. These include both commercial devices of proprietary design and devices discussed in the literature. For pipeline flows, see the references under flow inverters and static mixing elements previously discussed in the "Incompressible Flow in Pipes and Channels" subsection. For large area changes, as at the entrance to a vessel, it is sometimes necessary to diffuse the momentum of the inlet jet discharging from the feed pipe in order to produce a more uniform velocity profile within the vessel. Methods for this application exist, but remain largely in the domain of proprietary, commercial design.

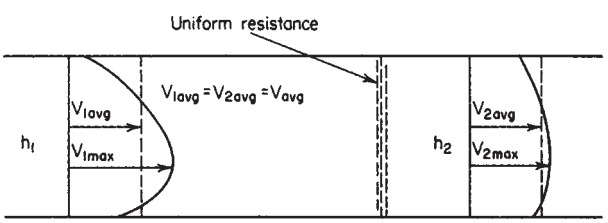

FIG. 6-38 Smoothing out a nonuniform profile in a channel.

FLUID MIXING

Mixing of fluids is a discipline of fluid mechanics. Fluid motion is used to accelerate the otherwise slow processes of diffusion and conduction to bring about uniformity of concentration and temperature, blend materials, facilitate chemical reactions, bring about intimate contact of multiple phases, and so on. As the subject is too broad to cover fully, only a brief introduction and some references for further information are given here.

Several texts are available. These include Harnby, Edwards, and Nienow (*Mixing in the Process Industries*, 2d ed., Butterworths, London, 1992), Oldshue (*Fluid Mixing Technology,* McGraw-Hill, New York, 1983), Tatterson (*Fluid Mixing and Gas Dispersion in Agitated Tanks,* McGraw-Hill, New York, 1991), Uhl and Gray (*Mixing,* vols. I–III, Academic, New York, 1966, 1967, 1986), and Nagata (*Mixing: Principles and Applications,* Wiley, New York, 1975). A good overview of stirred tank agitation is given in the series of articles from *Chemical Engineering* (110–114, Dec. 8, 1975; 139–145, Jan. 5, 1976; 93–100, Feb. 2, 1976; 102–110, Apr. 26, 1976; 144–150, May 24, 1976; 141–148, July 19, 1976; 89–94, Aug. 2, 1976; 101–108, Aug. 30, 1976; 109–112, Sept. 27, 1976; 119–126, Oct. 25, 1976; 127–133, Nov. 8, 1976).

Process mixing is commonly carried out in pipeline and vessel geometries. The terms **radial mixing** and **axial mixing** are commonly used. Axial mixing refers to mixing of materials which pass a given point at different times, and thus leads to **backmixing.** For example, backmixing or axial mixing occurs in stirred tanks where fluid elements entering the tank at different times are intermingled. Mixing of elements initially at different axial positions in a pipeline is axial mixing. Radial mixing occurs between fluid elements passing a given point at the same time, as, for example, between fluids mixing in a pipeline tee.

Turbulent flow, by means of the chaotic eddy motion associated with velocity fluctuation, is conducive to rapid mixing and, therefore, is the preferred flow regime for mixing. **Laminar mixing** is carried out when high viscosity makes turbulent flow impractical.

Stirred Tank Agitation Turbine impeller agitators, of a variety of shapes, are used for stirred tanks, predominantly in turbulent flow. Figure 6-39 shows typical stirred tank configurations and time-averaged flow patterns for axial flow and radial flow impellers. In order to prevent formation of a **vortex,** four vertical baffles are normally installed. These cause top-to-bottom mixing and prevent mixing-ineffective swirling motion.

For a given impeller and tank geometry, the impeller Reynolds number determines the flow pattern in the tank:

$$\mathrm{Re}_I = \frac{D^2 N \rho}{\mu} \tag{6-155}$$

where D = impeller diameter, N = rotational speed, and ρ and μ are the liquid density and viscosity. Rotational speed N is typically reported in revolutions per minute, or revolutions per second in SI units. Radians per second are almost never used. Typically, $\mathrm{Re}_I > 10^4$ is required for fully turbulent conditions throughout the tank. A wide transition region between laminar and turbulent flow occurs over the range $10 < \mathrm{Re}_I < 10^4$.

The power P drawn by the impeller is made dimensionless in a group called the power number:

$$\mathrm{N}_P = \frac{P}{\rho N^3 D^5} \tag{6-156}$$

Figure 6-40 shows power number vs. impeller Reynolds number for a typical configuration. The similarity to the friction factor vs. Reynolds number behavior for pipe flow is significant. In laminar flow, the power number is inversely proportional to Reynolds number, reflecting the dominance of viscous forces over inertial forces. In turbulent flow, where inertial forces dominate, the power number is nearly constant.

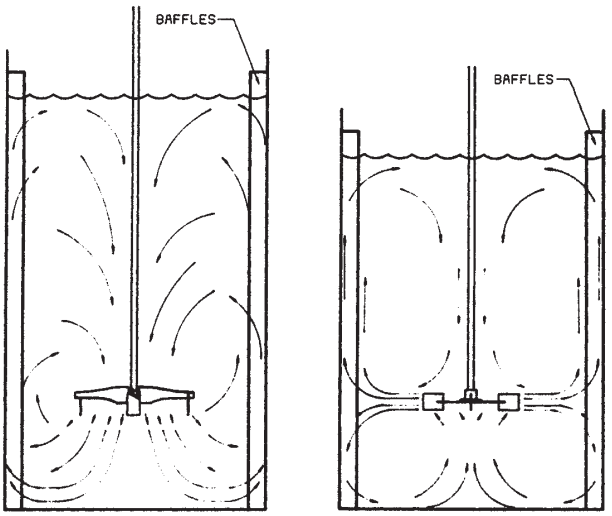

FIG. 6-39 Typical stirred tank configurations, showing time-averaged flow patterns for axial flow and radial flow impellers. (*From Oldshue,* Fluid Mixing Technology, *McGraw-Hill, New York, 1983.*)

Impellers are sometimes viewed as pumping devices; the total volumetric flow rate Q discharged by an impeller is made dimensionless in a pumping number:

$$N_Q = \frac{Q}{ND^3} \tag{6-157}$$

Blend time t_b, the time required to achieve a specified maximum standard deviation of concentration after injection of a tracer into a stirred tank, is made dimensionless by multiplying by the impeller rotational speed:

$$N_b = t_b N \tag{6-158}$$

Dimensionless pumping number and blend time are independent of Reynolds number under fully turbulent conditions. The magnitude of concentration fluctuations from the final well-mixed value in batch mixing decays exponentially with time.

The design of mixing equipment depends on the desired process result. There is often a tradeoff between operating cost, which depends mainly on power, and capital cost, which depends on agitator size and torque. For some applications bulk flow throughout the vessel is desired, while for others high local turbulence intensity is required. Multiphase systems introduce such design criteria as solids suspension and gas dispersion. In very viscous systems, helical ribbons, extruders, and other specialized equipment types are favored over turbine agitators.

Pipeline Mixing Mixing may be carried out with **mixing tees, inline** or **motionless mixing elements,** or in empty pipe. In the latter case, large pipe lengths may be required to obtain adequate mixing. Coaxially injected streams require lengths on the order of 100 pipe diameters. Coaxial mixing in turbulent single-phase flow is characterized by the turbulent diffusivity (eddy diffusivity) D_E which determines the rate of radial mixing. Davies (*Turbulence Phenomena,* Academic, New York, 1972) provides an equation for D_E which may be rewritten as

$$D_E \sim 0.015 DV\mathrm{Re}^{-0.125} \tag{6-159}$$

where D = pipe diameter
V = average velocity
Re = pipe Reynolds number, $DV\rho/\mu$
ρ = density
μ = viscosity

Properly designed tee mixers, with due consideration given to main stream and injected stream momentum, are capable of producing high degrees of uniformity in just a few diameters. Forney (*Jet Injection for Optimum Pipeline Mixing,* in "Encyclopedia of Fluid Mechanics," vol. 2., Chap. 25, Gulf Publishing, 1986) provides a thorough discussion of tee mixing. Inline or motionless mixers are generally of

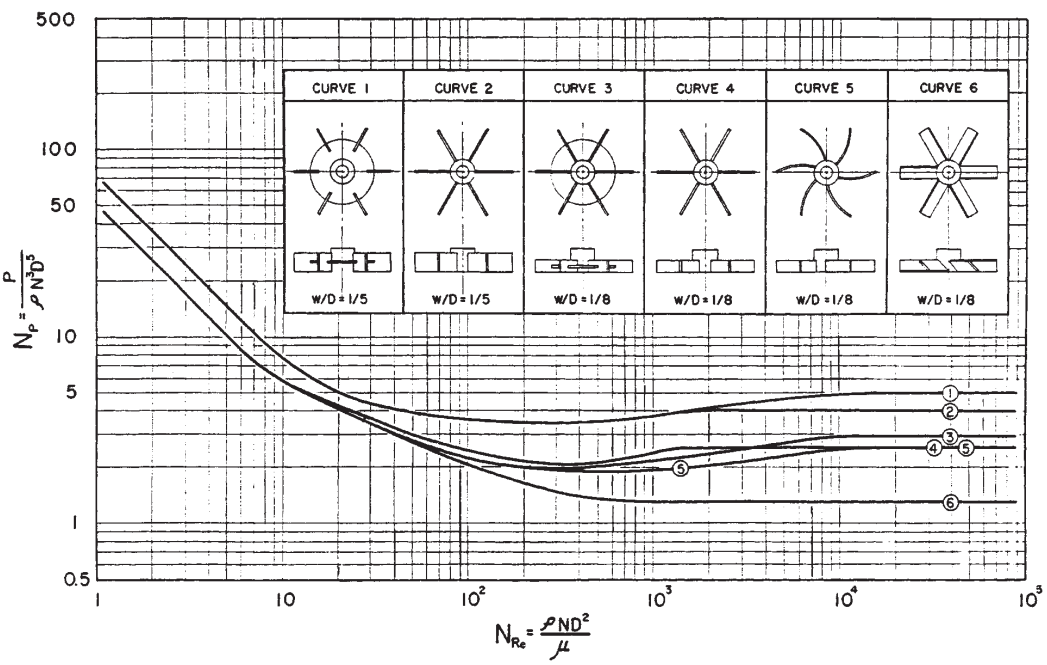

FIG. 6-40 Dimensionless power number in stirred tanks. (*Reprinted with permission from Bates, Fondy, and Corpstein,* Ind. Eng. Chem. Process Design Develop., **2,** *310 [1963].*)

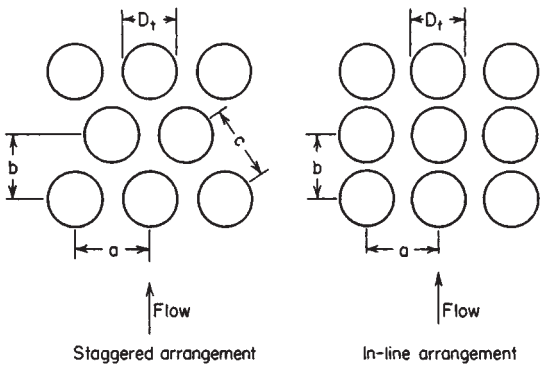

FIG. 6-41 Tube-bank configurations.

proprietary commercial design, and may be selected for viscous or turbulent, single or multiphase mixing applications. They substantially reduce required pipe length for mixing.

TUBE BANKS

Pressure drop across tube banks may not be correlated by means of a single, simple friction factor—Reynolds number curve, owing to the variety of tube configurations and spacings encountered, two of which are shown in Fig. 6-41. Several investigators have allowed for configuration and spacing by incorporating spacing factors in their friction factor expressions or by using multiple friction factor plots. Commercial computer codes for heat-exchanger design are available which include features for estimating pressure drop across tube banks.

Turbulent Flow The correlation by Grimison (*Trans. ASME,* **59,** 583–594 [1937]) is recommended for predicting pressure drop for turbulent flow (Re ≥ 2,000) across staggered or in-line tube banks for tube spacings [(a/D_t), (b/D_t)] ranging from 1.25 to 3.0. The pressure drop is given by

$$\Delta p = \frac{4 f N_r \rho V_{\max}^2}{2} \tag{6-160}$$

where f = friction factor
N_r = number of rows of tubes in the direction of flow
ρ = fluid density
$V_{\max}$ = fluid velocity through the minimum area available for flow.

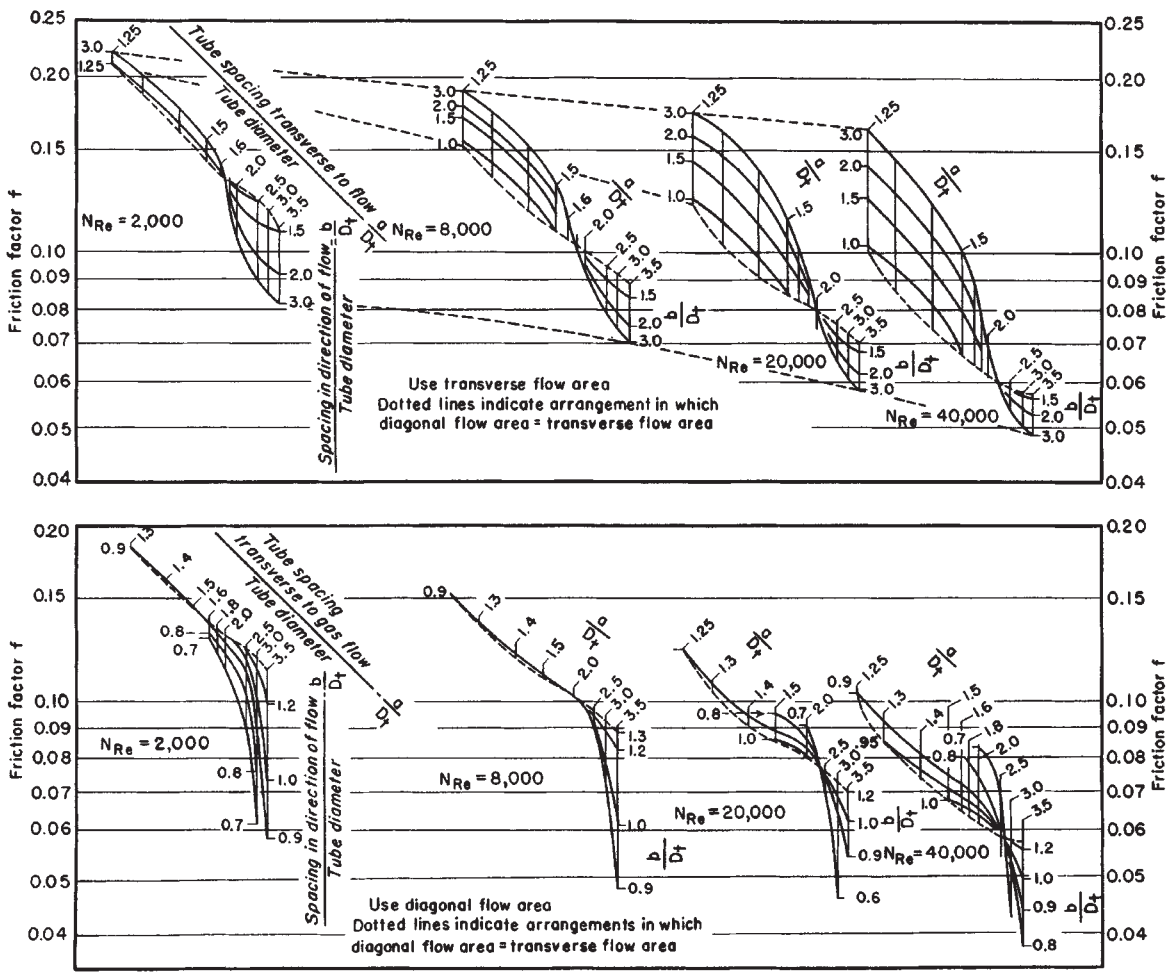

FIG. 6-42 Upper chart: Friction factors for staggered tube banks with minimum fluid flow area in transverse openings. Lower chart: Friction factors for staggered tube banks with minimum fluid flow area in diagonal openings. (*From Grimison,* Trans. ASME, ***59,*** *583 [1937].*)

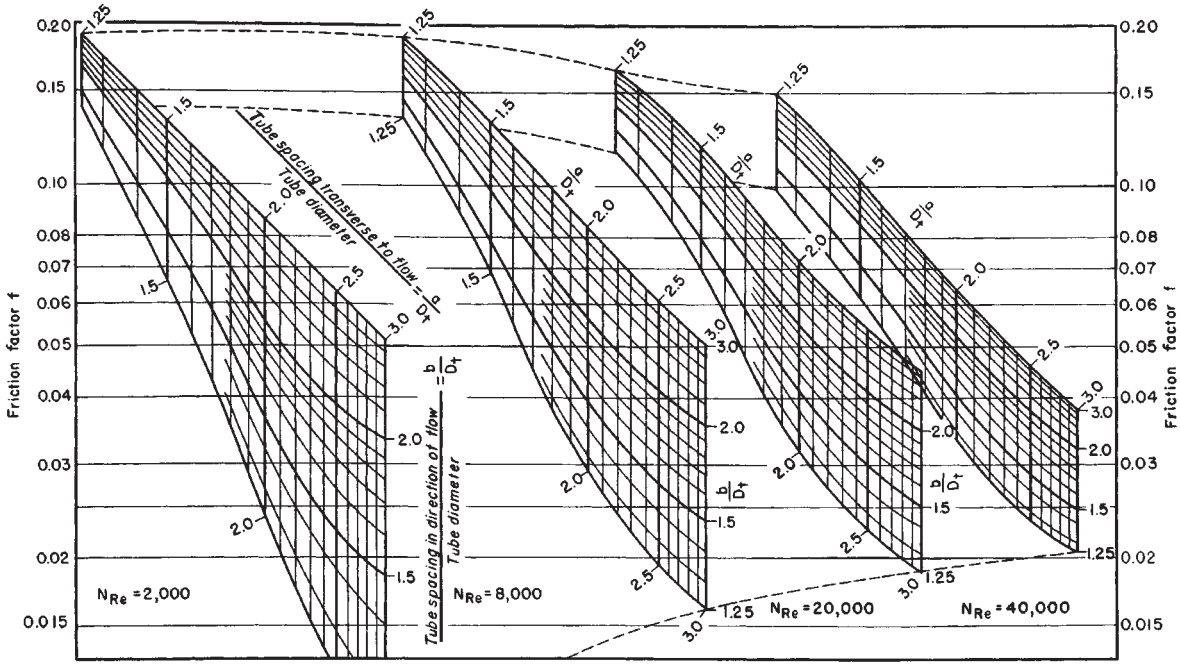

FIG. 6-43 Friction factors for in-line tube banks. (*From Grimison,* Trans. ASME, ***59,*** *583 [1937].*)

For banks of **staggered tubes,** the friction factor for isothermal flow is obtained from Fig. (6-42). Each "fence" (group of parametric curves) represents a particular Reynolds number defined as

$$\mathrm{Re} = \frac{D_t V_{\max} \rho}{\mu} \qquad (6\text{-}161)$$

where D_t = tube outside diameter and μ = fluid viscosity. The numbers along each fence represent the transverse and inflow-direction spacings. The upper chart is for the case in which the minimum area for flow is in the transverse openings, while the lower chart is for the case in which the minimum area is in the diagonal openings. In the latter case, $V_{\max}$ is based on the area of the diagonal openings and N_r is the number of rows in the direction of flow minus 1. A critical comparison of this method with all the data available at the time showed an average deviation of the order of ±15 percent. (Boucher and Lapple, *Chem. Eng. Prog.,* **44,** 117–134 [1948]). For tube spacings greater than 3 tube diameters, the correlation by Gunter and Shaw (*Trans. ASME,* **67,** 643–660 [1945]) can be used as an approximation. As an **approximation,** the pressure drop can be taken as 0.72 velocity head (based on $V_{\max}$ per row of tubes for tube spacings commonly encountered in practice (Lapple, et al., *Fluid and Particle Mechanics,* University of Delaware, Newark, 1954).

For banks of **in-line tubes,** f for isothermal flow is obtained from Fig. 6-43. Average deviation from available data is on the order of ±15 percent. For tube spacings greater than $3D_t$, the charts of Gram, Mackey, and Monroe (*Trans. ASME,* **80,** 25–35 [1958]) can be used. As an **approximation,** the pressure drop can be taken as 0.32 velocity head (based on $V_{\max}$) per row of tubes (Lapple, et al., *Fluid and Particle Mechanics,* University of Delaware, Newark, 1954).

For turbulent flow through **shallow** tube banks, the average friction factor per row will be somewhat greater than indicated by Figs. 6-42 and 6-43, which are based on 10 or more rows depth. A 30 percent increase per row for 2 rows, 15 percent per row for 3 rows and 7 percent per row for 4 rows can be taken as the maximum likely to be encountered (Boucher and Lapple, *Chem. Eng. Prog.,* **44,** 117–134 [1948]).

For a **single row of tubes,** the friction factor is given by Curve B in Fig. 6-44 as a function of tube spacing. This curve is based on the the data of several experimenters, all adjusted to a Reynolds number of 10,000. The values should be substantially independent of Re for $1{,}000 < \mathrm{Re} < 100{,}000$.

For **extended surfaces,** which include fins mounted perpendicularly to the tubes or spiral-wound fins, pin fins, plate fins, and so on, friction data for the specific surface involved should be used. For details, see Kays and London (*Compact Heat Exchangers,* 2d ed., McGraw-Hill, New York, 1964). If specific data are unavailable, the correlation by Gunter and Shaw (*Trans. ASME,* **67,** 643–660 [1945]) may be used as an approximation.

When a large temperature change occurs in a gas flowing across a

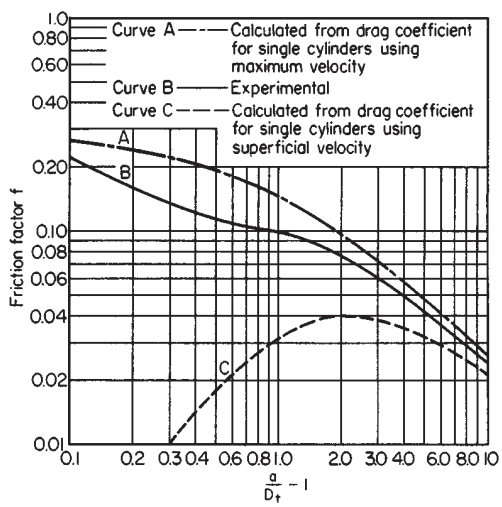

FIG. 6-44 Friction factors vs. transverse spacing for single row of tubes. (*From Boucher and Lapple,* Chem. Eng. Prog., ***44,*** *117 [1948].*)

tube bundle, gas properties should be evaluated at the mean temperature

$$T_m = T_t + K\,\Delta T_{lm} \tag{6-162}$$

where T_t = average tube-wall temperature
K = constant
ΔT_{lm} = log-mean temperature difference between the gas and the tubes.

Values of K averaged from the recommendations of Chilton and Genereaux (*Trans. AIChE,* **29,** 151–173 [1933]) and Grimison (*Trans. ASME,* **59,** 583–594 [1937]) are as follows: for in-line tubes, 0.9 for cooling and –0.9 for heating; for staggered tubes, 0.75 for cooling and –0.8 for heating.

For nonisothermal flow of **liquids** across tube bundles, the friction factor is increased if the liquid is being cooled and decreased if the liquid is being heated. The factors previously given for nonisothermal flow of liquids in pipes ("Incompressible Flow in Pipes and Channels") should be used.

For two-phase gas/liquid horizontal cross flow through tube banks, the method of Diehl and Unruh (*Pet. Refiner,* **37**[10], 124–128 [1958]) is available.

Transition Region This region extends roughly over the range $200 < \mathrm{Re} < 2{,}000$. Figure 6-45 taken from Bergelin, Brown, and Doberstein (*Trans. ASME,* **74,** 953–960 [1952]) gives curves for friction factor f_T for five different configurations. Pressure drop for liquid flow is given by

$$\Delta p = \frac{4 f_T N_r \rho V_{\max}^2}{2}\left(\frac{\mu_s}{\mu_b}\right)^{0.14} \tag{6-163}$$

where N_r = number of major restrictions encountered in flow through the bank (equal to number of rows when minimum flow area occurs in transverse openings, and to number of rows minus 1 when it occurs in the diagonal openings); ρ = fluid density; $V_{\max}$ = velocity through minimum flow area; μ_s = fluid viscosity at tube-surface temperature and μ_b = fluid viscosity at average bulk temperature. This method gives the friction factor within about ±25 percent.

Laminar Region Bergelin, Colburn, and Hull (*Univ. Delaware Eng. Exp. Sta. Bull.,* **2** [1950]) recommend the following equations for pressure drop with laminar flow ($\mathrm{Re}_v < 100$) of liquids across banks of plain tubes with pitch ratios P/D_t of 1.25 and 1.50:

$$\Delta p = \frac{280 N_r}{\mathrm{Re}_v}\left(\frac{D_t}{P}\right)^{1.6}\left(\frac{\mu_s}{\mu_b}\right)^{m}\left(\frac{\rho V_{\max}^2}{2}\right) \tag{6-164}$$

$$m = \frac{0.57}{(\mathrm{Re}_v)^{0.25}} \tag{6-165}$$

where $\mathrm{Re}_v = D_v V_{\max}\rho/\mu_b$; D_v = volumetric hydraulic diameter [(4 × free-bundle volume)/(exposed surface area of tubes)]; P = pitch (= a for in-line arrangements, = a or c [whichever is smaller] for staggered arrangements), and other quantities are as defined following Eq. (6-163). Bergelin, et al. (ibid.) show that pressure drop per row is independent of the number of rows in the bank with laminar flow. The pressure drop is predicted within about ±25 percent.

The validity of extrapolating Eq. (6-164) to pitch ratios larger than 1.50 is unknown. The correlation of Gunter and Shaw (*Trans. ASME,* **67,** 643–660 [1945]) may be used as an approximation in such cases.

For laminar flow of non-Newtonian fluids across tube banks, see Adams and Bell (*Chem. Eng. Prog., Symp. Ser.,* **82,** 133–145 [1968]).

Flow-induced **tube vibration** occurs at critical fluid velocities through tube banks, and is to be avoided because of the severe damage that can result. Methods to predict and correct vibration problems may be found in Eisinger (*Trans. ASME J. Pressure Vessel Tech.,* **102,** 138–145 [May 1980]) and Chen (*J. Sound Vibration,* **93,** 439–455 [1984]).

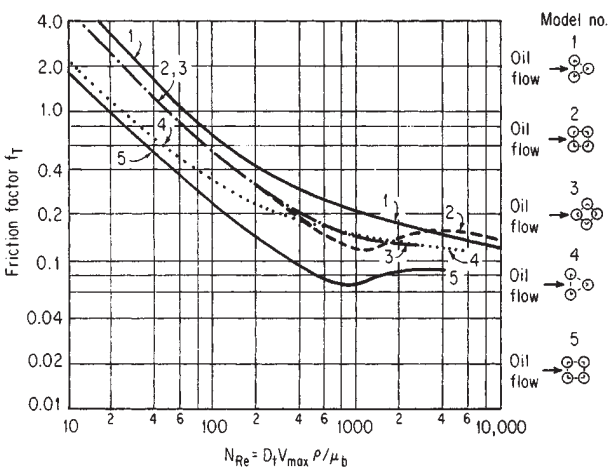

Model	Rows	D_t, in	Pitch/D_t
1	10	¾	1.25
2	10	¾	1.25
3	14	¾	1.25
4	10	¾	1.50
5	10	¾	1.50

FIG. 6-45 Friction factors for transition region flow across tube banks. (Pitch is the minimum center-to-center tube spacing.) (*From Bergelin, Brown, and Doberstein,* Trans. ASME, **74,** *953 [1952].*)

BEDS OF SOLIDS

Fixed Beds of Granular Solids Pressure-drop prediction is complicated by the variety of granular materials and of their packing arrangement. For flow of a **single incompressible fluid** through an incompressible bed of granular solids, the pressure drop may be estimated by the correlation given in Fig. 6-46 (Leva, *Chem. Eng.,* **56**[5], 115–117 [1949]), or *Fluidization,* McGraw-Hill, New York, 1959). The modified friction factor and Reynolds number are defined by

$$f_m \equiv \frac{D_p \rho \phi_s^{3-n} \epsilon^3 |\Delta p|}{2G^2 L(1-\epsilon)^{3-n}} \tag{6-166}$$

$$\mathrm{Re}' \equiv \frac{D_p G}{\mu} \tag{6-167}$$

where $-\Delta p$ = pressure drop
L = depth of bed
D_p = average particle diameter, defined as the diameter of a sphere of the same volume as the particle
ϵ = void fraction
n = exponent given in Fig. 6-46 as a function of Re′
ϕ_s = shape factor defined as the area of sphere of diameter D_p divided by the actual surface area of the particle
G = fluid superficial mass velocity based on the empty chamber cross section
ρ = fluid density
μ = fluid viscosity

As for any incompressible single-phase flow, the equivalent pressure $P = p + \rho g z$ where g = acceleration of gravity z = elevation, may be used in place of p to account for gravitational effects in flows with vertical components.

In creeping flow (Re′ < 10),

$$f_m = \frac{100}{\mathrm{Re}'} \tag{6-168}$$

At high Reynolds numbers the friction factor becomes nearly constant, approaching a value of the order of unity for most packed beds.

In terms of S, particle surface area per unit volume of bed,

$$D_p = \frac{6(1-\epsilon)}{\phi_s S} \tag{6-169}$$

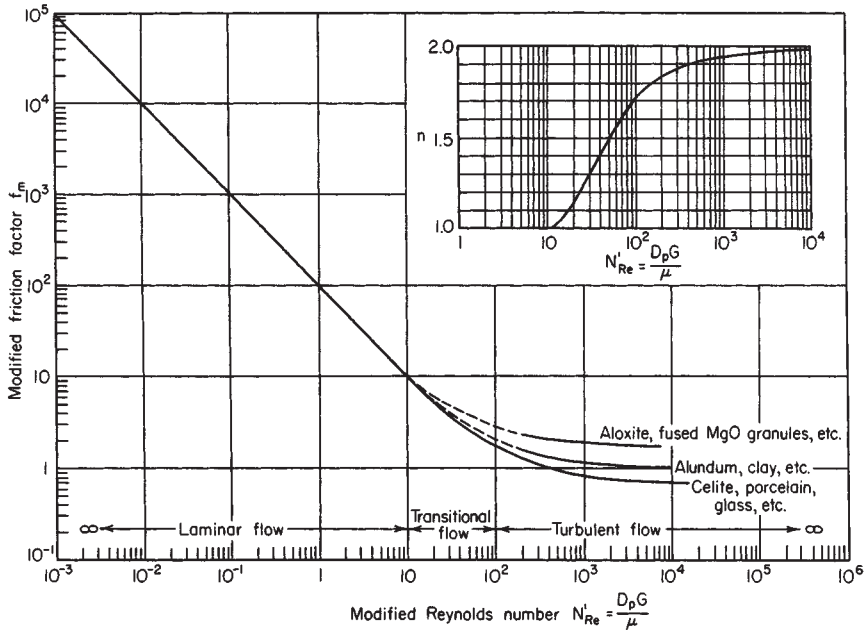

FIG. 6-46 Friction factor for beds of solids. (*From Leva,* Fluidization, *McGraw-Hill, New York, 1959, p. 49.*)

Porous Media Packed beds of granular solids are one type of the general class referred to as **porous media,** which include geological formations such as petroleum reservoirs and aquifers, manufactured materials such as sintered metals and porous catalysts, burning coal or char particles, and textile fabrics, to name a few. Pressure drop for incompressible flow across a porous medium has the same qualitative behavior as that given by Leva's correlation in the preceding. At low Reynolds numbers, viscous forces dominate and pressure drop is proportional to fluid viscosity and superficial velocity, and at high Reynolds numbers, pressure drop is proportional to fluid density and to the square of superficial velocity.

Creeping flow ($Re' <\sim 1$) through porous media is often described in terms of the **permeability** k and Darcy's Law:

$$\frac{-\Delta P}{L} = \frac{\mu}{k} V \tag{6-170}$$

where V = superficial velocity. The SI units for permeability are m^2. Creeping flow conditions generally prevail in geological porous media. For **multidimensional flows** through **isotropic** porous media, the superficial velocity **V** and pressure gradient ∇P vectors replace the corresponding one-dimensional variables in Eq. (6-170).

$$\nabla P = -\frac{\mu}{k} \mathbf{V} \tag{6-171}$$

For isotropic homogeneous porous media (uniform permeability and porosity), the pressure for creeping incompressible single phase-flow may be shown to satisfy the LaPlace equation:

$$\nabla^2 P = 0 \tag{6-172}$$

For **anisotropic** or **oriented** porous media, as are frequently found in geological media, permeability varies with direction and a **permeability tensor K,** with nine components K_{ij} giving the velocity compenent in the i direction due to a pressure gradient in the j direction, may be introduced. For further information, see Slattery (*Momentum, Energy and Mass Transfer in Continua,* Krieger, Huntington, New York, 1981, p. 193–218). See also Dullien (*Chem. Eng. J.* [*Laussanne*], **10,** 1,034 [1975]) for a review of pressure-drop methods in single-phase flow. Solutions for Darcy's law for several geometries of interest in petroleum reservoirs and aquifers, for both incompressible and compressible flows, are given in Craft and Hawkins (*Applied Petroleum Reservoir Engineering,* Prentice-Hall, Englewood Cliffs, N.J., 1959). See also Todd (*Groundwater Hydrology,* 2nd ed., Wiley, New York, 1980).

For granular solids of **mixed sizes** the average particle diameter may be calculated as

$$\frac{1}{D_p} = \sum_i \frac{x_i}{D_{p,i}} \tag{6-173}$$

where x_i = weight fraction of particles of size $D_{p,i}$.

For **isothermal compressible flow** of a gas with constant compressibility factor Z through a packed bed of granular solids, an equation similar to Eq. (6-114) for pipe flow may be derived:

$$p_1^2 - p_2^2 = \frac{2ZRG^2T}{M_w}\left[\ln\frac{v_2}{v_1} + \frac{2f_m L(1-\epsilon)^{3-n}}{\phi_s^{3-n}\epsilon^3 D_p}\right] \tag{6-174}$$

where p_1 = upstream absolute pressure
p_2 = downstream absolute pressure
R = gas constant
T = absolute temperature
M_w = molecular weight
v_1 = upstream specific volume of gas
v_2 = downstream specific volume of gas

For creeping flow of **power law** non-Newtonian fluids, the method of Christopher and Middleton (*Ind. Eng. Chem. Fundam.,* **4,** 422–426 [1965]) may be used:

$$-\Delta p = \frac{150HLV^n(1-\epsilon)^2}{D_p^2\phi_s^2\epsilon^3} \tag{6-175}$$

$$H = \frac{K}{12}\left(9 + \frac{3}{n}\right)^n \left[\frac{D_p^2\phi_s^2\epsilon^4}{(1-\epsilon)^2}\right]^{(1-n)/2} \tag{6-176}$$

where $V = G/\rho$ = superficial velocity, K, n = power law material constants, and all other variables are as defined in Eq. (6-166). This correlation is supported by data from Christopher and Middleton (ibid.), Gregory and Griskey (*AIChE J.,* **13,** 122–125 [1967]), Yu, Wen, and Bailie (*Can. J. Chem. Eng.,* **46,** 149–154 [1968]), Siskovic, Gregory, and Griskey (*AIChE J.,* **17,** 176–187 [1978]), Kemblowski and Mertl (*Chem. Eng. Sci.,* **29,** 213–223 [1974]), and Kemblowski and Dziu-

minski (*Rheol. Acta,* **17,** 176–187 [1978]). The measurements cover the range $n = 0.50$ to 1.60, and modified Reynolds number $\mathrm{Re}' = 10^{-8}$ to 10, where

$$\mathrm{Re}' = \frac{D_p V^{2-n}\rho}{H} \tag{6-177}$$

For the case $n = 1$ (Newtonian fluid), Eqs. (6-175) and (6-176) give a pressure drop 25 percent less than that given by Eqs. (6-166) through (6-168).

For **viscoelastic fluids** see Marshall and Metzner (*Ind. Eng. Chem. Fundam.,* **6,** 393–400 [1967]), Siskovic, Gregory, and Griskey (*AIChE J.,* **13,** 122–125 [1967]) and Kemblowski and Dziubinski (*Rheol. Acta,* **17,** 176–187 [1978]).

For gas flow through porous media with small pore diameters, the slip flow and molecular flow equations previously given (see the "Vacuum Flow" subsection) may be applied when the pore is of the same or smaller order as the mean free path, as described by Monet and Vermeulen (*Chem. Eng. Prog., Symp. Ser.,* **55,** *Symp. Ser.,* **25** [1959]).

Tower Packings For the flow of a **single fluid** through a bed of tower packing, pressure drop may be estimated using the preceding methods. See also Sec. 14 of this *Handbook.* For **countercurrent gas/liquid flow** in commercial tower packings, both structured and unstructured, several sources of data and correlations for pressure drop and flooding are available. See, for example, Strigle (*Random Packings and Packed Towers, Design and Applications,* Gulf Publishing, Houston, 1989; *Chem. Eng. Prog.,* **89**[8], 79–83 [August 1993]), Hughmark (*Ind. Eng. Chem. Fundam.,* **25,** 405–409 [1986]), Chen (*Chem. Eng. Sci.,* **40,** 2139–2140 [1985]), Billet and Mackowiak (*Chem. Eng. Technol.,* **11,** 213–217 [1988]), Krehenwinkel and Knapp (*Chem. Eng. Technol.,* **10,** 231–242 [1987]), Mersmann and Deixler (*Ger. Chem. Eng.,* **9,** 265–276 [1986]) and Robbins (*Chem. Eng. Progr.,* **87**[5], 87–91 [May 1991]). Data and correlations for flooding and pressure drop for structured packings are given by Fair and Bravo (*Chem. Eng. Progr.,* **86**[1], 19–29 [January 1990]).

Fluidized Beds When gas or liquid flows upward through a vertically unconstrained bed of particles, there is a minimum fluid velocity at which the particles will begin to move. Above this minimum velocity, the bed is said to be *fluidized.* Fluidized beds are widely used, in part because of their excellent mixing and heat and mass transfer characteristics. See Sec. 17 of this *Handbook* for detailed information.

BOUNDARY LAYER FLOWS

Boundary layer flows are a special class of flows in which the flow far from the surface of an object is inviscid, and the effects of viscosity are manifest only in a thin region near the surface where steep velocity gradients occur to satisfy the no-slip condition at the solid surface. The thin layer where the velocity decreases from the inviscid, potential flow velocity to zero (relative velocity) at the solid surface is called the *boundary layer.* The thickness of the boundary layer is indefinite because the velocity asymptotically approaches the free-stream velocity at the outer edge. The boundary layer thickness is conventionally taken to be the distance for which the velocity equals 0.99 times the free-stream velocity. The boundary layer may be either laminar or turbulent. Particularly in the former case, the equations of motion may be simplified by scaling arguments. Schlichting (*Boundary Layer Theory,* 8th ed., McGraw-Hill, New York, 1987) is the most comprehensive source for information on boundary layer flows.

Flat Plate, Zero Angle of Incidence For flow over a wide, thin flat plate at zero angle of incidence with a uniform free-stream velocity, as shown in Fig. 6-47, the **critical Reynolds number** at which the boundary layer becomes turbulent is normally taken to be

$$\mathrm{Re}_x = \frac{xV\rho}{\mu} = 500{,}000 \tag{6-178}$$

where V = free-stream velocity
ρ = fluid density
μ = fluid viscosity
x = distance from leading edge of the plate

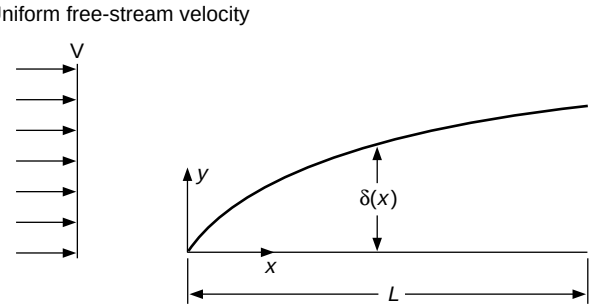

FIG. 6-47 Boundary layer on a flat plate at zero angle of incidence.

However, the transition Reynolds number depends on free-stream turbulence and may range from 3×10^5 to 3×10^6. The **laminar boundary layer** thickness δ is a function of distance from the leading edge:

$$\delta \approx 5.0x\mathrm{Re}_x^{-0.5} \tag{6-179}$$

The total drag on the plate of length L and width b for a laminar boundary layer, including the drag on both surfaces, is:

$$F_D = 1.328bL\rho V^2\mathrm{Re}_L^{-0.5} \tag{6-180}$$

For **non-Newtonian power law fluids** (Acrivos, Shah, and Peterson, *AIChE J.,* **6,** 312–317 [1960]; Hsu, *AIChE J.,* **15,** 367–370 [1969]),

$$F_D = CbL\rho V^2\mathrm{Re}_L'^{-1/(1+n)} \tag{6-181}$$

n =	0.2	0.3	0.4	0.5	0.6	0.7	0.8	0.9	1
C =	2.075	1.958	1.838	1.727	1.627	1.538	1.460	1.390	1.328

where $\mathrm{Re}_L' = \rho V^{2-n}L^n/K$ and K and n are the power law material constants (see Eq. [6-4]).

For a **turbulent boundary layer,** the thickness may be estimated as

$$\delta \approx 0.37x\mathrm{Re}_x^{-0.2} \tag{6-182}$$

and the total drag force on both sides of the plate of length L is

$$F_D = \left[\frac{0.455}{(\log \mathrm{Re}_L)^{2.58}} - \frac{1{,}700}{\mathrm{Re}_L}\right]\rho bLV^2 \qquad 5 \times 10^5 < \mathrm{Re}_L < 10^9 \tag{6-183}$$

Here the second term accounts for the laminar leading edge of the boundary layer and assumes that the critical Reynolds number is 500,000.

Cylindrical Boundary Layer Laminar boundary layers on cylindrical surfaces, with flow parallel to the cylinder axis, are described by Glauert and Lighthill (*Proc. R. Soc.* [*London*], **230A,** 188–203 [1955]), Jaffe and Okamura (*Z. Angew. Math. Phys.,* **19,** 564–574 [1968]) and Stewartson (*Q. Appl. Math.,* **13,** 113–122 [1955]). For a turbulent boundary layer, the total drag may be estimated as

$$F_D = \overline{c_j}\pi rL\rho V^2 \tag{6-184}$$

where r = cylinder radius, L = cylinder length, and the average friction coefficient is given by (White, *J. Basic Eng.,* **94,** 200–206 [1972])

$$\overline{c_j} = 0.0015 + \left[0.30 + 0.015\left(\frac{L}{r}\right)^{0.4}\right]\mathrm{Re}_L^{-1/3} \tag{6-185}$$

for $\mathrm{Re}_L = 10^6$ to 10^9 and $L/r < 10^6$.

Continuous Flat Surface Boundary layers on continuous surfaces drawn through a stagnant fluid are shown in Fig. 6-48. Figure 6-48*a* shows the continuous flat surface (Sakiadis, *AIChE J.,* **7,** 26–28, 221–225, 467–472 [1961]). The critical Reynolds number for transition to turbulent flow may be greater than the 500,000 value for the finite flat-plate case discussed previously (Tsou, Sparrow, and Kurtz, *J. Fluid Mech.,* **26,** 145–161 [1966]). For a laminar boundary layer, the thickness is given by

$$\delta = 6.37x\mathrm{Re}_x^{-0.5} \tag{6-186}$$

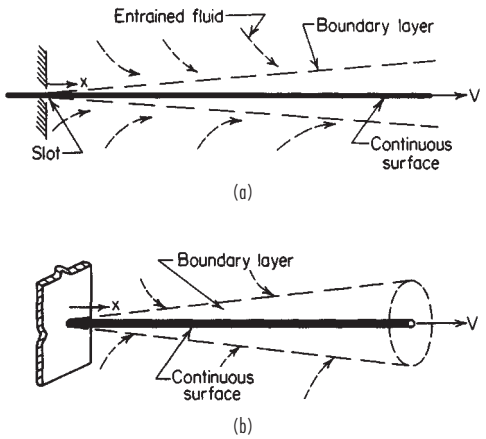

FIG. 6-48 Continuous surface: (*a*) continuous flat surface, (*b*) continuous cylindrical surface. (*From Sakiadis,* Am. Inst. Chem. Eng. J., **7,** *221, 467 [1961].*)

and the total drag exerted on the two surfaces is

$$F_D = 1.776bL\rho V^2 \mathrm{Re}_L^{-0.5} \tag{6-187}$$

The total flow rate of fluid entrained by the surface is

$$q = 3.232bLV\mathrm{Re}_L^{-0.5} \tag{6-188}$$

The theoretical velocity field was experimentally verified by Tsou, Sparrow, and Goldstein (*Int. J. Heat Mass Transfer,* **10,** 219–235 [1967]) and Szeri, Yates, and Hai (*J. Lubr. Technol.,* **98,** 145–156 [1976]). For **non-Newtonian power law fluids** see Fox, Erickson, and Fan (*AIChE J.,* **15,** 327–333 [1969]).

For a turbulent boundary layer, the thickness is given by

$$\delta = 1.01x\mathrm{Re}_x^{-0.2} \tag{6-189}$$

and the total drag on both sides by

$$F_D = 0.056bL\rho V^2 \mathrm{Re}_L^{-0.2} \tag{6-190}$$

and the total entrainment by

$$q = 0.252bLV\mathrm{Re}_L^{-0.2} \tag{6-191}$$

When the laminar boundary layer is a significant part of the total length of the object, the total drag should be corrected by subtracting a calculated turbulent drag for the length of the laminar section and then adding the laminar drag for the laminar section. Tsou, Sparrow, and Goldstein (*Int. J. Heat Mass Transfer,* **10,** 219–235 [1967]) give an improved analysis of the turbulent boundary layer; their data indicate that Eq. (6-190) underestimates the drag by about 15 percent.

Continuous Cylindrical Surface The continuous surface shown in Fig. 6-48*b* is applicable, for example, for a wire drawn through a stagnant fluid (Sakiadis, *AIChE J.,* **7,** 26–28, 221–225, 467–472 [1961]). The critical-length Reynolds number for transition is $\mathrm{Re}_x = 200{,}000$. The laminar boundary layer thickness, total drag, and entrainment flow rate may be obtained from Fig. 6-49; the drag and entrainment rate are obtained from the *momentum area* Θ and *displacement area* Δ evaluated at $x = L$.

$$F_D = \rho V^2 \Theta \tag{6-192}$$

$$q = V\Delta \tag{6-193}$$

Further laminar boundary layer analysis is given by Crane (*Z. Angew. Math. Phys.,* **23,** 201–212 [1972]).

For a turbulent boundary layer, the total drag may be roughly estimated using Eqs. (6-184) and (6-185) for finite cylinders. Measured forces by Kwon and Prevorsek (*J. Eng. Ind.,* **101,** 73–79 [1979]) are greater than predicted this way.

The laminar boundary layer on **deforming continuous surfaces** with velocity varying with axial position is discussed by Vleggaar

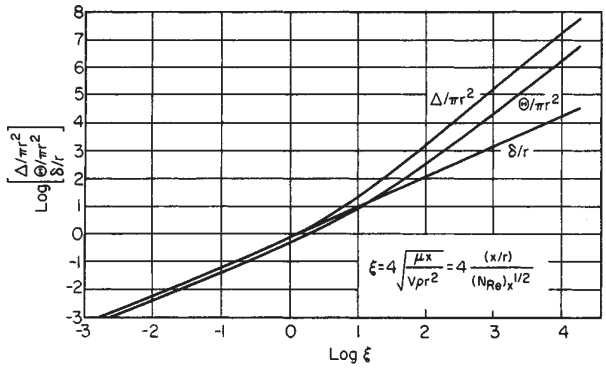

FIG. 6-49 Boundary layer parameters for continuous cylindrical surfaces. (*From Sakiadis,* Am. Inst. Chem. J., **7,** *467 [1961].*)

(*Chem. Eng. Sci.,* **32,** 1517–1525 [1977] and Crane (*Z. Angew. Math. Phys.,* **26,** 619–622 [1975]).

VORTEX SHEDDING

When fluid flows past objects or through orifices or similar restrictions, vortices may periodically be shed downstream. Objects such as smokestacks, chemical-processing columns, suspended pipelines, and electrical transmission lines can be subjected to damaging vibrations and forces due to the vortices, especially if the shedding frequency is close to a natural vibration frequency of the object. The shedding can also produce sound. See Krzywoblocki (*Appl. Mech. Rev.,* **6,** 393–397 [1953]) and Marris (*J. Basic Eng.,* **86,** 185–196 [1964]).

Development of a vortex street, or *von Kármán vortex street* is shown in Fig. 6-50. Discussions of the vortex street may be found in Panton (pp. 387–393). The Reynolds number is

$$\mathrm{Re} = \frac{DV\rho}{\mu} \tag{6-194}$$

where D = diameter of cylinder or effective width of object
V = free-stream velocity
ρ = fluid density
μ = fluid viscosity

For flow past a cylinder, the vortex street forms at Reynolds numbers above about 40. The vortices initially form in the wake, the point of formation moving closer to the cylinder as Re is increased. At a Reynolds number of 60 to 100, the vortices are formed from eddies attached to the cylinder surface. The vortices move at a velocity slightly less than V. The frequency of vortex shedding f is given in terms of the Strouhal number, which is approximately constant over a wide range of Reynolds numbers.

$$\mathrm{St} \equiv \frac{fD}{V} \tag{6-195}$$

For $40 < \mathrm{Re} < 200$ the vortices are laminar and the Strouhal number has a nearly constant value of 0.2 for flow past a cylinder. Between Re = 200 and 400 the Strouhal number is no longer constant and the wake becomes irregular. Above about Re = 400 the vortices become turbulent, the wake is once again stable, and the Strouhal number remains constant at about 0.2 up to a Reynolds number of about 10^5.

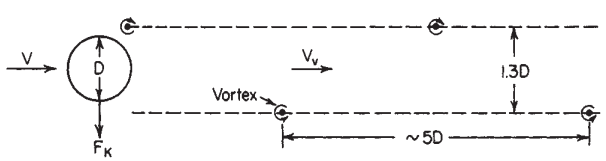

FIG. 6-50 Vortex street behind a cylinder.

Above Re = 10^5 the vortex shedding is difficult to see in flow visualization experiments, but velocity measurements still show a strong spectral component at St = 0.2 (Panton, p. 392). Experimental data suggest that the vortex street disappears over the range $5 \times 10^5 < \text{Re} < 3.5 \times 10^6$, but is reestablished at above 3.5×10^6 (Schlichting).

Vortex shedding exerts alternating lateral forces on a cylinder, perpendicular to the flow direction. Such forces may lead to severe vibration or mechanical failure of cylindrical elements such as heat-exchanger tubes, transmission lines, stacks, and columns when the vortex shedding frequency is close to resonant bending frequency. According to Den Hartog (*Proc. Nat. Acad. Sci.*, **40,** 155–157 [1954]), the vortex shedding and cylinder vibration frequency will shift to the resonant frequency when the calculated shedding frequency is within 20 percent of the resonant frequency. The well-known Tacoma Narrows bridge collapse resulted from resonance between a torsional oscillation and vortex shedding (Panton, p. 392). Spiral strakes are sometimes installed on tall stacks so that vortices at different axial positions are not shed simultaneously. The alternating lateral force F_K, sometimes called the *von Kármán force,* is given by (Den Hartog, *Mechanical Vibrations,* 4th ed., McGraw-Hill, New York, 1956, pp. 305–309):

$$F_K = C_K A \frac{\rho V^2}{2} \tag{6-196}$$

where C_K = von Kármán coefficient
A = projected area perpendicular to the flow
ρ = fluid density
V = free-stream fluid velocity

For a cylinder, $C_K = 1.7$. For a vibrating cylinder, the effective projected area exceeds, but is always less than twice, the actual cylinder projected area (Rouse, *Engineering Hydraulics,* Wiley, New York, 1950).

The following references pertain to discussions of vortex shedding in specific structures: steel stacks (Osker and Smith, *Trans. ASME,* **78,** 1381–1391 [1956]; Smith and McCarthy, *Mech. Eng.*, **87,** 38–41 [1965]); chemical-processing columns (Freese, *J. Eng. Ind.*, **81,** 77–91, [1959]); heat exchangers (Eisinger, *Trans. ASME J. Pressure Vessel Tech.*, **102,** 138–145 [May 1980]; Chen, *J. Sound Vibration,* **93,** 439–455 [1984]; Gainsboro, *Chem. Eng. Prog.*, **64**[3], 85–88 [1968]; "Flow-Induced Vibration in Heat Exchangers," *Symp. Proc.,* ASME, New York, 1970); suspended pipe lines (Baird, *Trans. ASME,* **77,** 797–804 [1955]); and suspended cable (Steidel, *J. Appl. Mech.*, **23,** 649–650 [1956]).

COATING FLOWS

In coating flows, liquid films are entrained on moving solid surfaces. For general discussions, see Ruschak (*Ann. Rev. Fluid Mech.*, **17,** 65–89 [1985]), Cohen and Gutoff (*Modern Coating and Drying Technology,* VCH Publishers, New York, 1992), and Middleman (*Fundamentals of Polymer Processing,* McGraw-Hill, New York, 1977). It is generally important to control the thickness and uniformity of the coatings.

In **dip coating,** or free withdrawal coating, a solid surface is withdrawn from a liquid pool, as shown in Fig. 6-51. It illustrates many of the features found in other coating flows, as well. Tallmadge and Gutfinger (*Ind. Eng. Chem.*, **59**[11], 19–34 [1967]) provide an early review of the theory of dip coating. The coating flow rate and film thickness are controlled by the withdrawal rate and the flow behavior in the meniscus region. For a withdrawal velocity V and an angle of inclination from the horizontal ϕ, the film thickness h may be estimated for low withdrawal velocities by

$$h\left(\frac{\rho g}{\sigma}\right)^{1/2} = \frac{0.944}{(1-\cos\phi)^{1/2}}\,\text{Ca}^{2/3} \tag{6-197}$$

where g = acceleration of gravity
$\text{Ca} = \mu V/\sigma$ = capillary number
μ = viscosity
σ = surface tension

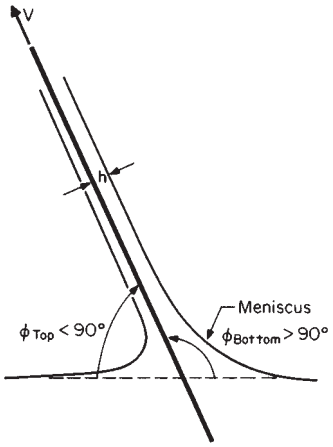

FIG. 6-51 Dip coating.

Equation (6-197) is asymptotically valid as Ca → 0 and agrees with experimental data up to capillary numbers in the range of 0.01 to 0.03. In practice, where high production rates require high withdrawal speeds, capillary numbers are usually too large for Eq. (6-197) to apply. Approximate analytical methods for larger capillary numbers have been obtained by numerous investigators, but none appears wholly satisfactory, and some are based on questionable assumptions (Ruschak, *Ann. Rev. Fluid Mech.*, **17,** 65–89 [1985]). With the availability of high-speed computers and the development of the field of computational fluid dynamics, numerical solutions accounting for two-dimensional flow aspects, along with gravitational, viscous, inertial, and surface tension forces are now the most effective means to analyze coating flow problems.

Other common coating flows include premetered flows, such as **slide** and **curtain coating,** where the film thickness is an independent parameter that may be controlled within limits, and the curvature of the mensiscus adjusts accordingly; the closely related **blade coating;** and **roll coating** and **extrusion coating.** See Ruschak (ibid.), Cohen and Gutoff (*Modern Coating and Drying Technology,* VCH Publishers, New York, 1992) and Middleman (*Fundamentals of Polymer Processing,* McGraw-Hill, New York, 1977). For dip coating of wires, see Taughy (*Int. J. Numerical Meth. Fluids,* **4,** 441–475 [1984]).

Many coating flows are subject to instabilities that lead to unacceptable coating defects. Three-dimensional flow instabilities lead to such problems as **ribbing.** Air entrainment is another common defect.

FALLING FILMS

Minimum Wetting Rate The minimum liquid rate required for complete wetting of a vertical surface is about 0.03 to 0.3 kg/m · s for water at room temperature. The minimum rate depends on the geometry and nature of the vertical surface, liquid surface tension, and mass transfer between surrounding gas and the liquid. See Ponter, et al. (*Int. J. Heat Mass Transfer,* **10,** 349–359 [1967]; *Trans. Inst. Chem. Eng.* [*London*], **45,** 345–352 [1967]), Stainthorp and Allen (*Trans. Inst. Chem. Eng.* [*London*], **43,** 85–91 [1967]) and Watanabe, et al. (*J. Chem. Eng.* [*Japan*], **8**[1], 75 [1975]).

Laminar Flow For films falling down **vertical flat surfaces,** as shown in Fig. 6-52, or vertical tubes with small film thickness compared to tube radius, laminar flow conditions prevail for Reynolds numbers less than about 2,000, where the Reynolds number is given by

$$\text{Re} = \frac{4\Gamma}{\mu} \tag{6-198}$$

where Γ = liquid mass flow rate per unit width of surface and μ = liq-

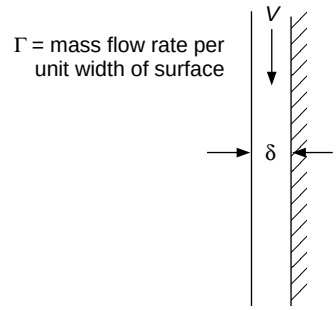

FIG. 6-52 Falling film.

uid viscosity. For a flat film surface, the following equations may be derived. The film thickness δ is

$$\delta = \left(\frac{3\Gamma\mu}{\rho^2 g}\right)^{1/3} \tag{6-199}$$

The average film velocity is

$$V = \frac{\Gamma}{\rho\delta} = \frac{g\rho\delta^2}{3\mu} \tag{6-200}$$

The downward velocity profile $u(x)$ where $x = 0$ at the solid surface and $x = \delta$ at the liquid/gas interface is given by

$$u = 1.5V\left[\frac{2x}{\delta} - \left(\frac{x}{\delta}\right)^2\right] \tag{6-201}$$

These equations assume that there is no drag force at the gas/liquid interface, such as would be produced by gas flow. For a flat surface **inclined** at an angle θ with the horizontal, the preceding equations may be modified by replacing g by $g \sin \theta$. For films falling inside vertical tubes with film thickness up to and including the full pipe radius, see Jackson (*AIChE J.*, **1,** 231–240 [1955]).

These equations have generally given good agreement with experimental results for low-viscosity liquids (<0.005 Pa · s) (< 5 cp) whereas Jackson (ibid.) found film thicknesses for higher-viscosity liquids (0.01 to 0.02 Pa·s (10 to 20 cp) were significantly less than predicted by Eq. (6-197). At Reynolds numbers of 25 or greater, **surface waves** will be present on the liquid film. West and Cole (*Chem. Eng. Sci.*, **22,** 1388–1389 [1967]) found that the surface velocity $u(x = \delta)$ is still within ±7 percent of that given by Eq. (6-201) even in wavy flow.

For laminar non-Newtonian film flow, see Bird, Armstrong, and Hassager (*Dynamics of Polymeric Liquids*, vol. 1: *Fluid Mechanics*, Wiley, New York, 1977, p. 215, 217), Astarita, Marrucci, and Palumbo (*Ind. Eng. Chem. Fundam.*, **3,** 333–339 [1964]) and Cheng (*Ind. Eng. Chem. Fundam.*, **13,** 394–395 [1974]).

Turbulent Flow In turbulent flow, Re > 2,000, for vertical surfaces, the film thickness may be estimated to within ±25 percent using

$$\delta = 0.304\left(\frac{\Gamma^{1.75}\mu^{0.25}}{\rho^2 g}\right)^{1/3} \tag{6-202}$$

Replace g by $g \sin \theta$ for a surface inclined at angle θ to the horizontal. The average film velocity is $V = \Gamma/\rho\delta$.

Tallmadge and Gutfinger (*Ind. Eng. Chem.*, **59**[11], 19–34 [1967]) discuss prediction of drainage rates from liquid films on flat and cylindrical surfaces.

Effect of Surface Traction If a drag is exerted on the surface of the film because of motion of the surrounding fluid, the film thickness will be reduced or increased, depending upon whether the drag acts with or against gravity. Thomas and Portalski (*Ind. Eng. Chem.*, **50,** 1081–1088 [1958]), Dukler (*Chem. Eng. Prog.*, **55**[10], 62–67 [1959]) and Kosky (*Int. J. Heat Mass Transfer*, **14,** 1220–1224 [1971]) have presented calculations of film thickness and film velocity. Film thickness data for falling water films with cocurrent and countercurrent air flow in pipes are given by Zhivaikin (*Int. Chem. Eng.*, **2,** 337–341 [1962]). Zabaras, Dukler, and Moalem-Maron (*AIChE J.*, **32,** 829–843 [1986]) and Zabaras and Dukler (*AIChE J.*, **34,** 389–396 [1988]) present studies of film flow in vertical tubes with both cocurrent and countercurrent gas flow, including measurements of film thickness, wall shear stress, wave velocity, wave amplitude, pressure drop, and flooding point for countercurrent flow.

Flooding With countercurrent gas flow, a condition is reached with increasing gas rate for which flow reversal occurs and liquid is carried upward. The mechanism for this flooding condition has been most often attributed to waves either bridging the pipe or reversing direction to flow upward at flooding. However, the results of Zabaras and Dukler (ibid.) suggest that flooding may be controlled by flow conditions at the liquid inlet and that wave bridging or upward wave motion does not occur, at least for the 50.8-mm diameter pipe used for their study. Flooding mechanisms are still incompletely understood. Under some circumstances, as when the gas is allowed to develop its normal velocity profile in a "calming length" of pipe beneath the liquid draw-off, the gas superficial velocity at flooding will be increased, and increases with decreasing length of wetted pipe (Hewitt, Lacy, and Nicholls, *Proc. Two-Phase Flow Symp.*, University of Exeter, paper 4H, AERE-4 4614 [1965]). A bevel cut at the bottom of the pipe with an angle 30° from the vertical will increase the flooding velocity in small-diameter tubes at moderate liquid flow rates. If the gas approaches the tube from the side, the taper should be oriented with the point facing the gas entrance. Figures 6-53 and 6-54 give correlations for flooding in tubes with square and slant bottoms (courtesy Holmes, DuPont Co.) The superficial mass velocities of gas and liquid G_G and G_L, and the physical property parameters λ and ψ are the same as those defined for the Baker chart ("Multiphase Flow" subsection, Fig. 6-25). For tubes larger than 50 mm (2 in), flooding velocity appears to be relatively insensitive to diameter and the flooding curves for 1.98-in diameter may be used.

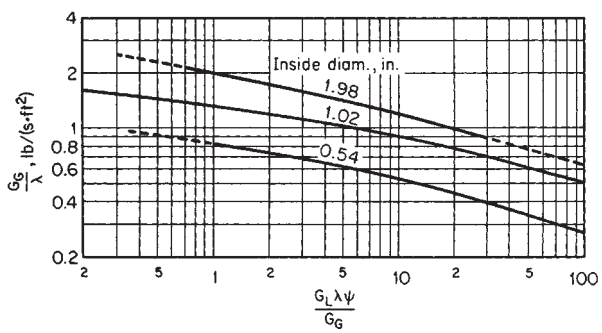

FIG. 6-53 Flooding in vertical tubes with square top and square bottom. To convert lbm/(ft²·s) to kg/(m²·s), multiply by 4.8824; to convert in to mm, multiply by 25.4. (*Courtesy of E. I. du Pont de Nemours & Co.*)

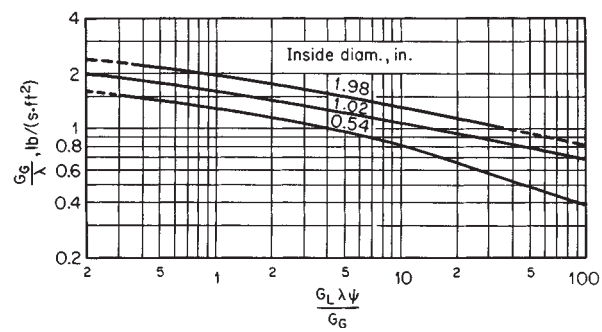

FIG. 6-54 Flooding in vertical tubes with square top and slant bottom. To convert lbm/(ft²·s) to kg/(m²·s), multiply by 4.8824; to convert in to mm, multiply by 25.4. (*Courtesy of E. I. du Pont de Nemours & Co.*)

HYDRAULIC TRANSIENTS

Many transient flows of liquids may be analyzed by using the full time-dependent equations of motion for incompressible flow. However, there are some phenomena that are controlled by the small compressibility of liquids. These phenomena are generally called **hydraulic transients.**

Water Hammer When liquid flowing in a pipe is suddenly decelerated to zero velocity by a fast-closing valve, a pressure wave propagates upstream to the pipe inlet, where it is reflected; a pounding of the line commonly known as **water hammer** is often produced. For an instantaneous flow stoppage of a truly incompressible fluid in an inelastic pipe, the pressure rise would be infinite. Finite compressibility of the fluid and elasticity of the pipe limit the pressure rise to a finite value. The Joukowski formula gives the maximum pressure rise as

$$\Delta p = \rho a \Delta V \tag{6-203}$$

where ρ = liquid density
ΔV = change in liquid velocity
a = pressure wave velocity

The wave velocity is given by

$$a = \frac{\sqrt{\beta/\rho}}{\sqrt{1 + (\beta/E)(D/b)}} \tag{6-204}$$

where β = liquid bulk modulus of elasticity
E = elastic modulus of pipe wall
D = pipe inside diameter
b = pipe wall thickness

The numerator gives the wave velocity for perfectly rigid pipe, and the denominator corrects for wall elasticity. This formula is for thin-walled pipes; for thick-walled pipes, the factor D/b is replaced by

$$2\,\frac{(D_o^2 + D_i^2)}{(D_o^2 - D_i^2)}$$

where D_o = pipe outside diameter
D_i = pipe inside diameter

Example 10: Response to Instantaneous Valve Closing Compute the wave speed and maximum pressure rise for instantaneous valve closing, with an initial velocity of 2.0 m/s, in a 4-in Schedule 40 steel pipe with elastic modulus 207×10^9 Pa. Repeat for a plastic pipe of the same dimensions, with $E = 1.4 \times 10^9$ Pa. The liquid is water with $\beta = 2.2 \times 10^9$ Pa and $\rho = 1{,}000$ kg/m^3.

For the steel pipe, $D = 102.3$ mm, $b = 6.02$ mm, and the wave speed is

$$a = \frac{\sqrt{\beta/\rho}}{\sqrt{1 + (\beta/E)(D/b)}}$$

$$= \frac{\sqrt{2.2 \times 10^9/1000}}{\sqrt{1 + (2.2 \times 10^9/207 \times 10^9)(102.3/6.02)}}$$

$$= 1365 \text{ m/s}$$

The maximum pressure rise is

$$\Delta p = \rho a \Delta V$$

$$= 1{,}000 \times 1{,}365 \times 2.0 = 2.73 \times 10^6 \text{ Pa}$$

For the plastic pipe,

$$a = \frac{\sqrt{2.2 \times 10^9/1000}}{\sqrt{1 + (2.2 \times 10^9/1.4 \times 10^9)(102.3/6.02)}}$$

$$= 282 \text{ m/s}$$

$$\Delta p = \rho a \Delta V = 1{,}000 \times 282 \times 2.0 = 5.64 \times 10^5 \text{ Pa}$$

The maximum pressure surge is obtained when the valve closes in less time than the period τ required for the pressure wave to travel from the valve to the pipe inlet and back, a total distance of $2L$.

$$\tau = \frac{2L}{a} \tag{6-205}$$

The pressure surge will be reduced when the time of flow stoppage exceeds the pipe period τ, due to cancellation between direct and reflected waves. Wood and Jones (*Proc. Am. Soc. Civ. Eng., J. Hydraul. Div.*, **99,** (HY1), 167–178 [1973]) present charts for reliable estimates of water-hammer pressure for different valve closure modes. Wylie and Streeter (*Hydraulic Transients,* McGraw-Hill, New York, 1978) describe several solution methods for hydraulic transients, including the method of characteristics, which is well suited to computer methods for accurate solutions. A rough approximation for the peak pressure for cases where the valve closure time t_c exceeds the pipe period τ is (Daugherty and Franzini, *Fluid Mechanics with Engineering Applications,* McGraw-Hill, New York, 1985):

$$\Delta p \approx \left(\frac{\tau}{t_c}\right)\rho a \Delta V \tag{6-206}$$

Successive reflections of the pressure wave between the pipe inlet and the closed valve result in alternating pressure increases and decreases, which are gradually attenuated by fluid friction and imperfect elasticity of the pipe. Periods of reduced pressure occur while the reflected pressure wave is traveling from inlet to valve. Degassing of the liquid may occur, as may vaporization if the pressure drops below the vapor pressure of the liquid. Gas and vapor bubbles decrease the wave velocity. Vaporization may lead to what is often called *liquid column separation;* subsequent collapse of the vapor pocket can result in pipe rupture.

In addition to water hammer induced by changes in valve setting, including closure, numerous other hydraulic transient flows are of interest, as, for example (Wylie and Streeter, *Hydraulic Transients,* McGraw-Hill, New York, 1978), those arising from starting or stopping of pumps; changes in power demand from turbines; reciprocating pumps; changing elevation of a reservoir; waves on a reservoir; turbine governor hunting; vibration of impellers or guide vanes in pumps, fans, or turbines; vibration of deformable parts such as valves; draft-tube instabilities due to vortexing; and unstable pump or fan characteristics. Tube failure in heat exchangers may be added to this list.

Pulsating Flow Reciprocating machinery (pumps and compressors) produces flow pulsations, which adversely affect flow meters and process control elements and can cause vibration and equipment failure, in addition to undesirable process results. Vibration and damage can result not only from the fundamental frequency of the pulse producer but also from higher harmonics. Multipiston double-acting units reduce vibrations. Pulsation dampeners are often added. Damping methods are described by M. W. Kellogg Co. (*Design of Piping Systems,* rev. 2d ed., Wiley, New York, 1965). For liquid phase pulsation damping, gas-filled surge chambers, also known as accumulators, are commonly used; see Wylie and Streeter (*Hydraulic Transients,* McGraw-Hill, New York, 1978).

Software packages are commercially available for simulation of hydraulic transients. These may be used to analyze piping systems to reveal unsatisfactory behavior, and they allow the assessment of design changes such as increases in pipe-wall thickness, changes in valve actuation, and addition of check valves, surge tanks, and pulsation dampeners.

Cavitation Loosely regarded as related to water hammer and hydraulic transients because it may cause similar vibration and equipment damage, **cavitation** is the phenomenon of collapse of vapor bubbles in flowing liquid. These bubbles may be formed anywhere the local liquid pressure drops below the vapor pressure, or they may be injected into the liquid, as when steam is sparged into water. Local low-pressure zones may be produced by local velocity increases (in accordance with the Bernoulli equation; see the preceding "Conservation Equations" subsection) as in eddies or vortices, or near boundary contours; by rapid vibration of a boundary; by separation of liquid during water hammer; or by an overall reduction in static pressure, as due to pressure drop in the suction line of a pump.

Collapse of vapor bubbles once they reach zones where the pressure exceeds the vapor pressure can cause objectionable noise and vibration and extensive erosion or pitting of the boundary materials. The critical cavitation number at inception of cavitation, denoted σ_i, is useful in correlating equipment performance data:

$$\sigma_i = \frac{(p - p_v)}{\rho V^2/2} \tag{6-207}$$

where p = static pressure in undisturbed flow
p_v = vapor pressure
ρ = liquid density
V = free-stream velocity of the liquid

The value of the cavitation number for incipient cavitation for a specific piece of equipment is a characteristic of that equipment. Cavitation numbers for various head forms of cylinders, for disks, and for various hydrofoils are given by Holl and Wislicenus (*J. Basic Eng.*, **83,** 385–398 [1961]) and for various surface irregularities by Arndt and Ippen (*J. Basic Eng.*, **90,** 249–261 [1968]), Ball (*Proc. ASCE J. Constr. Div.*, **89**(C02), 91–110 [1963]), and Holl (*J. Basic Eng.*, **82,** 169–183 [1960]). As a guide only, for blunt forms the cavitation number is generally in the range of 1 to 2.5, and for somewhat streamlined forms the cavitation number is in the range of 0.2 to 0.5. Critical cavitation numbers generally depend on a characteristic length dimension of the equipment in a way that has not been explained. This renders scale-up of cavitation data questionable.

For cavitation in flow through orifices, Fig. 6-55 (Thorpe, *Int. J. Multiphase Flow,* **16,** 1023–1045 [1990]) gives the critical cavitation number for inception of cavitation. To use this cavitation number in Eq. (6-207), the pressure p is the orifice backpressure downstream of the vena contracta after full pressure recovery, and V is the average velocity through the orifice. Fig. 6-55 includes data from Tullis and Govindarajan (*ASCE J. Hydraul. Div.*, **HY13,** 417–430 [1973]) modified to use the same cavitation number definition; their data also include critical cavitation numbers for 30.50- and 59.70-cm pipes (12.00- to 23.50-in). Very roughly, compared with the 15.40-cm pipe, the cavitation number is about 20 percent greater for the 30.50-cm (12.01-in) pipe and about 40 percent greater for the 59.70-cm (23.50-in) diameter pipe. Inception of cavitation appears to be related to release of dissolved gas and not merely vaporization of the liquid. For further discussion of cavitation, see Eisenberg and Tulin (Streeter, *Handbook of Fluid Dynamics,* Sec. 12, McGraw-Hill, New York, 1961).

TURBULENCE

Turbulent flow occurs when the Reynolds number exceeds a critical value above which laminar flow is unstable; the critical Reynolds number depends on the flow geometry. There is generally a transition regime between the critical Reynolds number and the Reynolds number at which the flow may be considered fully turbulent. The transition regime is very wide for some geometries. In turbulent flow, variables such as velocity and pressure fluctuate chaotically; statistical methods are used to quantify turbulence.

Time Averaging In turbulent flows it is useful to define time-averaged and fluctuation values of flow variables such as velocity components. For example, the x-component velocity fluctuation v_x' is the difference between the actual instantaneous velocity v_x and the time-averaged velocity $\overline{v_x}$:

$$v_x'(x, y, z, t) = v_x(x, y, z, t) - \overline{v_x}(x, y, z) \tag{6-208}$$

The actual and fluctuating velocity components are, in general, functions of the three spatial coordinates x, y, and z and of time t. The time-averaged velocity $\overline{v_x}$ is independent of time for a **stationary** flow. Nonstationary processes may be considered where averages are defined over time scales long compared to the time scale of the turbulent fluctuations, but short compared to longer time scales over which the time-averaged flow variables change due, for example, to time-varying boundary conditions. The time average over a time interval $2T$ centered at time t of a turbulently fluctuating variable $\zeta(t)$ is defined as

$$\overline{\zeta(t)} = \frac{1}{2T}\int_{t-T}^{t+T} \zeta(\tau)\, d\tau \tag{6-209}$$

where τ = dummy integration variable. For stationary turbulence, $\overline{\zeta}$ does not vary with time.

$$\overline{\zeta} = \lim_{T\to\infty} \frac{1}{2T}\int_{t-T}^{t+T} \zeta(\tau)\, d\tau \tag{6-210}$$

The time average of a fluctuation $\overline{\zeta'} = \overline{\zeta - \overline{\zeta}} = 0$. Fluctuation magnitudes are quantified by root mean squares.

$$\tilde{v}_x' = \sqrt{\overline{(v_x')^2}} \tag{6-211}$$

In **isotropic** turbulence, statistical measures of fluctuations are equal in all directions.

$$\tilde{v}_x' = \tilde{v}_y' = \tilde{v}_z' \tag{6-212}$$

In **homogeneous** turbulence, turbulence properties are independent of spatial position. **The kinetic energy of turbulence** k is given by

$$k = \frac{1}{2}(\tilde{v}_x'^2 + \tilde{v}_y'^2 + \tilde{v}_z'^2) \tag{6-213}$$

Turbulent velocity fluctuations ultimately dissipate their kinetic energy through viscous effects. Macroscopically, this energy dissipation requires pressure drop, or velocity decrease. The **energy dissipation rate** per unit mass is usually denoted ϵ. For steady flow in a pipe, the average energy dissipation rate per unit mass is given by

$$\epsilon = \frac{2fV^3}{D} \tag{6-214}$$

where ρ = fluid density
f = Fanning friction factor
D = pipe inside diameter

When the continuity equation and the Navier-Stokes equations for incompressible flow are time averaged, equations for the time-averaged velocities and pressures are obtained which appear identical to the original equations (6-18 through 6-28), except for the appearance of additional terms in the Navier-Stokes equations. Called **Reynolds stress** terms, they result from the nonlinear effects of momentum transport by the velocity fluctuations. In each i-component ($i = x, y, z$) Navier-Stokes equation, the following additional terms appear on the right-hand side:

$$\sum_{j=1}^{3} \frac{\partial \tau_{ji}^{(t)}}{\partial x_j}$$

with j components also being x, y, z. The Reynolds stresses are given by

$$\tau_{ij}^{(t)} = -\rho\overline{v_i' v_j'} \tag{6-215}$$

The Reynolds stresses are nonzero because the velocity fluctuations in different coordinate directions are correlated so that $\overline{v_i' v_j'}$ in general is nonzero.

Although direct numerical simulations under limited circumstances have been carried out to determine (unaveraged) fluctuating velocity fields, in general the solution of the equations of motion for turbulent flow is based on the time-averaged equations. This requires semi-

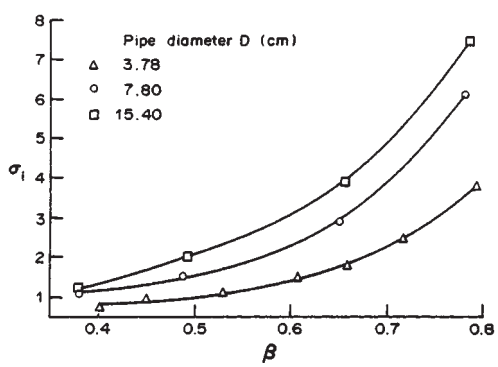

FIG. 6-55 Critical cavitation number vs. diameter ratio β. (*Reprinted from Thorpe, "Flow regime transitions due to cavitation in the flow through an orifice,"* Int. J. Multiphase Flow, ***16,*** *1023–1045. Copyright © 1990, with kind permission from Elsevier Science, Ltd., The Boulevard, Langford Lane, Kidlington OX5 1GB, United Kingdom.*)

empirical models to express the Reynolds stresses in terms of time-averaged velocities. This is the **closure** problem of turbulence. In all but the simplest geometries, numerical methods are required.

Closure Models Many closure models have been proposed. A few of the more important ones are introduced here. Many employ the Boussinesq approximation, simplified here for incompressible flow, which treats the Reynolds stresses as analogous to viscous stresses, introducing a scalar quantity called the turbulent or eddy viscosity μ_t.

$$-\rho\overline{v_i' v_j'} = \mu_t\left(\frac{\partial \overline{v_i}}{\partial x_j} + \frac{\partial \overline{v_j}}{\partial x_i}\right) \tag{6-216}$$

An additional *turbulence pressure* term equal to $-\frac{2}{3}k\delta_{ij}$, where k = turbulent kinetic energy and $\delta_{ij} = 1$ if $i = j$ and $\delta_{ij} = 0$ if $i \neq j$, is sometimes included in the right-hand side. To solve the equations of motion using the Boussinesq approximation, it is necessary to provide equations for the single scalar unknown μ_t (and k, if used) rather than the nine unknown tensor components $\tau_{ij}^{(t)}$. With this approximation, and using the effective viscosity $\mu_{\text{eff}} = \mu + \mu_t$, the time-averaged momentum equation is similar to the original Navier-Stokes equation, with time-averaged variables and μ_{eff} replacing the instantaneous variables and molecular viscosity. However, solutions to the time-averaged equations for turbulent flow are not identical to those for laminar flow because μ_{eff} is not a constant.

The universal turbulent velocity profile near the pipe wall presented in the preceding subsection "Incompressible Flow in Pipes and Channels" may be developed using the Prandtl mixing length approximation for the eddy viscosity,

$$\mu_t = \rho l_P^2 \left|\frac{d\overline{v_x}}{dy}\right| \tag{6-217}$$

where l_P is the Prandtl mixing length. The turbulent core of the universal velocity profile is obtained by assuming that the mixing length is proportional to the distance from the wall. The proportionality constant is one of two constants adjusted to fit experimental data.

The Prandtl mixing length concept is useful for shear flows parallel to walls, but is inadequate for more general three-dimensional flows. A more complicated semiempirical model commonly used in numerical computations, and found in most commercial software for computational fluid dynamics (CFD; see the following subsection), is the k–ϵ model described by Launder and Spaulding (*Lectures in Mathematical Models of Turbulence,* Academic, London, 1972). In this model the eddy viscosity is assumed proportional to the ratio k^2/ϵ.

$$\mu_t = \rho C_\mu \frac{k^2}{\epsilon} \tag{6-218}$$

where the value $C_\mu = 0.09$ is normally used. Semiempirical partial differential conservation equations for k and ϵ derived from the Navier-Stokes equations with simplifying closure assumptions are coupled with the equations of continuity and momentum:

$$\frac{\partial}{\partial t}(\rho k) + \frac{\partial}{\partial x_i}(\rho \overline{v_i} k) = \frac{\partial}{\partial x_i}\left(\frac{\mu_t}{\sigma_k}\frac{\partial k}{\partial x_i}\right) + \mu_t\left(\frac{\partial \overline{v_i}}{\partial x_j} + \frac{\partial \overline{v_j}}{\partial x_i}\right)\frac{\partial \overline{v_i}}{\partial x_j} - \rho\epsilon \tag{6-219}$$

$$\frac{\partial}{\partial t}(\rho \epsilon) + \frac{\partial}{\partial x_i}(\rho \overline{v_i} \epsilon) = \frac{\partial}{\partial x_i}\left(\frac{\mu_t}{\sigma_\epsilon}\frac{\partial \epsilon}{\partial x_i}\right) + C_{1\epsilon}\frac{\epsilon \mu_t}{k}\left(\frac{\partial \overline{v_i}}{\partial x_j} + \frac{\partial \overline{v_j}}{\partial x_i}\right)\frac{\partial \overline{v_i}}{\partial x_j} - C_{2\epsilon}\frac{\rho\epsilon^2}{k} \tag{6-220}$$

In these equations summations over repeated indices are implied. The values for the empirical constants $C_{1\epsilon} = 1.44$, $C_{2\epsilon} = 1.92$, $\sigma_k = 1.0$, and $\sigma_\epsilon = 1.3$ are widely accepted (Launder and Spaulding, *The Numerical Computation of Turbulent Flows,* Imperial Coll. Sci. Tech. London, NTIS N74-12066 [1973]). The k–ϵ model has proved reasonably accurate for many flows without highly curved streamlines or significant swirl. It usually underestimates flow separation and overestimates turbulence production by normal straining. The k–ϵ model is suitable for high Reynolds number flows. See Virendra, Patel, Rodi, and Scheuerer (*AIAA J.,* **23,** 1308–1319 [1984]) for a review of low Reynolds number k–ϵ models.

More advanced models, more complex and computationally intensive, are being developed. For example, the renormalization group theory (Yakhot and Orszag, *J. Scientific Computing,* **1,** 1–51 [1986]; Yakhot, Orszag, Thangam, Gatski, and Speziale, *Phys. Fluids A,* **4,** 1510–1520 [1992]) modification of the k–ϵ model provides theoretical values of the model constants and provides substantial improvement in predictions of flows with stagnation, separation, normal straining, transient behavior such as vortex shedding, and relaminarization. Stress transport models provide equations for all nine Reynolds stress components, rather than introducing eddy viscosity. Algebraic closure equations for the Reynolds stresses are available, but are no longer in common use. Differential Reynolds stress models (e.g., Launder, Reece, and Rodi, *J. Fluid Mech.,* **68,** 537–566 [1975]) use differential conservation equations for all nine Reynolds stress components.

In **direct numerical simulation** of turbulent flows, the solution of the unaveraged equations of motion is sought. Due to the extreme computational intensity, solutions to date have been limited to relatively low Reynolds numbers (Re < about 10,000 to 20,000) in simple geometries such as channel flow. See, for example, Kim, Moin, and Moser (*J. Fluid Mech.,* **177,** 133 [1987]). Since computational grids must be sufficiently fine to resolve even the smallest eddies, the computational difficulty rapidly becomes prohibitive as Reynolds number increases. **Large eddy simulations** use models for subgrid turbulence while solving for larger-scale fluctuations.

Eddy Spectrum The energy that produces and sustains turbulence is extracted from velocity gradients in the mean flow, principally through vortex stretching. At Reynolds numbers well above the critical value there is a wide spectrum of eddy sizes, often described as a cascade of energy from the largest down to the smallest eddies. The largest eddies are of the order of the equipment size. The smallest are those for which viscous forces associated with the eddy velocity fluctuations are of the same order as inertial forces, so that turbulent fluctuations are rapidly damped out by viscous effects at smaller length scales. Most of the turbulent kinetic energy is contained in the larger eddies, while most of the dissipation occurs in the smaller eddies. Large eddies, which extract energy from the mean flow velocity gradients, are generally anisotropic. At smaller length scales, the directionality of the mean flow exerts less influence, and **local isotropy** is approached. The range of eddy scales for which local isotropy holds is called the **equilibrium range.**

Davies (*Turbulence Phenomena,* Academic, New York, 1972) presents a good discussion of the spectrum of eddy lengths for well-developed isotropic turbulence. The smallest eddies, usually called *Kolmogorov eddies* (Kolmogorov, *Compt. Rend. Acad. Sci. URSS,* **30,** 301; **32,** 16 [1941]), have a characteristic velocity fluctuation $\tilde{v}_K'$ given by

$$\tilde{v}_K' = (\nu\epsilon)^{1/4} \tag{6-221}$$

where ν = kinematic viscosity and ϵ = energy dissipation per unit mass. The size of the Kolmogorov eddy scale is

$$l_K = (\nu^3/\epsilon)^{1/4} \tag{6-222}$$

The Reynolds number for the Kolmogorov eddy, $\text{Re}_K = l_K \tilde{v}_K'/\nu$, is equal to unity by definition. In the equilibrium range, which exists for well-developed turbulence and extends from the medium eddy sizes down to the smallest, the energy dissipation at the smaller length scales is supplied by turbulent energy drawn from the bulk flow and passed down the spectrum of eddy lengths according to the scaling rule

$$\epsilon = \frac{(\tilde{v}')^3}{l} \tag{6-223}$$

which is consistent with Eqs. (6-221) and (6-222). For the medium, or energy-containing, eddy size,

$$\epsilon = \frac{(\tilde{v}_e')^3}{l_e} \tag{6-224}$$

For turbulent pipe flow, the friction velocity $u_* = \sqrt{\tau_w/\rho}$ used earlier in describing the universal turbulent velocity profile may be used as an estimate for $\tilde{v}_e'$. Together with the Blasius equation for the friction fac-

tor from which ϵ may be obtained (Eq. 6-214), this provides an estimate for the energy-containing eddy size in turbulent pipe flow:

$$l_e = 0.05D\mathrm{Re}^{-1/8} \tag{6-225}$$

where D = pipe diameter and Re = pipe Reynolds number. Similarly, the Kolmogorov eddy size is

$$l_K = 4D\mathrm{Re}^{-0.78} \tag{6-226}$$

Most of the energy dissipation occurs on a length scale about 5 times the Kolmogorov eddy size. The characteristic fluctuating velocity for these energy-dissipating eddies is about 1.7 times the Kolmogorov velocity.

The eddy spectrum is normally described using Fourier transform methods; see, for example, Hinze (*Turbulence,* McGraw-Hill, New York, 1975), and Tennekes and Lumley (*A First Course in Turbulence,* MIT Press, Cambridge, 1972). The spectrum $E(\kappa)$ gives the fraction of turbulent kinetic energy contained in eddies of wavenumber between κ and $\kappa + d\kappa$, so that $k = \int_0^\infty E(\kappa)\, d\kappa$. The portion of the equilibrium range excluding the smallest eddies, those which are affected by dissipation, is the **inertial subrange.** The Kolmogorov law gives $E(\kappa) \propto \kappa^{-5/3}$ in the inertial subrange.

Several texts are available for further reading on turbulent flow, including Tennekus and Lumley (ibid.), Hinze (*Turbulence,* McGraw-Hill, New York, 1975), Landau and Lifshitz (*Fluid Mechanics,* 2d ed., Chap. 3, Pergamon, Oxford, 1987) and Panton (*Incompressible Flow,* Wiley, New York, 1984).

COMPUTATIONAL FLUID DYNAMICS

Computational fluid dynamics (CFD) emerged in the 1980s as a significant tool for fluid dynamics both in research and in practice, enabled by rapid development in computer hardware and software. Commercial CFD software is widely available. Computational fluid dynamics is the numerical solution of the equations of continuity and momentum (Navier-Stokes equations for incompressible Newtonian fluids) along with additional conservation equations for energy and material species in order to solve problems of nonisothermal flow, mixing, and chemical reaction.

Textbooks include Fletcher (*Computational Techniques for Fluid Dynamics,* vol. 1: *Fundamental and General Techniques,* and vol. 2: *Specific Techniques for Different Flow Categories,* Springer-Verlag, Berlin, 1988), Hirsch (*Numerical Computation of Internal and External Flows,* vol. 1: *Fundamentals of Numerical Discretization,* and vol. 2: *Computational Methods for Inviscid and Viscous Flows,* Wiley, New York, 1988), Peyret and Taylor (*Computational Methods for Fluid Flow,* Springer-Verlag, Berlin, 1990), Canuto, Hussaini, Quarteroni, and Zang (*Spectral Methods in Fluid Dynamics,* Springer-Verlag, Berlin, 1988), Anderson, Tannehill, and Pletcher (*Computational Fluid Mechanics and Heat Transfer,* Hemisphere, New York, 1984), and Patankar (*Numerical Heat Transfer and Fluid Flow,* Hemisphere, Washington, D.C., 1980).

A wide variety of numerical methods has been employed, but three basic steps are common to all CFD methods:

1. **Subdivision or discretization of the flow domain into cells or elements.** There are methods, called *boundary element methods,* in which the surface of the flow domain, rather than the volume, is discretized, but the vast majority of CFD work uses volume discretization. Discretization produces a set of **grid** lines or curves which define a **mesh** and a set of **nodes** at which the flow variables are to be calculated. The equations of motion are solved approximately on a domain defined by the grid. Curvilinear or **body-fitted** coordinate system grids may be used to ensure that the discretized domain accurately represents the true problem domain.

2. **Discretization of the governing equations.** In this step, the exact partial differential equations to be solved are replaced by approximate algebraic equations written in terms of the nodal values of the dependent variables. Among the numerous discretization methods, **finite difference, finite volume,** and **finite element** methods are the most common. The *finite difference* method estimates spatial derivatives in terms of the nodal values and spacing between nodes. The governing equations are then written in terms of the nodal unknowns at each interior node. *Finite volume* methods, related to finite difference methods, may be derived by a volume integration of the equations of motion, with application of the divergence theorem, reducing by one the order of the differential equations. Equivalently, macroscopic balance equations are written on each cell. *Finite element* methods are weighted residual techniques in which the unknown dependent variables are expressed in terms of **basis functions** interpolating among the nodal values. The basis functions are substituted into the equations of motion, resulting in error residuals which are multiplied by the weighting functions, integrated over the control volume, and set to zero to produce algebraic equations in terms of the nodal unknowns. Selection of the weighting functions defines the various finite element methods. For example, Galerkin's method uses the nodal interpolation basis functions as weighting functions. Each method also has its own method for implementing **boundary conditions.** The end result after discretization of the equations and application of the boundary conditions is a set of algebraic equations for the nodal unknown variables. Discretization in time is also required for the $\partial/\partial t$ time derivative terms in unsteady flow; finite differencing in time is often used. The descretized equations represent an approximation of the exact equations, and their solution gives an approximation for the flow variables. The accuracy of the solution improves as the grid is **refined;** that is, as the number of nodal points is increased.

3. **Solution of the algebraic equations.** For creeping flows, the algebraic equations are linear and a linear matrix equation is to be solved. Both direct and iterative solvers have been used. For most flows, the nonlinear inertial terms in the momentum equation are important and the algebraic discretized equations are therefore nonlinear. Solution yields the nodal values of the unknowns.

CFD solutions, especially for complex three-dimensional flows, generate very large quantities of solution data. Computer graphics have greatly improved the ability to examine CFD solutions and visualize flow.

CFD methods are used for incompressible and compressible, creeping, laminar and turbulent, Newtonian and non-Newtonian, and isothermal and nonisothermal flows. Chemically reacting flows, particularly in the field of combustion, have been simulated. Solution accuracy must be considered from several perspectives. These include convergence of the algorithms for solving the nonlinear discretized equations and convergence with respect to refinement of the mesh so that the discretized equations better approximate the exact equations and, in some cases, so that the mesh more accurately fits the true geometry. The possibility that steady-state solutions are unstable must always be considered. In addition to numerical sources of error, modeling errors are introduced in turbulent flow, where semiempirical closure models are used to solve time-averaged equations of motion, as discussed previously. Most commercial CFD codes include the k–ϵ turbulence model, which has been by far the most widely used. More accurate models, such as differential Reynolds stress and renormalization group theory models, are also becoming available. Significant solution error is known to result in some problems from inadequacy of the turbulence model. Closure models for nonlinear chemical reaction source terms may also contribute to inaccuracy. **Direct numerical simulation** and **large eddy simulation,** which involve solutions for velocity fluctuations, under limited conditions or with certain modeling assumptions, remain primarily research areas.

In its general sense, multiphase flow is not currently solvable by computational fluid dynamics. However, in certain cases reasonable solutions are possible. These include well-separated flows where the phases are confined to relatively well-defined regions separated by one or a few interfaces and flows in which a second phase appears as discrete particles of known size and shape whose motion may be approximately computed with drag coefficient formulations, or rigorously computed with refined meshes applying boundary conditions at the particle surface. **Two-fluid modeling,** in which the phases are treated as overlapping continua, with each phase occupying a volume fraction that is a continuous function of position (and time) is a useful approximation which is becoming available in commercial software. See Elghobashi and Abou-Arab (*J. Physics Fluids,* **26,** 931–938 [1983]) for a k–ϵ model for two-fluid systems.

Figure 6-56 gives an example CFD calculation for time-dependent flow past a square cylinder at a Reynolds number of 22,000 (Choudhury, et al., *Trans. ASME Fluids Div.,* Lake Tahoe, Nev. [1994]). The computation was done with an implementation of the renormalization group theory k–ϵ model. The series of contour plots of stream function shows a sequence in time over about 1 vortex-shedding period. The calculated Strouhal number (Eq. [6-195]) is 0.146, in excellent agreement with experiment, as is the time-averaged drag coefficient, $C_D = 2.24$. Similar computations for a circular cylinder at Re = 14,500 have given excellent agreement with experimental measurements for St and C_D (*Introduction to the Renormalization Group Method and Turbulence Modeling,* Fluent, Inc., 1993).

DIMENSIONLESS GROUPS

For purposes of data correlation, model studies, and scale-up, it is useful to arrange variables into dimensionless groups. Table 6-7 lists many of the dimensionless groups commonly found in fluid mechanics problems, along with their physical interpretations and areas of application. More extensive tabulations may be found in Catchpole and Fulford (*Ind. Eng. Chem.,* **58**[3], 46–60 [1966]) and Fulford and Catchpole (*Ind. Eng. Chem.,* **60**[3], 71–78 [1968]).

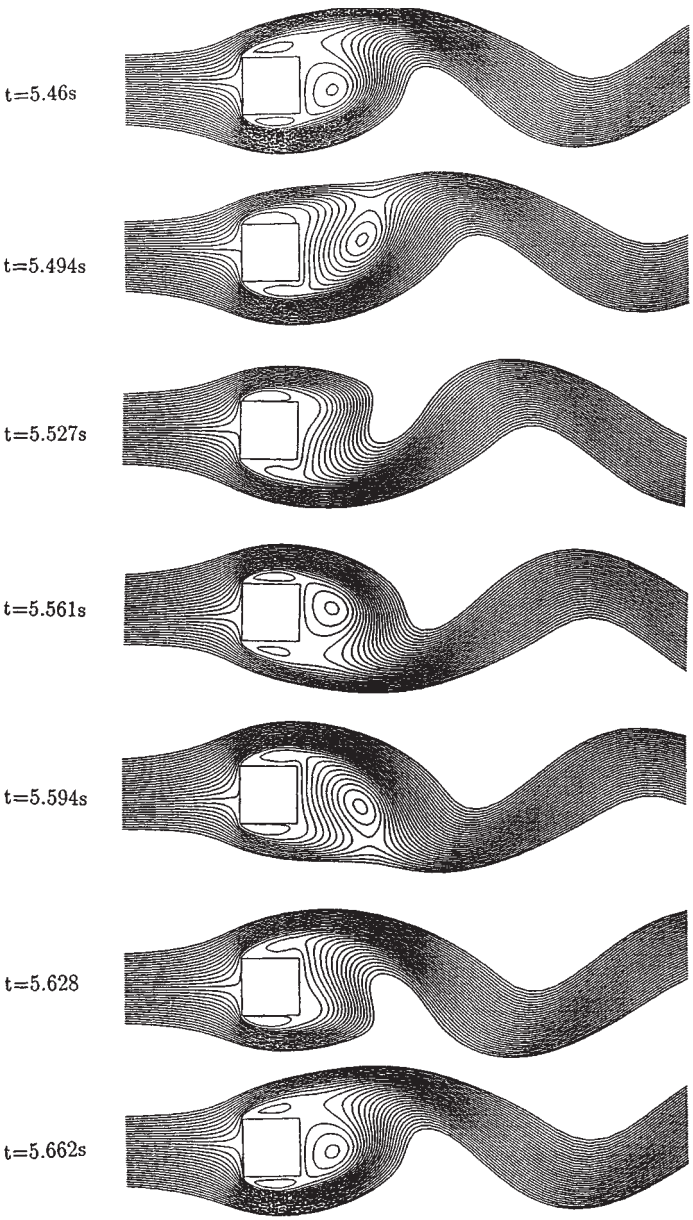

FIG. 6-56 Computational fluid dynamic simulation of flow over a square cylinder, showing one vortex shedding period. (*From Choudhury, et al.,* Trans. ASME Fluids Div., *TN-076 [1994].*)

TABLE 6-7 Dimensionless Groups and Their Significance

Name	Symbol	Formula	Physical interpretation	Comments
Archimedes number	Ar	$\frac{gL^3(\rho_p - \rho)\rho}{\mu^2}$	$\frac{\text{inertial forces} \times \text{buoyancy forces}}{(\text{viscous forces})^2}$	Particle settling
Bingham number	Bm	$\frac{\tau_y L}{\mu_\infty V}$	$\frac{\text{yield stress}}{\text{viscous stress}}$	Flow of Bingham plastics = yield number, Y
Bingham Reynolds number	Re_B	$\frac{LV\rho}{\mu_\infty}$	$\frac{\text{inertial force}}{\text{viscous force}}$	Flow of Bingham plastics
Blake number	B	$\frac{V\rho}{\mu(1-\epsilon)s}$	$\frac{\text{inertial force}}{\text{viscous force}}$	Beds of solids
Bond number	Bo	$\frac{(\rho_L - \rho_G)L^2 g}{\sigma}$	$\frac{\text{gravitational force}}{\text{surface-tension force}}$	Atomization = Eotvos number, Eo
Capillary number	Ca	$\frac{\mu V}{\sigma}$	$\frac{\text{viscous force}}{\text{surface-tension force}}$	Two-phase flows, free surface flows
Cauchy number	C	$\frac{\rho V^2}{\beta}$	$\frac{\text{inertial force}}{\text{compressibility force}}$	Compressible flow, hydraulic transients
Cavitation number	σ	$\frac{p - p_v}{\rho V^2/2}$	$\frac{\text{excess pressure above vapor pressure}}{\text{velocity head}}$	Cavitation
Dean number	D_e	$\frac{\text{Re}}{(Dc/D)^{1/2}}$	$\text{Reynolds number} \times \frac{\text{inertial force}}{\text{centrifugal force}}$	Flow in curved channels
Deborah number	De	$\lambda\omega$	$\frac{\text{fluid relaxation time}}{\text{flow characteristic time}}$	Viscoelastic flow
Drag coefficient	C_D	$\frac{F_D}{A\rho V^2/2}$	$\frac{\text{drag force}}{\text{projected area} \times \text{velocity head}}$	Flow around objects, particle settling
Elasticity number	El	$\frac{\lambda\mu}{\rho L^2}$	$\frac{\text{elastic force}}{\text{inertial force}}$	Viscoelastic flow
Euler number	Eu	$\frac{\Delta p}{\rho V^2}$	$\frac{\text{frictional pressure loss}}{2 \times \text{velocity head}}$	Fluid friction in conduits
Fanning friction factor	f	$\frac{D\Delta p}{2\rho V^2 L} = \frac{2\tau_w}{\rho V^2}$	$\frac{\text{wall shear stress}}{\text{velocity head}}$	Fluid friction in conduits Darcy friction factor = $4f$
Froude number	Fr	$\frac{V^2}{gL}$	$\frac{\text{inertial force}}{\text{gravity force}}$	Often defined as $\text{Fr} = V/\sqrt{gL}$
Densometric Froude number	Fr′	$\frac{\rho V^2}{(\rho_d - \rho)gL}$	$\frac{\text{inertial force}}{\text{gravity force}}$	or $\text{Fr}' = \frac{V}{\sqrt{(\rho_d - \rho)gL/\rho}}$
Hedstrom number	He	$\frac{L^2\tau_y\rho}{\mu_\infty^2}$	Bingham Reynolds number × Bingham number	Flow of Bingham plastics
Hodgson number	H	$\frac{V'\omega\Delta p}{\overline{q}\,\overline{p}}$	$\frac{\text{time constant of system}}{\text{period of pulsation}}$	Pulsating gas flow
Mach number	M	$\frac{V}{c}$	$\frac{\text{fluid velocity}}{\text{sonic velocity}}$	Compressible flow
Newton number				
Ohnesorge number	Z	$\frac{\mu}{(\rho L\sigma)^{1/2}}$	$\frac{\text{viscous force}}{(\text{inertial force} \times \text{surface tension force})^{1/2}}$	$\text{Atomization} = \frac{\text{Weber number}}{\text{Reynolds number}}$
Peclet number	Pe	$\frac{LV}{D}$	$\frac{\text{convective transport}}{\text{diffusive transport}}$	Heat, mass transfer, mixing
Pipeline parameter	Pn	$\frac{aV_o}{2gH}$	$\frac{\text{maximum water-hammer pressure rise}}{2 \times \text{static pressure}}$	Water hammer

TABLE 6-7 Dimensionless Groups and Their Significance (*Concluded*)

Name	Symbol	Formula	Physical interpretation	Comments
Power number	Po	$\frac{P}{\rho N^3 L^5}$	$\frac{\text{impeller drag force}}{\text{inertial force}}$	Agitation
Prandtl velocity ratio	v^+	$\frac{v}{(\tau_w/\rho)^{1/2}}$	velocity normalized by friction velocity	Turbulent flow near a wall, friction velocity $= \sqrt{\tau_w/\rho}$
Reynolds number	Re	$\frac{LV\rho}{\mu}$	$\frac{\text{inertial force}}{\text{viscous force}}$	
Strouhal number	St	$\frac{f'L}{V}$	vortex shedding frequency × characteristic flow time scale	Vortex shedding, von Karman vortex streets
Weber number	We	$\frac{\rho V^2 L}{\sigma}$	$\frac{\text{inertial force}}{\text{surface tension force}}$	Bubble, drop formation

Nomenclature		SI Units	Nomenclature		SI Units
a	Wave speed	m/s	P	Power	Watts
A	Projected area	m	$\overline{q}$	Average volumetric flow rate	m^3/s
c	Sonic velocity	m/s	s	Particle area/particle volume	1/m
D	Diameter of pipe	m	v	Local fluid velocity	m/s
D_c	Diameter of curvature	m	V	Characteristic or average fluid velocity	m/s
D'	Diffusivity	m^2/s	V'	System volume	m^3
f'	Vortex shedding frequency	1/s	β	Bulk modulus	Pa
F_D	Drag force	N	ϵ	Void fraction	m^3
g	Acceleration of gravity	m/s	λ	Fluid relaxation time	s
H	Static head	m	μ	Fluid viscosity	Pa · s
L	Characteristic length	m	μ_∞	Infinite shear viscosity (Bingham plastics)	Pa · s
N	Rotational speed	1/s	ρ	Fluid density	kg/m^3
p	Pressure	Pa	ρ_G, ρ_L	Gas, liquid densities	kg/m^3
p_v	Vapor pressure	Pa	ρ_d	Dispersed phase density	kg/m^3
$\overline{p}$	Average static pressure	Pa	σ	Surface tension	N/m
Δp	Frictional pressure drop	Pa	ω	Characteristic frequency or reciprocal time scale of flow	1/s

PARTICLE DYNAMICS

General References: Brodkey, *The Phenomena of Fluid Motions*, Addison-Wesley, Reading, Mass., 1967; Clift, Grace, and Weber, *Bubbles, Drops and Particles*, Academic, New York, 1978; Govier and Aziz, *The Flow of Complex Mixtures in Pipes*, Van Nostrand Reinhold, New York, 1972, Krieger, Huntington, N.Y., 1977; Lapple, et al., *Fluid and Particle Mechanics*, University of Delaware, Newark, 1951; Levich, *Physicochemical Hydrodynamics*, Prentice-Hall, Englewood Cliffs, N.J., 1962; Orr, *Particulate Technology*, Macmillan, New York, 1966; Shook and Roco, *Slurry Flow*, Butterworth-Heinemann, Boston, 1991; Wallis, *One-dimensional Two-phase Flow*, McGraw-Hill, New York, 1969.

DRAG COEFFICIENT

Whenever relative motion exists between a particle and a surrounding fluid, the fluid will exert a drag upon the particle. In steady flow, the drag force on the particle is

$$F_D = \frac{C_D A_P \rho u^2}{2} \tag{6-227}$$

where F_D = drag force
C_D = drag coefficient
A_P = projected particle area in direction of motion
ρ = density of surrounding fluid
u = relative velocity between particle and fluid

The drag force is exerted in a direction parallel to the fluid velocity. Equation (6-227) defines the **drag coefficient.** For some solid bodies, such as aerofoils, a lift force component perpendicular to the liquid velocity is also exerted. For free-falling particles, lift forces are generally not important. However, even spherical particles experience lift forces in shear flows near solid surfaces.

TERMINAL SETTLING VELOCITY

A particle falling under the action of gravity will accelerate until the drag force balances gravitational force, after which it falls at a constant **terminal** or **free-settling velocity** u_t, given by

$$u_t = \sqrt{\frac{2gm_p(\rho_p - \rho)}{\rho \rho_p A_P C_D}} \tag{6-228}$$

where g = acceleration of gravity
m_p = particle mass
ρ_p = particle density

and the remaining symbols are as previously defined.

Settling particles may undergo fluctuating motions owing to vortex shedding, among other factors. Oscillation is enhanced with increasing separation between the mass and geometric centers of the particle. Variations in mean velocity are usually less than 10 percent. The drag force on a particle fixed in space with fluid moving is somewhat lower than the drag force on a particle freely settling in a stationary fluid at the same relative velocity.

Spherical Particles For spherical particles of diameter d_p, Eq. (6-228) becomes

$$u_t = \sqrt{\frac{4gd_p(\rho_p - \rho)}{3\rho C_D}} \tag{6-229}$$

The drag coefficient for rigid spherical particles is a function of particle Reynolds number, $\mathrm{Re}_p = d_p \rho u/\mu$ where μ = fluid viscosity, as shown in Fig. 6-57. At low Reynolds number, **Stokes' Law** gives

$$C_D = \frac{24}{\mathrm{Re}_p} \qquad \mathrm{Re}_p < 0.1 \tag{6-230}$$

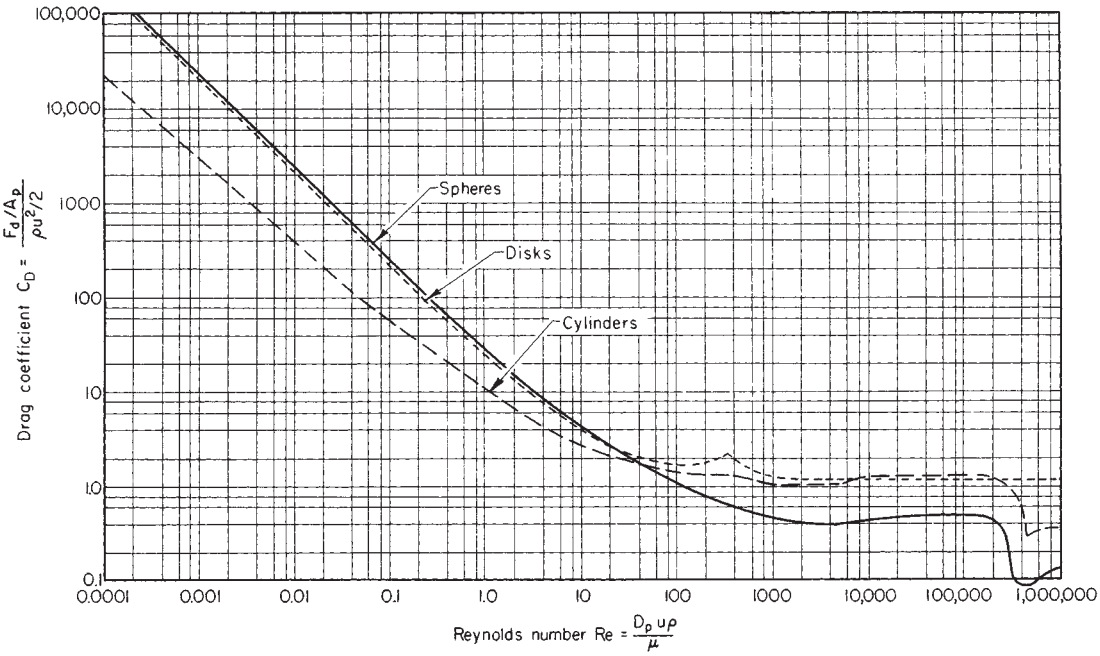

FIG. 6-57 Drag coefficients for spheres, disks, and cylinders: A_p = area of particle projected on a plane normal to direction of motion; C = overall drag coefficient, dimensionless; D_p = diameter of particle; F_d = drag or resistance to motion of body in fluid; Re = Reynolds number, dimensionless; u = relative velocity between particle and main body of fluid; μ = fluid viscosity; and ρ = fluid density. (*From Lapple and Shepherd,* Ind. Eng. Chem., **32,** *605 [1940].*)

which may also be written

$$F_D = 3\pi\mu u d_p \qquad \mathrm{Re}_p < 0.1 \tag{6-231}$$

and gives for the terminal settling velocity

$$u_t = \frac{g d_p^2 (\rho_p - \rho)}{18\mu} \qquad \mathrm{Re}_p < 0.1 \tag{6-232}$$

In the **intermediate regime** ($0.1 < \mathrm{Re}_p < 1{,}000$), the drag coefficient may be estimated within 6 percent by

$$C_D = \left(\frac{24}{\mathrm{Re}_p}\right)\left(1 + 0.14\mathrm{Re}_p^{0.70}\right) \qquad 0.1 < \mathrm{Re}_p < 1{,}000 \tag{6-233}$$

In the **Newton's Law** regime, which covers the range $1{,}000 < \mathrm{Re}_p < 350{,}000$, $C_D = 0.445$, within 13 percent. In this region, Eq. (6-227) becomes

$$u_t = 1.73\sqrt{\frac{g d_p(\rho_p - \rho)}{\rho}} \qquad 1{,}000 < \mathrm{Re}_p < 350{,}000 \tag{6-234}$$

Between about $\mathrm{Re}_p = 350{,}000$ and 1×10^6, the drag coefficient drops dramatically in a **drag crisis** owing to the transition to turbulent flow in the boundary layer around the particle, which delays aft separation, resulting in a smaller wake and less drag. Beyond $\mathrm{Re} = 1 \times 10^6$, the drag coefficient may be estimated from (Clift, Grace, and Weber):

$$C_D = 0.19 - \frac{8 \times 10^4}{\mathrm{Re}_p} \qquad \mathrm{Re}_p > 1 \times 10^6 \tag{6-235}$$

Drag coefficients may be affected by turbulence in the free-stream flow; the drag crisis occurs at lower Reynolds numbers when the free stream is turbulent. Torobin and Guvin (*AIChE J.,* **7,** 615–619 [1961]) found that the drag crisis Reynolds number decreases with increasing free-stream turbulence, reaching a value of 400 when the relative turbulence intensity, defined as $\sqrt{u'}/\overline{U}_R$ is 0.4. Here $\sqrt{u'}$ is the rms fluctuating velocity and $\overline{U}_R$ is the relative velocity between the particle and the fluid.

For particles settling in **non-Newtonian** fluids, correlations are given by Dallon and Christiansen (Preprint 24C, *Symposium on Selected Papers,* part III, 61st Ann. Mtg. AIChE, Los Angeles, Dec. 1–5, 1968) for spheres settling in shear-thinning liquids, and by Ito and Kajiuchi (*J. Chem. Eng. Japan,* **2**[1], 19–24 [1969]) and Pazwash and Robertson (*J. Hydraul. Res.,* **13,** 35–55 [1975]) for spheres settling in Bingham plastics. Beris, Tsamopoulos, Armstrong, and Brown (*J. Fluid Mech.,* **158** [1985]) present a finite element calculation for creeping motion of a sphere through a Bingham plastic.

Nonspherical Rigid Particles The drag on a nonspherical particle depends upon its shape and orientation with respect to the direction of motion. The orientation in free fall as a function of Reynolds number is given in Table 6-8.

The drag coefficients for **disks** (flat side perpendicular to the direction of motion) and for **cylinders** (infinite length with axis perpendicular to the direction of motion) are given in Fig. 6-57 as a function of Reynolds number. The effect of length-to-diameter ratio for cylinders in the Newton's law region is reported by Knudsen and Katz (*Fluid Mechanics and Heat Transfer,* McGraw-Hill, New York, 1958).

Pettyjohn and Christiansen (*Chem. Eng. Prog.,* **44,** 157–172 [1948]) present correlations for the effect of particle shape on free-settling velocities of **isometric particles.** For $\mathrm{Re} < 0.05$, the terminal or free-settling velocity is given by

TABLE 6-8 Free-Fall Orientation of Particles

Reynolds number*	Orientation
0.1–5.5	All orientations are stable when there are three or more perpendicular axes of symmetry.
5.5–200	Stable in position of maximum drag.
200–500	Unpredictable. Disks and plates tend to wobble, while fuller bluff bodies tend to rotate.
500–200,000	Rotation about axis of least inertia, frequently coupled with spiral translation.

SOURCE: From Becker, *Can. J. Chem. Eng.,* **37,** 85–91 (1959).
*Based on diameter of a sphere having the same surface area as the particle.

$$u_t = K_1 \frac{g d_s^2 (\rho_p - \rho)}{18\mu} \tag{6-236}$$

$$K_1 = 0.843 \log\left(\frac{\psi}{0.065}\right) \tag{6-237}$$

where ψ = sphericity, the surface area of a sphere having the same volume as the particle, divided by the actual surface area of the particle; d_s = equivalent diameter, equal to the diameter of the equivalent sphere having the same volume as the particle; and other variables are as previously defined.

In the **Newton's law region,** the terminal velocity is given by

$$u_t = \sqrt{\frac{4 d_s (\rho_p - \rho) g}{3 K_3 \rho}} \tag{6-238}$$

$$K_3 = 5.31 - 4.88\psi \tag{6-239}$$

Equations (6-236) to (6-239) are based on experiments on cube-octahedrons, octahedrons, cubes, and tetrahedrons for which the sphericity ψ ranges from 0.906 to 0.670, respectively. See also Clift, Grace, and Weber. A graph of drag coefficient vs. Reynolds number with ψ as a parameter may be found in Brown, et al. (*Unit Operations,* Wiley, New York, 1950) and in Govier and Aziz.

For particles with $\psi < 0.67$, the correlations of Becker (*Can. J. Chem. Eng.,* **37,** 85–91 [1959]) should be used. Reference to this paper is also recommended for **intermediate region** flow. Settling characteristics of nonspherical particles are discussed by Clift, Grace, and Weber, Chaps. 4 and 6.

The terminal velocity of **axisymmetric particles in axial motion** can be computed from Bowen and Masliyah (*Can. J. Chem. Eng.,* **51,** 8–15 [1973]) for low–Reynolds number motion:

$$u_t = \frac{V'}{K_2} \frac{g D_s^2 (\rho_p - \rho)}{18\mu} \tag{6-240}$$

$$K_2 = 0.244 + 1.035\Sigma - 0.712\Sigma^2 + 0.441\Sigma^3 \tag{6-241}$$

where D_s = diameter of sphere with perimeter equal to maximum particle projected perimeter
V' = ratio of particle volume to volume of sphere with diameter D_s
Σ = ratio of surface area of particle to surface area of a sphere with diameter D_s

and other variables are as defined previously.

Hindered Settling When particle concentration increases, particle settling velocities decrease because of hydrodynamic interaction between particles and the upward motion of displaced liquid. The suspension viscosity increases. Hindered settling is normally encountered in sedimentation and transport of concentrated slurries. Below 0.1 percent volumetric particle concentration, there is less than a 1 percent reduction in settling velocity. Several expressions have been given to estimate the effect of particle volume fraction on settling velocity. Maude and Whitmore (*Br. J. Appl. Phys.,* **9,** 477–482 [1958]) give, for uniformly sized spheres,

$$u_t = u_{t0}(1 - c)^n \tag{6-242}$$

where u_t = terminal settling velocity
u_{t0} = terminal velocity of a single sphere (infinite dilution)
c = volume fraction solid in the suspension
n = function of Reynolds number $\mathrm{Re}_p = d_p u_{t0} \rho/\mu$ as given Fig. 6-58

In the Stokes' law region ($\mathrm{Re}_p < 0.3$), $n = 4.65$ and in the Newton's law region ($\mathrm{Re}_p > 1{,}000$), $n = 2.33$. Equation (6-242) may be applied to particles of any size in a polydisperse system, provided the volume fraction corresponding to all the particles is used in computing terminal velocity (Richardson and Shabi, *Trans. Inst. Chem. Eng.* [*London*], **38,** 33–42 [1960]). The concentration effect is greater for nonspherical and angular particles than for spherical particles (Steinour, *Ind. Eng. Chem.,* **36,** 840–847 [1944]). Theoretical developments for low–Reynolds number flow assemblages of spheres are given by Happel and Brenner (*Low Reynolds Number Hydrodynamics,* Prentice-Hall, Englewood Cliffs, N.J., 1965) and Famularo and Happel (*AIChE J.,* **11,** 981 [1965]) leading to an equation of the form

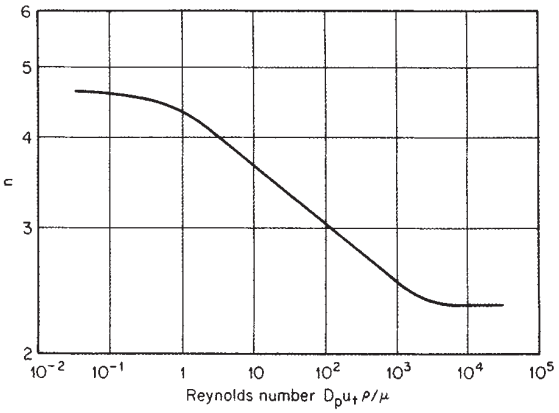

FIG. 6-58 Values of exponent n for use in Eq. (6-240). (*From Maude and Whitmore,* Br. J. Appl. Phys., **9,** *481 [1958]. Courtesy of the Institute of Physics and the Physical Society.*)

$$u_t = \frac{u_{t0}}{1 + \gamma c^{1/3}} \tag{6-243}$$

where γ is about 1.3. As particle concentration increases, resulting in interparticle contact, hindered settling velocities are difficult to predict. Thomas (*AIChE J.,* **9,** 310 [1963]) provides an empirical expression reported to be valid over the range $0.08 < u_t/u_{t0} < 1$:

$$\ln\left(\frac{u_t}{u_{t0}}\right) = -5.9c \tag{6-244}$$

Time-Dependent Motion The time-dependent motion of particles is computed by application of Newton's second law, equating the rate of change of particle motion to the net force acting on the particle. Rotation of particles may also be computed from the net torque. For large particles moving through low-density gases, it is usually sufficient to compute the force due to fluid drag from the relative velocity and the drag coefficient computed for steady flow conditions. For two- and three-dimensional problems, the velocity appearing in the particle Reynolds number and the drag coefficient is the amplitude of the relative velocity. The drag force, not the relative velocity, is to be resolved into vector components to compute the particle acceleration components. Clift, Grace, and Weber (*Bubbles, Drops and Particles,* Academic, London, 1978) discuss the complexities that arise in the computation of transient drag forces on particles when the transient nature of the flow is important. Analytical solutions for the case of a single particle in creeping flow ($\mathrm{Re}_p = 0$) are available. For example, the creeping motion of a sphericial particle released from rest in a stagnant fluid is described by

$$\rho_p V \frac{dU}{dt} = g(\rho_p - \rho)V - 3\pi\mu d_p U - \frac{\rho}{2} V \frac{dU}{dt} - \left(\frac{3}{2}\right) d_p^2 \sqrt{\pi\rho\mu} \int_0^t \frac{(dU/dt)_{t=s}\, ds}{\sqrt{t - s}} \tag{6-245}$$

Here, U = particle velocity, positive in the direction of gravity, and V = particle volume. The first term on the right-hand side is the net gravitational force on the particle, accounting for buoyancy. The second is the steady-state Stokes drag (Eq. 6-231). The third is the **added mass** or **virtual mass** term, which may be interpreted as the inertial effect of the fluid which is accelerated along with the particle. The volume of the added mass of fluid is half the particle volume. The last term, the **Basset force,** depends on the entire history of the transient motion, with past motions weighted inversely with the square root of elapsed time. Clift, et al. provide integrated solutions. In **turbulent flows,** particle velocity will closely follow fluid eddy velocities when (Clift et al.)

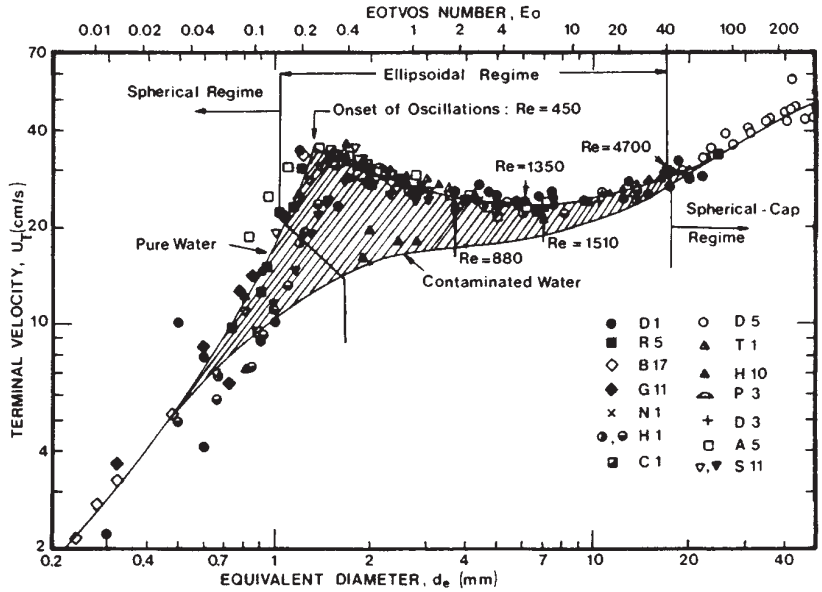

FIG. 6-59 Terminal velocity of air bubbles in water at 20°C. (*From Clift, Grace, and Weber,* Bubbles, Drops and Particles, *Academic, New York, 1978*).

$$\tau_0 >> \frac{d_p^2[(2\rho_p/\rho) + 1]}{36\nu} \qquad (6\text{-}246)$$

where τ_0 = oscillation period or eddy time scale, the right-hand side expression is the **particle relaxation time,** and ν = kinematic viscosity.

Gas Bubbles Fluid particles, unlike rigid solid particles, may undergo deformation and internal circulation. Figure 6-59 shows rise velocity data for air bubbles in stagnant water. In the figure, Eo = Eotvos number, $g(\rho_L - \rho_G)d_b^2/\sigma$, where ρ_L = liquid density, ρ_G = gas density, d_b = bubble diameter, and σ = surface tension. Small bubbles (<1-mm [0.04-in] diameter) remain spherical and rise in straight lines. The presence of surface active materials generally renders small bubbles rigid, and they rise roughly according to the drag coefficient and terminal velocity equations for spherical solid particles. Bubbles roughly in the range 2- to 8-mm (0.079- to 0.32-in) diameter assume flattened, ellipsoidal shape, and rise in a zig-zag or spiral pattern. This motion increases dissipation and drag, and the rise velocity may actually decrease with increasing bubble diameter in this region, characterized by rise velocities in the range of 20 to 30 cm/s (0.7 to 1.0 ft/s). Large bubbles, >8-mm (0.32-in) diameter, are greatly deformed, assuming a mushroomlike, spherical cap shape. These bubbles are unstable and may break into smaller bubbles. Carefully purified water, free of surface active materials, allows bubbles to freely circulate even when they are quite small. Under creeping flow conditions $Re_b = d_b u_r \rho_L/\mu_L < 1$, where u_r = bubble rise velocity and μ_L = liquid viscosity, the bubble rise velocity may be computed analytically from the Hadamard-Rybczynski formula (Levich, *Physicochemical Hydrodynamics*, Prentice-Hall, Englewood Cliffs, N.J., 1962, p. 402). When $\mu_G/\mu_L << 1$, which is normally the case, the rise velocity is 1.5 times the rigid sphere Stokes law velocity. However, in practice, most liquids, including ordinary distilled water, contain sufficient surface active materials to render small bubbles rigid. Larger bubbles undergo deformation in both purified and ordinary liquids; however, the variation in rise velocity for large bubbles with degree of purity is quite evident in Fig. 6-59. For additional discussion, see Clift, et al., Chap. 7. Figure 6-60 gives the drag coefficient as a function of bubble or drop Reynolds number for air bubbles in water and water drops in air, compared with the standard drag curve for rigid spheres. Information on bubble motion in **non-Newtonian** liquids may be found in Astarita and Apuzzo (*AIChE J.*, **11,** 815–820 [1965]); Calderbank, Johnson, and Loudon (*Chem. Eng. Sci.*, **25,** 235–256 [1970]); and Acharya, Mashelkar, and Ulbrecht (*Chem. Eng. Sci.*, **32,** 863–872 [1977]).

Liquid Drops in Liquids Very small liquid drops in immisicibile liquids behave like rigid spheres, and the terminal velocity can be approximated by use of the drag coefficient for solid spheres up to a Reynolds number of about 10 (Warshay, Bogusz, Johnson, and Kintner, *Can. J. Chem. Eng.*, **37,** 29–36 [1959]). Between Reynolds numbers of 10 and 500, the terminal velocity exceeds that for rigid spheres owing to internal circulation. In normal practice, the effect of drop phase viscosity is neglected. Grace, Wairegi, and Nguyen (*Trans. Inst. Chem. Eng.*, **54,** 167–173 [1976]; Clift, et al., op. cit., pp. 175–177) present a correlation for terminal velocity valid in the range

$$M < 10^{-3} \qquad \text{Eo} < 40 \qquad \text{Re} > 0.1 \qquad (6\text{-}247)$$

where M = Morton number = $g\mu^4\Delta\rho/\rho^2\sigma^3$
Eo = Eotvos number = $g\Delta\rho d^2/\sigma$
Re = Reynolds number = $du\rho/\mu$
$\Delta\rho$ = density difference between the phases
ρ = density of continuous liquid phase
d = drop diameter
μ = continuous liquid viscosity
σ = surface tension
u = relative velocity

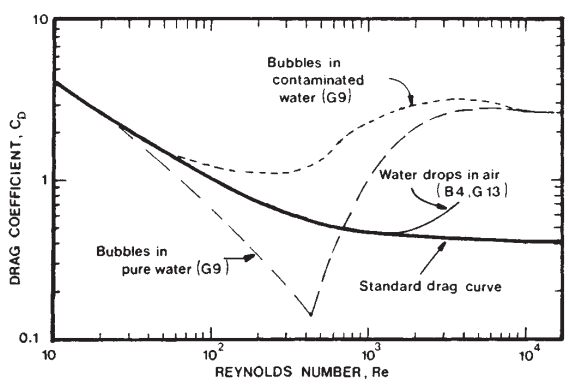

FIG. 6-60 Drag coefficient for water drops in air and air bubbles in water. Standard drag curve is for rigid spheres. (*From Clift, Grace, and Weber,* Bubbles, Drops and Particles, *Academic, New York, 1978.*)

The correlation is represented by

$$J = 0.94H^{0.757} \qquad (2 < H \le 59.3) \tag{6-248}$$

$$J = 3.42H^{0.441} \qquad (H > 59.3) \tag{6-249}$$

where

$$H = \frac{4}{3}\,\mathrm{Eo}M^{-0.149}\left(\frac{\mu}{\mu_w}\right)^{-0.14} \tag{6-250}$$

$$J = \mathrm{Re}M^{0.149} + 0.857 \tag{6-251}$$

Note that the terminal velocity may be evaluated explicitly from

$$u = \frac{\mu}{\rho d}\,M^{-0.149}(J - 0.857) \tag{6-252}$$

In Eq. (6-250), μ = viscosity of continuous liquid and μ_w = viscosity of water, taken as 0.9 cP (0.0009 Pa · s).

For drop velocities in non-Newtonian liquids, see Mhatre and Kinter (*Ind. Eng. Chem.*, **51,** 865–867 [1959]); Marrucci, Apuzzo, and Astarita (*AIChE J.*, **16,** 538–541 [1970]); and Mohan, et al. (*Can. J. Chem. Eng.*, **50,** 37–40 [1972]).

Liquid Drops in Gases Liquid drops falling in stagnant gases appear to remain spherical and follow the rigid sphere drag relationships up to a Reynolds number of about 100. Large drops will deform, with a resulting increase in drag, and in some cases will shatter. The largest water drop which will fall in air at its terminal velocity is about 8 mm (0.32 in) in diameter, with a corresponding velocity of about 9 m/s (30 ft/s). Drops shatter when the Weber number defined as

$$\mathrm{We} = \frac{\rho_G u^2 d}{\sigma} \tag{6-253}$$

exceeds a critical value. Here, ρ_G = gas density, u = drop velocity, d = drop diameter, and σ = surface tension. A value of $\mathrm{We}_c = 13$ is often cited for the critical Weber number.

Terminal velocities for water drops in air have been correlated by Berry and Prnager (*J. Appl. Meteorol.*, **13,** 108–113 [1974]) as

$$\mathrm{Re} = \exp\left[-3.126 + 1.013 \ln N_D - 0.01912(\ln N_D)^2\right] \tag{6-254}$$

for $2.4 < N_D < 10^7$ and $0.1 < \mathrm{Re} < 3550$. The dimensionless group N_D (often called the *Best* number [Clift, et al.]) is given by

$$N_D = \frac{4\rho\Delta\rho g d^3}{3\mu^2} \tag{6-255}$$

and is proportional to the similar Archimedes and Galileo numbers.

Figure 6-61 gives calculated settling velocities for solid spherical particles settling in air or water using the standard drag coefficient curve for spherical particles. For fine particles settling in air, the **Stokes-Cunningham correction** has been applied to account for particle size comparable to the mean free path of the gas. The correction is less than 1 percent for particles larger than 16 μm settling in air. Smaller particles are also subject to **Brownian motion.** Motion of particles smaller than 0.1 μm is dominated by Brownian forces and gravitational effects are small.

Wall Effects When the diameter of a settling particle is significant compared to the diameter of the container, the settling velocity is reduced. For rigid spherical particles settling with Re < 1, the correction given in Table 6-9 may be used. The factor k_w is multiplied by the settling velocity obtained from Stokes' law to obtain the corrected settling rate. For values of diameter ratio β = particle diameter/vessel diameter less than 0.05, $k_w = 1/(1 + 2.1\beta)$ (Zenz and Othmer, *Fluidization and Fluid-Particle Systems,* Reinhold, New York, 1960, pp. 208–209). In the range $100 < \mathrm{Re} < 10{,}000$, the computed terminal velocity for rigid spheres may be multiplied by k'_w to account for wall effects, where k'_w is given by (Harmathy, *AIChE J.*, **6,** 281 [1960])

$$k'_w = \frac{1 - \beta^2}{\sqrt{1 + \beta^4}} \tag{6-256}$$

For gas bubbles in liquids, there is little wall effect for β < 0.1. For β > 0.1, see Uto and Kintner (*AIChE J.*, **2,** 420–424 [1956]), Maneri and Mendelson (*Chem. Eng. Prog.*, **64,** *Symp. Ser.*, **82,** 72–80 [1968]), and Collins (*J. Fluid Mech.*, **28,** part 1, 97–112 [1967]).

TABLE 6-9 Wall Correction Factor for Rigid Spheres in Stokes' Law Region

β*	k_w	β	k_w
0.0	1.000	0.4	0.279
0.05	0.885	0.5	0.170
0.1	0.792	0.6	0.0945
0.2	0.596	0.7	0.0468
0.3	0.422	0.8	0.0205

SOURCE: From Haberman and Sayre, *David W. Taylor Model Basin Report* 1143, 1958.

*β = particle diameter divided by vessel diameter.

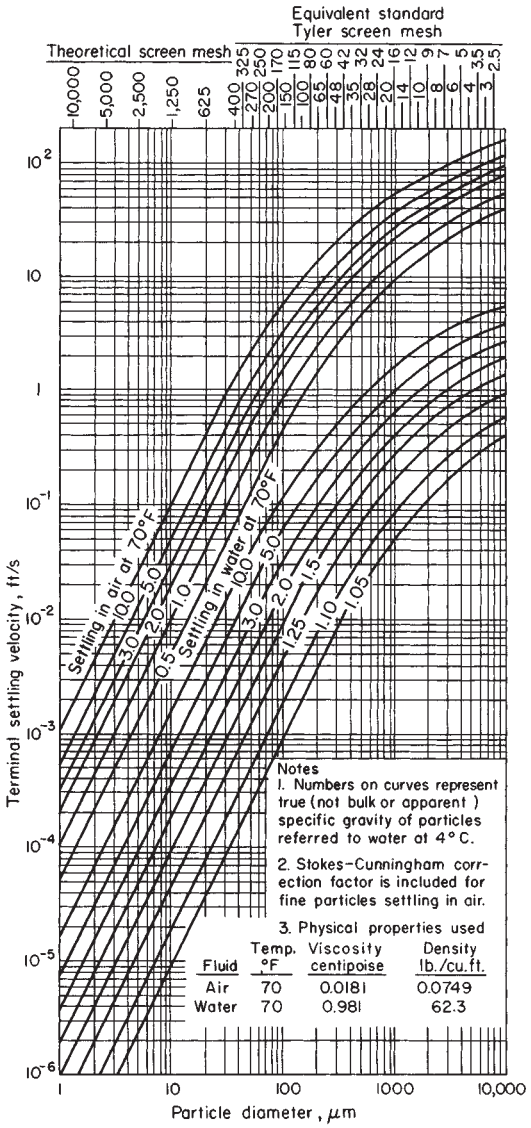

FIG. 6-61 Terminal velocities of spherical particles of different densities settling in air and water at 70°F under the action of gravity. To convert ft/s to m/s, multiply by 0.3048. (*From Lapple, et al.*, Fluid and Particle Mechanics, *University of Delaware, Newark, 1951, p. 292.*)